

**EXPERIMENTAL STUDY ON THE EFFECT OF LINTEL
ON INFILLED FRAMES UNDER CYCLIC LOADING**

MD. MAHIR ASIF

MASTER OF SCIENCE IN CIVIL ENGINEERING (STRUCTURAL)



DEPARTMENT OF CIVIL ENGINEERING
BANGLADESH UNIVERSITY OF ENGINEERING AND TECHNOLOGY
Dhaka, Bangladesh

July, 2022

EXPERIMENTAL STUDY ON THE EFFECT OF LINTEL ON INFILLED FRAMES UNDER CYCLIC LOADING

A Thesis Submitted by

MD. MAHIR ASIF

Student ID - 0417042339

A Thesis Submitted to the Department of Civil Engineering in
Partial Fulfillment of the Requirements for the Degree of
Master of Science in Civil and Structural Engineering



DEPARTMENT OF CIVIL ENGINEERING
BANGLADESH UNIVERSITY OF ENGINEERING AND TECHNOLOGY
Dhaka, Bangladesh

July, 2022

DEDICATED
TO
MY PARENTS

The thesis titled “Experimental Study on The Effect of Lintel on Infilled Frames under Cyclic Loading” submitted by Md. Mahir Asif, Roll No.: 0417042339P, Session: April 2017, has been accepted as satisfactory in partial fulfillment of the requirement for the degree of Master of Science in Civil and Structural Engineering on the 23rd July, 2022.

BOARD OF EXAMINERS



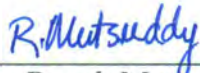
Dr. Raquib Ahsan
Professor
Department of Civil Engineering
BUET, Dhaka-1000

Chairman
(Supervisor)



Dr. Md. Delwar Hossain
Professor and Head
Department of Civil Engineering
BUET, Dhaka-1000

Member
(Ex- officio)



Dr. Rupak Mutsuddy
Assistant Professor
Department of Civil Engineering
BUET, Dhaka-1000

Member



Dr. Ali Ahmed
Professor, Department of Civil Engineering
Dean, Faculty of Engineering and Applied Sciences
BUBT, Dhaka-1216

Member
(External)

DECLARATION

It is hereby declared that this thesis has been composed solely by the author, and that it has not been submitted in whole or in part for the award of any degree (except for publication). Apart from where states otherwise by reference or acknowledgment, the work presented is entirely by the author.



Md. Mahir Asif

ACKNOWLEDGEMENT

I will commence by expressing my gratitude to ALLAH, the All-Mighty, for granting me the chance, resolve, and fortitude to accomplish my thesis work satisfactorily.

I would like to express whole-hearted gratitude and obligation to my respected supervisor, Dr. Raquib Ahsan (Professor, Department of Civil Engineering, BUET). Without his rigorous direction, constructive comments, encouragement, and passionate support throughout the development of this thesis, it would not have been possible to complete it.

Sincere appreciation to Dr. Md. Delwar Hossain (Professor, and Head of the Department of Civil Engineering, BUET) for his support from the Department. The author states his gratitude to Dr. Rupak Mutsuddy (Assistant Professor, Department of Civil Engineering, BUET) and Dr. Ali Ahmed (Professor, Department of Civil Engineering, BUBT) for giving their valuable comments, thoughtful insights, and suggestions.

I will express my thankfulness to GPH Ispat, Eco Ceramics Industries Limited and Crowne Cement Especially to Md. Delwar Hossain and Md. Arifuzzaman. Without their material support, it would be difficult to conduct the experiments.

I would like to thank Mr. Soumya Suhreed Das (MSc student, BUET) for providing me with necessary information about the state of Hydraulic Jacks. And Ms. Sadia Sabrin (Research Assistant, BUET) for assisting in experimental works.

A special thanks to the technical staff of the „Concrete & Materials Lab“ and the „Strength of The Materials Lab“ for their friendly attitude and helpful mentality during the experiment work. Special thanks also to the office staff for their valuable information in different steps.

I would like to acknowledge the research grant received for this study from the Committee for Advanced Studies and Research (CASR) of BUET, Dhaka.

Finally, I am indebted to my parents, sister, wife, and family members for their love, concern, care, and faith without their support this thesis work would not come into reality.

ABSTRACT

Numerous new and existing reinforced concrete frame structures have unreinforced masonry infill walls, establishing a composite program known as an infilled frame structure. These structures are one of the most extensively exploited structural systems in the world. Identically, these structures are profusely renowned in Bangladesh. However, every year a plethora of natural calamities ensue here and these structures are drastically subjected to cyclic excitation.

In our country, in most of the cases solid clay brick is used in the masonry wall. These buildings composed of solid clay brick perform miserably, especially in cyclic loading. Consequently, alternative material is necessary to address the defects and deficiencies uncovered by previous investigations which resulted in the development of the lightweight perforated clay brick. On the other hand, Lintel has a novel function to transfer loads of the masonry above the opening to the side walls nevertheless; its relevance is totally dismissed in structural design. Hence, these two parameters in infilled frame structure would be interesting to assess.

Four one-story and one-bay infilled frame structures have been constructed at half Scale. Two specimens have been built with solid clay brick masonry (the first one is a normal infilled frame structure and the second one includes lintel connecting one column to another) and the other two have been cast with perforated clay brick masonry (the first one is normal infilled frame structure and the second one includes lintel connecting one column to another). Afterward, they have been subjected to lateral cyclic loading.

From the experiment, it is found that specimens having lintel considerably increase the ductility (52%-81%), ultimate load carrying capacity (7%-23%), and energy dissipation (1.5-5 times). On the other hand, specimens containing perforated clay brick significantly enhance the ductility (10%-30%), and energy dissipation (1.1-4 times).

TABLE OF CONTENTS

	<u>Page No.</u>
DECLARATION	i
ACKNOWLEDGEMENT	ii
ABSTRACT	iii
TABLE OF CONTENTS	iv
LIST OF FIGURES	vii
LIST OF TABLES	xi
NOTATIONS	xii
LIST OF ABBREVIATIONS	xiii
Chapter 1: INTRODUCTION	1
1.1 General	1
1.2 Historical Background of the Research	2
1.3 Core Parameters of the study	4
1.4 Objective of the Study	4
1.5 Scope of the Investigation	5
1.6 Methodology of the Study	5
1.7 Outline of the Thesis	6
Chapter 2: LITERATURE REVIEW	7
2.1 Introduction	7
2.2 Behavior of Masonry Infilled RC Frame Structure under Cyclic Loading	8
2.3 Different Failure Modes of Masonry Infilled RC Frame Structures	16
2.4 Disasters and Cyclic Loads on Masonry infilled RC frame Structures	25
2.5 Solid Clay Brick and Perforated Clay Brick	32
2.5.1 Energy conservation	32
2.5.2 Cost-effective and low maintenance	32
2.5.3 Time-saving	32
2.5.4 Less dead load	33
2.5.5 Environment-friendly construction	33
2.5.6 Easy electrical installation	33
2.6 Lintel	33
2.6.1 Withstanding load above the opening	34
2.6.2 Resisting deflection	34
2.6.3 Transferring loads	34
2.6.4 Structural Contribution	34
2.7 Previous Investigation of MIRCF Structures under Cyclic Loading	34
2.8 Codes	42

	<u>Page No.</u>
Chapter 3: EXPERIMENTAL SCHEME	48
3.1 Introduction	48
3.2 Material Properties	48
3.2.1 Cement	48
3.2.2 Fine aggregate	48
3.2.3 Coarse aggregate	48
3.2.4 Reinforcement	49
3.2.5 Clay brick	49
3.2.6 Water	50
3.2.7 Mortar	50
3.2.8 Concrete	51
3.2.9 Prism Test	51
3.3 Details of Specimens	52
3.4 Preparation of Specimens	57
3.5 Experimental Setup	61
3.5.1 Firm base	61
3.5.2 Anchor bolt and steel plate	62
3.5.3 Reaction frame	63
3.5.4 Tripod stands	63
3.5.5 Dial gauges	63
3.5.6 Hydraulic jack	64
3.6 Test Procedure	65
Chapter 4: RESULTS AND DISCUSSION	66
4.1 Introduction	66
4.2 Summary of The Experimental Results of The Specimens	66
4.3 Damage Assessment and Failure Mode of the Specimens	67
4.3.1 SB (Solid Brick Infill)	67
4.3.2 SBL (Solid Brick Infill with Lintel)	72
4.3.3 PB (Perforated Brick Infill)	76
4.3.4 PBL (Perforated Brick Infill with Lintel)	81
4.4 Comparative Study	86
4.4.1 Comparison between SB and SBL	86
4.4.2 Comparison between PB and PBL	89
4.4.3 Comparison between SB and PB	92
4.4.4 Comparison between SBL and PBL	95
4.5 Overall Comparison of All Specimens	98
Chapter 5: CONCLUSIONS AND RECOMMENDATIONS	102
5.1 Introduction	102
5.2 Conclusions from the Experiments	102
5.3 Recommendations for Future Study	103
REFERENCES	105

		<u>Page No.</u>
Appendix-A	YIELD STRENGTH AND ULTIMATE STRENGTH OF REINFORCEMENT	119
Appendix-B	COMPRESSIVE STRENGTH OF SOLID AND PERFORATED CLAY BRICK	120
Appendix-C	ABSORPTION CAPACITY OF SOLID AND PERFORATED CLAY BRICK	122
Appendix-D	COMPRESSIVE STRENGTH OF MORTAR CUBE	124
Appendix-E	COMPRESSIVE STRENGTH OF CONCRETE CYLINDER	125
Appendix-F	COMPRESSIVE STRENGTH OF SOLID AND PERFORATED BRICK PRISM	126
Appendix-G	HYDRAULIC JACKS	127
Appendix-H	VALUES OF LOAD-DISPLACEMENT	129
Appendix-I	SAMPLE CALCULATION FOR STIFFNESS, STORY DRIFT AND CUMULATIVE ENERGY DISSIPATION	137

LIST OF FIGURES

		<u>Page No.</u>
Figure 2.1	Equivalent truss mechanisms for infill frame	7
Figure 2.2	Normal and shear stresses acting in the infilled frame	9
Figure 2.3	(a) Double arching effect, (b) Proposed equivalent method	10
Figure 2.4	Bending moment, Shear force, and axial force diagram for a typical infilled frame	10
Figure 2.5	(a) Interactive behavior of frame and infills, (b) analogous braced frame	11
Figure 2.6	Testing device	12
Figure 2.7	Modeling of seismic behavior before and after detachment of masonry infill	13
Figure 2.8	Change in the lateral load transfer mechanism owing to the inclusion of masonry infill walls	13
Figure 2.9	Behavior of soft-story in the earthquake	14
Figure 2.10	Buildings with open ground story (a) actual building (b) building being assumed in current design practice	15
Figure 2.11	Formation of Short columns due to partial height of brick masonry infill wall	16
Figure 2.12	(a) Mode of infill failures (b) mode of frame failures	18
Figure 2.13	Failure mechanisms of infilled frames	19
Figure 2.14	Typical degree of damage for bed joint sliding	19
Figure 2.15	Typical degree of damage for corner crushing	20
Figure 2.16	Typical degree of damage for diagonal tension cracking	20
Figure 2.17	Typical degree of damage for both corner crushing and diagonal cracking	21
Figure 2.18	Collapse mechanism of solid infill masonry with reinforced concrete frame	22
Figure 2.19	Modes of failure of infilled frames	22
Figure 2.20	Samples of collapses occurred for irregular distribution of infills over the height	23
Figure 2.21	Frame-infill interaction effects: local collapse due to the different infill–column height: (a) short column double plastic hinge mechanism; (b) short column shear failure	23
Figure 2.22	Effects of local infill–frame interaction: Sample of the local shear collapse of column ends and joints due to the interaction with the infills	24
Figure 2.23	(a) Corner crushing of the infill; (b) in-plane cracking and crushing of masonry wall (c) horizontal bed joint sliding	24
Figure 2.24	Crustal plate boundaries	26
Figure 2.25	Tectonic setup of Bangladesh and plate boundaries	27
Figure 2.26	Seismic zoning map of Bangladesh	28
Figure 2.27	Formation and pathways of storms	29
Figure 2.28	Basic wind speed (V, m/s) map of Bangladesh	30
Figure 2.29	Cyclone storm tracks in Bangladesh	31

	<u>Page No.</u>	
Figure 2.30	Flexural requirements for beams (IMF)	46
Figure 2.31	Transverse reinforcement requirements for beams (IMF)	46
Figure 2.32	Transverse reinforcement requirements for columns (IMF)	47
Figure 3.1	(a) Front / back elevation, (b) plan view, (c) side elevation of a full-scale solid clay brick (Every unit is in mm)	49
Figure 3.2	(a) Front / back elevation, (b) plan view, (c) side elevation of a full scale perforated clay brick (Every unit is in mm)	50
Figure 3.3	Compressive strength of mortar cube	51
Figure 3.4	Compressive strength of concrete cylinder	51
Figure 3.5	Schematic drawing of SB (Every unit is in mm)	53
Figure 3.6	Schematic drawing of SBL (Every unit is in mm)	54
Figure 3.7	Schematic drawing of PB (Every unit is in mm)	55
Figure 3.8	Schematic drawing of PBL (Every unit is in mm)	56
Figure 3.9	(a) lintel, (b) beam-column joint, (c) stirrups / ties, (d) column-base joint, (e) a full reinforced structure	57
Figure 3.10	Shuttering work	58
Figure 3.11	Measuring slump and concrete casting	58
Figure 3.12	(a) curing, (b) a concrete frame after 28 days of casting	59
Figure 3.13	Eight half-scale bricks produced from a single full-scale brick	59
Figure 3.14	Masonry work	60
Figure 3.15	Whitewashing	60
Figure 3.16	Schematic diagram of the experimental setup	61
Figure 3.17	Firm base	62
Figure 3.18	Anchor bolt and steel plate	62
Figure 3.19	(a) Reaction frame, (b) tripod stand	63
Figure 3.20	Dial gauges at (a) top-left corner at the specimen, (b) top-right corner of the specimen, (c) bottom-right corner of the base	64
Figure 3.21	(a) Hydraulic Jack 1, (b) hydraulic jack 2	64
Figure 3.22	Full experimental setup	65
Figure 3.23	Applied loading pattern during testing	65
Figure 4.1	Hysteretic load-displacement curve for SB	68
Figure 4.2	SB after the completion of cycle 1	70
Figure 4.3	SB after the completion of cycle 2	70
Figure 4.4	SB after the completion of cycle 3	71
Figure 4.5	SB at complete failure (at cycle 4)	71
Figure 4.6	Hysteretic load-displacement curve for SBL	73
Figure 4.7	SBL after the completion of cycle 1	74
Figure 4.8	SBL after the completion of cycle 2	75
Figure 4.9	SBL after the completion of cycle 3	75
Figure 4.10	SBL at complete failure (at cycle 4)	76
Figure 4.11	Hysteretic load-displacement curve for PB	77
Figure 4.12	PB after the completion of cycle 1	79
Figure 4.13	PB after the completion of cycle 2	79

	<u>Page No.</u>	
Figure 4.14	PB after the completion of cycle 3	80
Figure 4.15	PB at complete failure (at cycle 4)	80
Figure 4.16	Hysteretic load-displacement curve for PBL	82
Figure 4.17	PBL after the completion of cycle 1	84
Figure 4.18	PBL after the completion of cycle 2	84
Figure 4.19	PBL after the completion of cycle 3	85
Figure 4.20	PBL after the completion of cycle 4	85
Figure 4.21	PBL at complete failure (at cycle 5)	86
Figure 4.22	Relation between lateral load and story drift	87
Figure 4.23	Relation between stiffness and story drift	88
Figure 4.24	Relation between cumulative energy dissipation vs. story drift	88
Figure 4.25	Maximum displacement at each cycle	89
Figure 4.26	Stiffness at maximum displacement at each cycle	89
Figure 4.27	Relation between lateral load and story drift	90
Figure 4.28	Relation between stiffness and story drift	91
Figure 4.29	Relation between cumulative energy dissipation vs. story drift	91
Figure 4.30	Maximum displacement at each cycle	92
Figure 4.31	Stiffness at maximum displacement at each cycle	92
Figure 4.32	Relation between lateral load and story drift	93
Figure 4.33	Relation between stiffness and story drift	94
Figure 4.34	Relation between cumulative energy dissipation vs. story drift	94
Figure 4.35	Maximum displacement at each cycle	95
Figure 4.36	Stiffness at maximum displacement at each cycle	95
Figure 4.37	Relation between lateral load and story drift	96
Figure 4.38	Relation between stiffness and story drift	97
Figure 4.39	Relation between cumulative energy dissipation vs. story drift	97
Figure 4.40	Maximum displacement at each cycle	98
Figure 4.41	Stiffness at maximum displacement at each cycle	98
Figure 4.42	Relation between lateral load and story drift	99
Figure 4.43	Relation between stiffness and story drift	99
Figure 4.44	Relation between cumulative energy dissipation vs. story drift	100
Figure 4.45	Maximum displacement at each cycle	100
Figure 4.46	Stiffness at maximum displacement at each cycle	101
Figure A.1	Testing of rebar	119
Figure B.1	(a) Capping of bricks before testing, (b) Compressive strength testing of brick	121
Figure C.1	Weighting of (a) solid clay brick and (b) perforated clay brick during absorption capacity testing	123
Figure D.1	(a) Prepared mortar cubes (b) mortar testing	124
Figure E.1	(a) Prepared concrete cylinders (b) cylinder testing	125

	<u>Page No.</u>
Figure F.1 (a) Prepared prisms (b) testing of prisms	126
Figure G.1 Calibration curve of hydraulic jack 1	127
Figure G.2 Calibration curve of hydraulic jack 2	128

LIST OF TABLES

		<u>Page No.</u>
Table 3.1	Results of rebar testing	49
Table 3.2	Compressive strength of brick	50
Table 3.3	Water absorption capacity of brick	50
Table 3.4	Compressive strength of brick prism	52
Table 3.5	Details of the specimens	52
Table 4.1	Summary of The Experimental Results of The Specimens	66
Table A.1	Yield strength and ultimate strength of reinforcement	119
Table B.1	Compressive strength of solid clay brick	120
Table B.2	Compressive strength of perforated clay brick	120
Table C.1	Absorption capacity of solid clay brick	122
Table C.2	Absorption capacity of perforated clay brick	122
Table D.1	Compressive strength of mortar cube	124
Table E.1	Compressive strength of concrete cylinder	125
Table F.1	Compressive strength of solid brick prism	126
Table F.2	Compressive strength of perforated brick prism	126
Table H.1	Load-Displacement values for SB	129
Table H.2	Load-Displacement values for SBL	131
Table H.3	Load-Displacement values for PB	133
Table H.4	Load-Displacement values for PBL	135
Table I.1	Sample Calculation for stiffness, story drift and cumulative energy dissipation of SB	137

NOTATIONS

Symbol	Description
η	Magnification Factor
ΔW_{Rw}	Strength Reduction of The Current Story with Respect to The Upper Infilled One
ΔW_{Sd}	Sum of The Seismic Shear Forces Acting at The Top of Considered Story.
T_a	Natural Period of MIRCFC
h	h Is The Height of The Building (meter)
d	the base dimension of building (meter)
a	Width of the Diagonal Compression Strut (inch)
h_{col}	Column Height Between Centerlines of Beams (inch)
h_{inf}	The Height of The Infill Panel (inch)
E_{fe}	Expected Modulus of Elasticity of Frame Material (ksi)
E_{me}	Expected Modulus of Elasticity Of Infill Material (ksi)
L_{inf}	Length of Infill Panel (inch)
r_{inf}	Diagonal Length of Infill Panel (inch)
t_{inf}	Thickness of Infill Panel And Equivalent Strut (inch)
θ	Angle Whose Tangent Is The Infill Height-To Length Aspect Ratio (radians)
λ_1	Coefficient Used to Determine Equivalent Width of Infill Strut

LIST OF ABBREVIATIONS

Symbol	Description
RC	Reinforced Concrete
URM	Unreinforced Masonry
MIRCF	Masonry Infilled Reinforced Concrete Frame
BNBC	Bangladesh National Building Code
FEMA	Federal Emergency Management Agency
IS	Indian Standard
NBC	Nepal National Building Code
NSR	Colombian Standards for Seismic Resistant Design and Construction
SB	Solid Brick Infill
SBL	Solid Brick Infill with Lintel
PB	Perforated Brick Infill
PBL	Perforated Brick Infill with Lintel

Chapter 1

INTRODUCTION

1.1 General

One of the most widely utilized structural systems in Bangladesh is reinforced concrete (RC) frames with unreinforced masonry (URM) infill walls. Though they have been damaged in past earthquakes resulting in a lot of loss of life and property, these kinds of structural systems are still prevalent in disaster-prone areas. Many new and existing reinforced concrete frame structures are constructed with unreinforced masonry infill walls, resulting in a composite system known as infilled frame structure. Masonry infilled reinforced concrete frame (MIRCF) structures are immensely popular in Bangladesh. One of the key advantages of employing masonry infill is the economy and convenience of construction as it uses indigenous materials and worker skills. It provides ample sound and heat insulation, as well as waterproofing capabilities, leading to superior occupant comfort (Bekele, 2016).

However, the infill wall is considered a non-structural element, and the interaction of it with the bounding RC frame is ignored in the design. Particularly, the in-plane action can cause significant damage, if the structural element is not intended to meet serviceability criteria for damage control (Ricci et al., 2018; De Angelis and Pecce, 2020). The infill wall exerts both beneficial and detrimental effects on the surrounding RC frame. The infill wall enhances the performance of the overall system by increasing stiffness. Moreover, it decreases the natural period of the frame, which might be beneficial depending on the frequency of the input motion (Mondal and Tesfamariam, 2013; Misir, 2014). On the other hand, when an infilled frame is subjected to cyclic load, undesirable consequences such as cracking, out-of-plane failure, the short-column effect, the soft-story effect, etc. are observed (Tang et al., 2019). Therefore, specialist structural engineers must comprehend the impact of local masonry infills on the dynamic performance of MIRCF structures in Bangladesh.

1.2 Historical Background of the Research

At present, reinforced concrete frame structures with masonry infill are prevalent even in regions with a greater susceptibility to natural disasters. However, the usage of these structures is not new and they have been constructed for quite a long time. There are important historical facts behind the development of today's masonry infilled frame structures.

According to Crisafulli (1997), the usage of infilled frame structure started at the commencement of the 20th century. In a multitude of places around the world, masonry structures have been used due to fire resistance, thermal & acoustic insulation, aesthetic view, easy construction technique, etc. These structures acquired enormous popularity day by day.

Gomez (2012) stated that at the beginning there was a prototype for skeleton constructions in timber structures, which were typically covered with masonry or adobe. The true growth of this type, however, ensued with the industrialization of reinforced concrete and steel. These materials became the most cost-effective and time-efficient building materials. These types of structures gained more popularity after the Second World War. Mixed constructions with peripheral structural masonry walls and interior columns, as well as reinforced concrete floor slabs, were more frequent in the beginning. However, the unexpected response of these structures under later force led them to be changed and new types of structures were finally developed recognized as reinforced concrete skeletons with non-structural masonry infills.

There are a plethora of experimental, theoretical, and numerical investigations regarding these structures throughout history. Since 1948, the topic of the contribution of the infill to the horizontal racking stiffness and strength of an infilled frame has been the focus of - separate studies at numerous universities (Samai, 1984). A substantial investigation was commenced by Polyakov (1960) and his novel path was followed by a multitude of researchers and engineers. Polyakov proposed that the infill panel could be represented by a band of material acting in between the loaded corners of the bounded frame. He

successfully managed to develop the concept of the diagonal strut which is one of the most adopted theories regarding the masonry infill frame wall. Later, enormous researches were conducted regarding the lateral stiffness, flexural capacity, shear capacity, and ductility of the infilled frame walls. Among them, the works of Holmes (1961), Smith (1966), Liauw and Kwan (1985), Mander et al. (1993), Saneinejad and Hobbs (1995), Mehrabi et al. (1996), Negro et al. (1996), Lourenco et al. (1997), Madan et al.(1997), Papia (1998), Bunapane and White (1999), Henderson (2003), etc. are significant.

MIRCF structures have to be designed not only to resist the gravity load but also to withstand the lateral dynamic loads applied due to natural and man-made disasters. Bangladesh is a small country that is susceptible to a myriad of natural calamities. Among them, earthquake is a common phenomenon producing substantial structural damage (Asif et al., 2021). Under the surface of Bangladesh, tectonic plates are continuously shifting position, and Bangladesh is situated at the intersection of three tectonic plates (the Indian plate, the Eurasian plate, and the Burmese plate) (Asif et al., 2020). Bangladesh is surrounded by a number of tectonic blocks named Bogra Fault Zone, Tripura Fault Zone, Shilong Plateau, Dauki Fault Zone, and Assam Fault Zone (Al-Zaman and Monira, 2017). These geographical formations have made Bangladesh one of the most tectonically active places in the world. Hence, this has become a challenge to construct and take care of the MIRCF structures considering the aforementioned seismic hazard.

Bangladesh is also extremely vulnerable to cyclones because of its location at the triangular head of the Bay of Bengal (Murty and Neralla, 1992). Most of the worst affected areas are either off-shore islands or coastal areas (Paul and Rahman, 2006), although the whole country suffered many times during the past few strong cyclones. During the cyclone, the structures not only experience high wind force but also encounter heavy surge and wave force, especially near the coastal areas. Therefore, given the aforesaid events, this has become an arduous task to build and maintain the MIRCF structures.

Most of the existing masonry infilled RC frame structures have been constructed before the development of proper codes of lateral cyclic excitement. Again, a lot of MIRCF structures

in our country are not being designed according to the updated codes and regulations. Hence, dedicated investigations are strongly required in this sector to study more about MIRCF structures, predominantly under cyclic loading.

1.3 Core Parameters of the study

MIRCF structure is one of the most widely used structures in Bangladesh. In most of the cases solid clay brick is used as masonry material in our country. However, these structures made of solid clay brick respond adversely, particularly under cyclic loading. Hence, an alternate material is required to rectify the flaws and inadequacies discovered in past investigations. Lightweight perforated clay brick may prove to be advantageous. Usage of perforated brick instead of solid brick can be beneficial for having lightweight, energy efficiency, thermal and acoustic insulation, and cost-effective characteristics (Antoniadis et al., 2012; Pavlik et al., 2012; Su et al., 2016; Cavaco et al., 2018, Yadav et al., 2019).

A lintel is a sort of beam used to support the above wall or partition material when doors, windows, and other apertures are required to provide a building framework. The major purpose of the lintel is to transfer loads originating from the high wall to the side wall. In construction, the lintel is not considered as a structural material and there is little research conducted regarding this theme (Stavroulaki and Liarakos 2012; Park et al., 2014). Hence, it would be interesting to investigate the contribution of the lintel to the behavior of the MIRCF structure under cyclic loading.

1.4 Objective of the Study

The main objectives of this research are:

- I. To conduct an experimental comparative study among infilled frame structures in terms of stiffness, ductility, energy dissipation, and load-carrying capacity by altering the presence of lintel under cyclic load.
- II. To observe the different cracking patterns and failure modes of the specimens.

- III. To investigate the performance of perforated clay brick as a masonry wall in comparison with solid clay brick.

1.5 Scope of the Investigation

The primary purpose of the study is to investigate the behavior of MIRCF structures subjected to cyclic loading. The effect of lintel and perforated clay bricks have been predominantly observed here. The scope of the study deals with:

- I. Usage of only two types of masonry materials.
- II. Engagement of only experimental investigations. Numerical analysis is not conducted here
- III. Leveraging the advantage of the MIRCF structure. URM structure has not been utilized.
- IV. Construction of specimens without opening.
- V. Application of only lateral load. Vertical load has not been executed here.
- VI. Usage of conventional concrete and mortar.

1.6 Methodology of the Study

The following steps have been adopted to complete the research:

- I. Four one-story and one-bay (1675 mm) infilled frame structures have been cast at half scale with concrete ratio of 1:1.5:3 (by volume) and mortar ratio of 1:4 (by volume). Concrete has been prepared with Ordinary Portland Cement and the W/C ratio has been kept at 0.45 in all cases. The lintel has been 125 mm × 100 mm in cross-sectional dimension. Two specimens have been built with solid clay brick masonry. The first option is a normal infilled frame structure and the second option includes lintel connecting one column to another. The other two have been cast with perforated clay brick masonry. The first option is normal infilled frame structure and the second option includes lintel connecting one column to another.

- II. An experimental setup has been established to investigate the behavior of the specimens under cyclic loading. The frame has been built on a strong base and the total system has been fixed firmly with strong bolts. Necessary action has been associated to measure the displacements of the specimens. After completing the experimental arrangement, the lateral cyclic load has been applied to each specimen. Eventually, experimental data of different specimens have been collected and compared.

1.7 Outline of the Thesis

Chapter 1 includes ‘Introduction’ which introduces the thesis work. It represents the historical background, core parameters, objective, outcome, and methodology of the study in brief.

Chapter 2 contains ‘Literature Review’ which discusses the past research about MIRCF structure, their general behavior and internal interactions, their failure mechanisms, parameters such as perforated brick and lintel detail discussion, natural disasters of the world and Bangladesh which exerts cyclic excitation on structures, and relevant codes.

Chapter 3 consists of ‘Experimental Scheme’ which covers material properties, details of specimens, preparation of specimens, experimental setup, and testing procedure.

Chapter 4 comprises ‘Results and Discussions’ which lists the summary of the experimental results and explains the cracking and failure mechanism of the specimens, and comparative studies.

Chapter 5 covers ‘Conclusions and Recommendations’ which summarize the overall outcome of the experiment, and prospects for future study.

Chapter 2

LITERATURE REVIEW

2.1 Introduction

Throughout the history of human civilization, lateral load resistivity has been regarded as a key concern due to the fact that different regions of the world have been subjected to a large number of catastrophic natural disasters. During the early phase of constructional development, most of the structures were designed to resist the vertical load only. A little concern was shown in the lateral load-carrying capacity of structures. As a result, a huge amount of asset and life losses were caused when those structures experienced medium or heavy cyclic load due to various natural disasters. By the passage of time, a lot of codes, rules, regulations, and systems were developed to counteract the effect of lateral excitation. According to Samai (1984), in reinforced concrete constructions, shear walls are typically the most practical means of securing lateral stability. He envisaged three types of shear walls. Firstly, the conventional shear wall where load-bearing walls resist all lateral stresses in structures primarily made of wall and floor slab sections. Secondly, Shear walls combined with frames where modern building techniques have led to the adoption of shear walls as the primary lateral-load-resisting element, which are constructed as vertical cantilevers. Thirdly, Infilled frames where structures composed of two dissimilar materials, frame and infill, that function together to withstand lateral loading.

The last type of structure is profoundly interesting where the infill masonry panel is surrounded by a frame. Currently, this type of structure is extremely popular throughout the world as well as in Bangladesh. It successfully attracts users because it not only increases the strength and stiffness but also enhances the capability of heat and sound insulation (Moretti et al., 2014). In general point of view, the infill works as a partition wall and its structural contribution is totally neglected in most of the cases. However, it is a matter of concern for researchers and engineers to analyze the combined effect of infill masonry material and the surrounding frame.

2.2 Behavior of Masonry Infilled RC Frame Structure under Cyclic Loading

Infilled RC frame wall is a heterogeneous structure comprised of RC frame and masonry infill. The contribution of infill to the surrounding frame is highly interesting. When masonry panels are erected in line with the frames, the stiffness and strength of the frames are greatly increased. In tests utilizing reinforced concrete frames, the strength enhancement varies from twice to more than quadruple that of a frame without infill (Ghosh and Amde, 2022). The infill also affects the dynamic response of the structures (Mohammadi and Nikfar, 2013). Abreast several beneficial effects, the infill also decreases the displacement and second-order effects of the whole structure (Zovkic, 2013). It can also cause extensive damage as it interacts with the enclosing frame and impacts the load-transfer mechanism and the damage pattern (Bolis et al., 2017). However, in seismic design calculations, the existence of masonry infill is typically overlooked on the assumption that it is a nonstructural component. This assumption may lead to erroneous assessments not only of the seismic performance, such as the lateral stiffness, strength, and ductility of the structures but also of the seismic demands associated with the dynamic properties (Maidiawati and Sanada, 2017). The contribution of infill is generally ignored because the mechanism of infill wall is not simple due to their highly nonlinear inelastic response. Furthermore, several mechanical parameters, particularly for masonry infill and the contact between the infill and the surrounding frame, are difficult to characterize (Kareem and Guneyisi, 2018). Hence, the combination and interaction between infill wall and surrounding frame are a matter of concern for engineers and researchers.

According to Polyakov (1960), the full combined structure of infill and frame behaves as a braced frame because the masonry panel interacts with each side of the frame at a shorter distance from the loaded corners. This phenomenon was explained as a diagonal strut by the early researchers and engineers as presented in Figure 2.1. There is an immediate formation of the compressive strut at the alternative diagonal whenever the direction of lateral load reverses. Although the phenomenon was firstly determined by Polyakov, later it was reported by Mallick and Severn (1967). Holmes (1961) also worked with the diagonal strut and he proposed that the width of the diagonal strut should be one-third of the length of the diagonal length. The thickness of the diagonal strut was considered the

same as the thickness of the masonry panel.

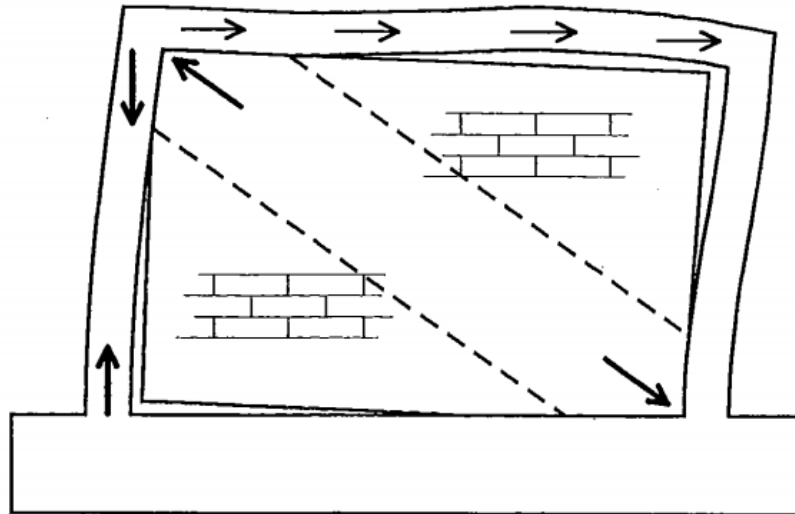


Figure 2.1: Equivalent truss mechanisms for infill frame (Polyakov, 1960).

Leuchars (1973) showed nonlinear normal stress distribution along the contact point of infill and frame relying on the loading condition as presented in Figure 2.2. He also demonstrated that the shear stress generated between the infill and frame is proportional to the normal stress.

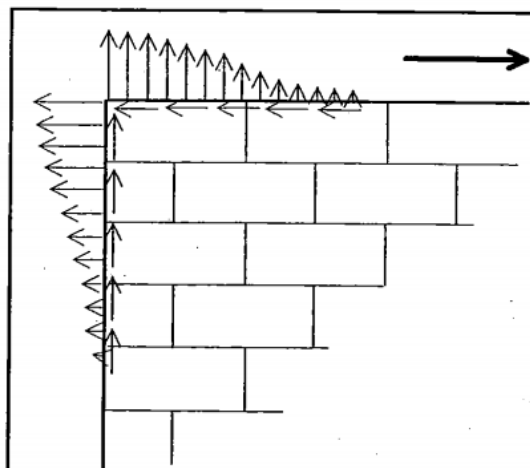


Figure 2.2: Normal and shear stresses acting in the infilled frame (Leuchars, 1973).

Smolira (1974) developed a qualitative model comprised of flexible frames and bricks without any other mortar or binder. In his experiment, he showed a double arching effect occurred in the panel as presented in Fig 2.3 (a) when the infilled frame is subjected to high lateral excitement. Again, Mainstone (1971) presented a similar type of experiment which dealt with the formation of two pinned diagonals as shown in Fig 2.3 (b) under high lateral load.

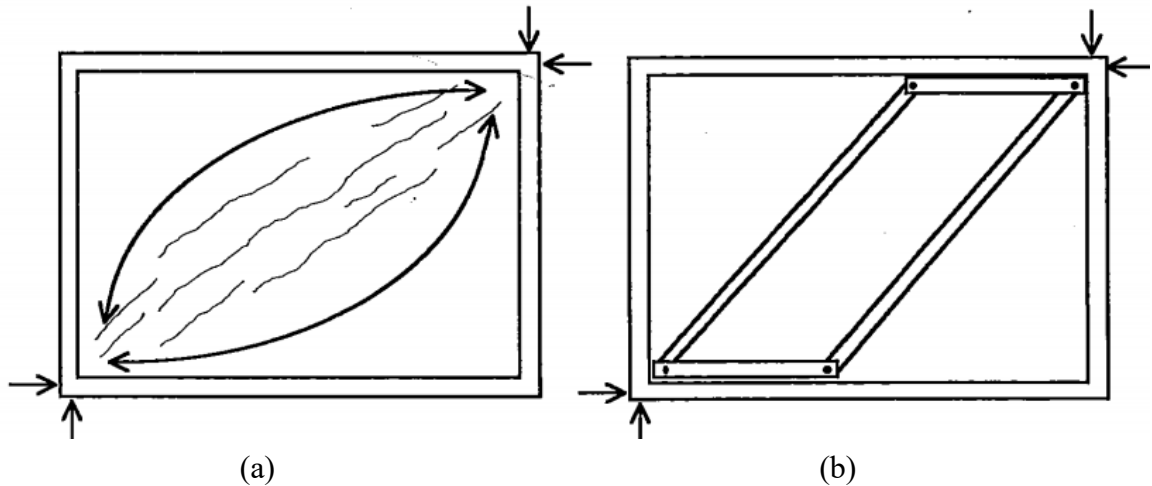


Figure 2.3: (a) Double arching effect (Smolira, 1974), (b) Proposed equivalent method (Mainstone, 1971).

Dhanasekar et al. (1985), illustrated typical bending moment, shear force and axial force after segregation occurs where the lateral load was applied along the top beam which was totally free from any sort of vertical loading. And the resulting formations are shown in Figure 2.4. And the bending moment was found much smaller in comparison to the bare frame.

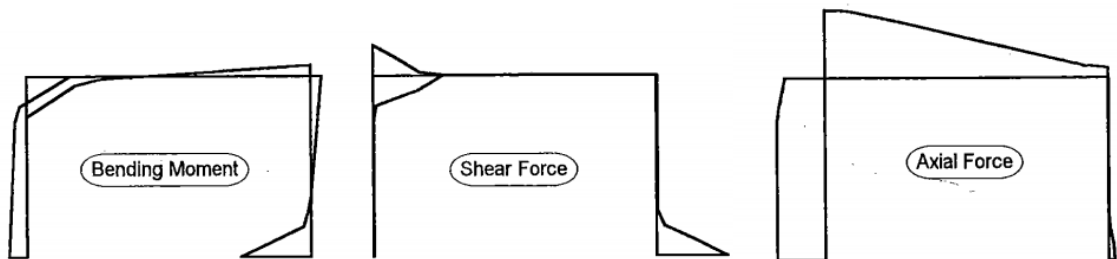


Figure 2.4: Bending moment, Shear force, and axial force diagram for a typical infilled frame (Dhanasekar et al., 1985).

According to Smith and Coull (1991), the infill possesses high in-plane shear rigidity and when it combines with flexible frame, it provides sufficient strength and stiffness to the whole combined system. The wall contributes to the frame by both in-plane shear resistance and diagonal bracing strut. Due to the translation of the top half of the column on each level and the contraction of the frame's leading diagonal, the column presses against the wall and compresses the wall along its diagonal. The whole behavior is illustrated in Figure 2.5.

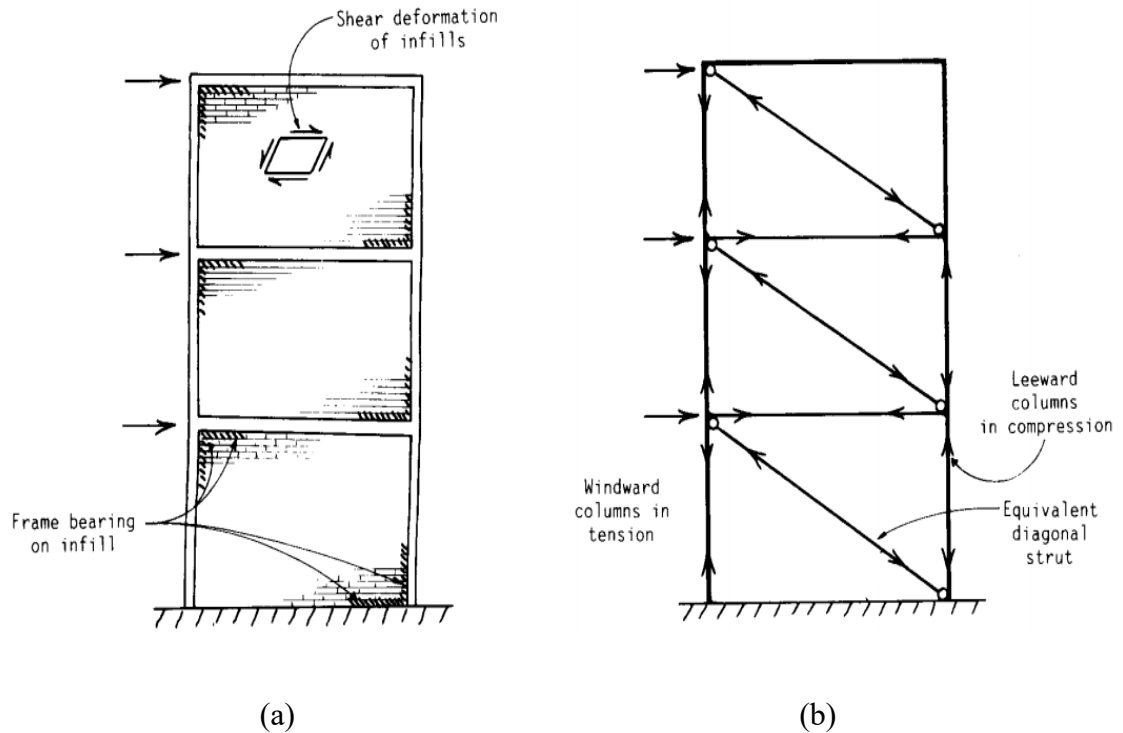


Figure 2.5: (a) Interactive behavior of frame and infills, (b) analogous braced frame (Smith and Coull, 1991).

Mander et al. (1993) developed multi-storied infilled steel frames with semi-rigid beam-column connections. The full arrangement has been demonstrated in Figure 2.6. They observed and disclosed that in this case, the diagonal strut connecting two opposite corners is not sufficient to resist heavy lateral forces. Therefore, they introduced a secondary strut mechanism.

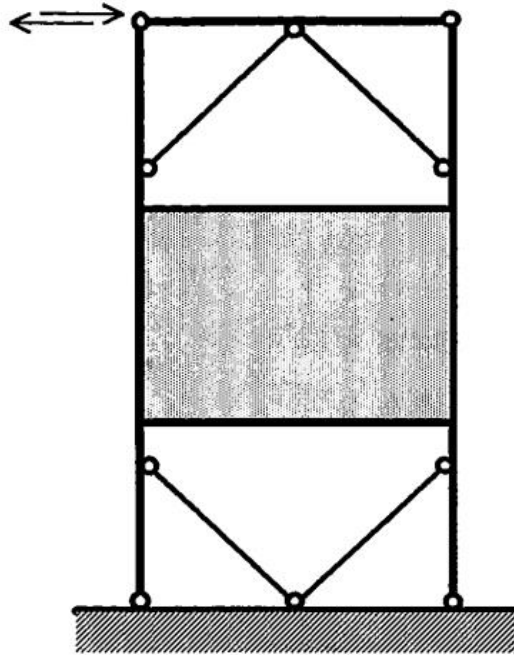


Figure 2.6: Testing device used by Mander et al. (1993).

Fardis et al. (1996) conducted a non-linear dynamic analysis and he demonstrated that the masonry infills influence positively the whole infilled frame structure, especially in the absence of irregularities. Furthermore, he showed that the masonry infill is highly beneficial to increase the stiffness and decrease the deformation of the whole system. The dynamic behavior of this type of structure is also improved because the system can dissipate sufficient energy through the slippage and friction action between the infill and the frame.

Tomazevic (1999) showed that an infilled frame operates as a monolithic load-resisting system at low lateral loads. Nevertheless, the crack is visible when there is an increment of loading. Moreover, the infill has a tendency to partially separate from the bounding frame as the load increases. This phenomenon is responsible for the formation of the compression strut mechanism. It may or may not develop into the principal load mechanism of the structure, contingent on the strength and stiffness characteristics of the infill relative to those of the frame. The behavior of this type of model is shown in Figure 2.7.

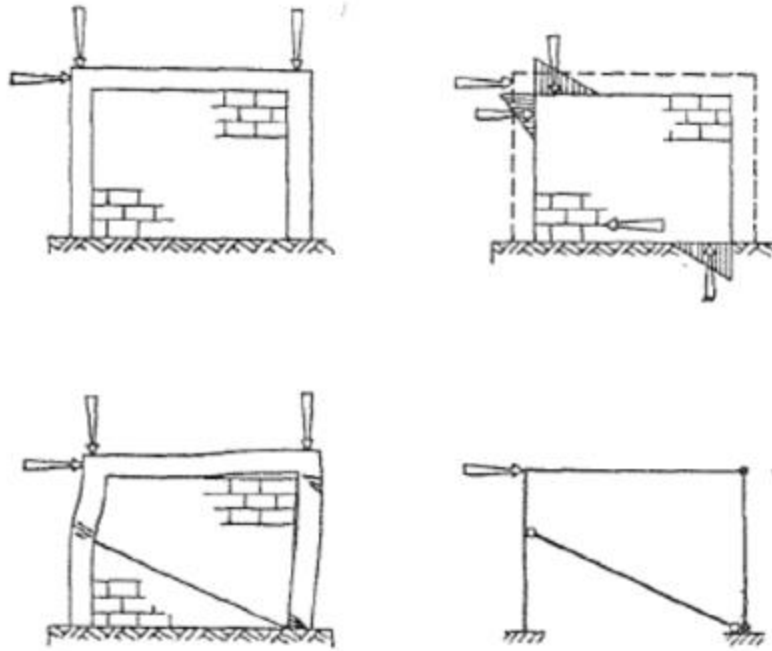


Figure 2.7: Modeling of seismic behavior before and after detachment of masonry infill (Tomazevic, 1999).

Murty and Jain (2000) stated that infills generate interference with the lateral deformations of the RC frame, which results in the segregation of the frame and the infill along one diagonal and the creation of a compression strut along the other diagonal. Therefore, infills contribute to the building's lateral rigidity. The frame action is replaced with a major truss action as the structural load transfer mechanism. As a result of this change, the frame columns are subjected to heavy axial forces, but they are also subjected to diminished bending moments and shear forces. The phenomenon is presented in Figure 2.8.

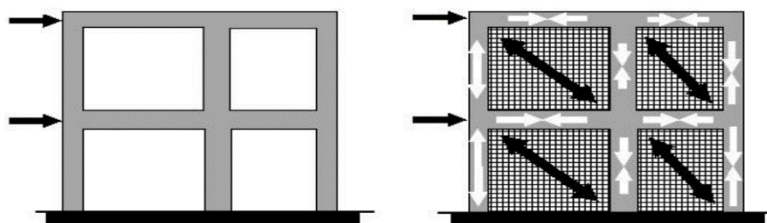


Figure 2.8: Change in the lateral load transfer mechanism owing to the inclusion of masonry infill walls (Murty and Jain, 2000).

Soft-story refers to a level of a building that is much less rigid or resistant to lateral loads than the stories above it and the floors or foundation below it. According to BNBC (1993) and UBC (1997), a soft story is one with lateral stiffness that is less than 70 percent of the preceding story or less than 80 percent of the average stiffness of the three preceding stories. For buildings with an open ground floor, the presence of walls in upper stories makes them substantially stiffer than the ground story. Thus, the majority of the building's horizontal displacement arises in the soft ground story. Hence, during earthquake trembling, such buildings move backwards and forwards and the columns in the open ground story are heavily affected. If the columns are not adequately designed to resist this incident, then significant damage or major collapse can ensue. Because of their substantial commencing stiffness, the associated contribution of different modes in infilled RC framed structures relies on the quantity and position of infills in the frame. Shailendra and Babulal (2015) illustrated this behavior which is presented in Figure 2.9.

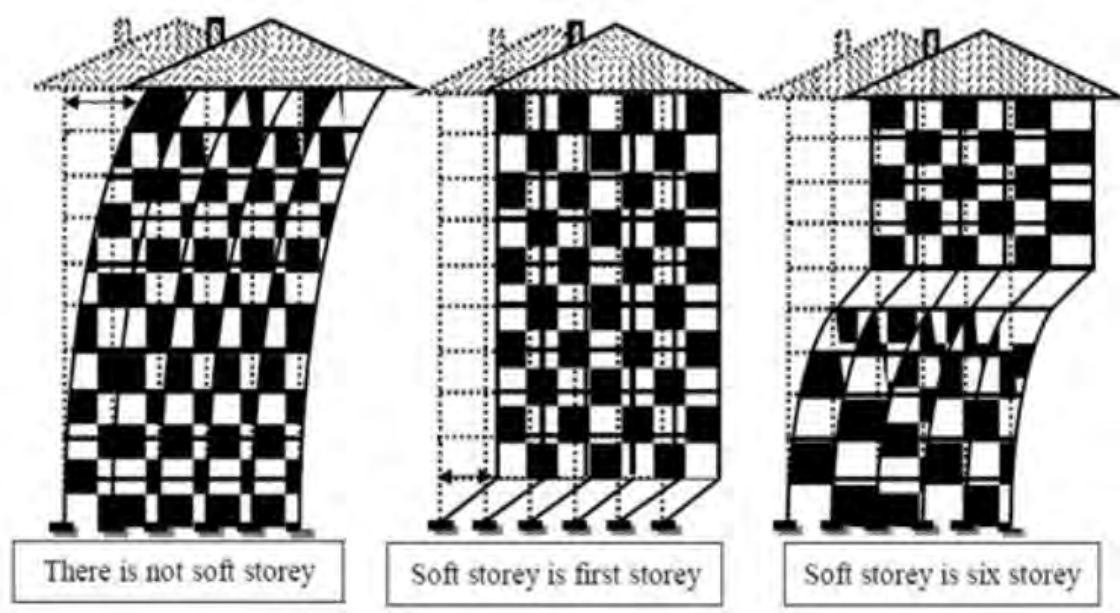


Figure 2.9: Behavior of soft-story in the earthquake (Shailendra and Babulal, 2015).

However, to avoid this type of damage, only bare frames are considered in modern design provisions. The effect of the infills is overlooked in these provisions as shown in Figure 2.10.

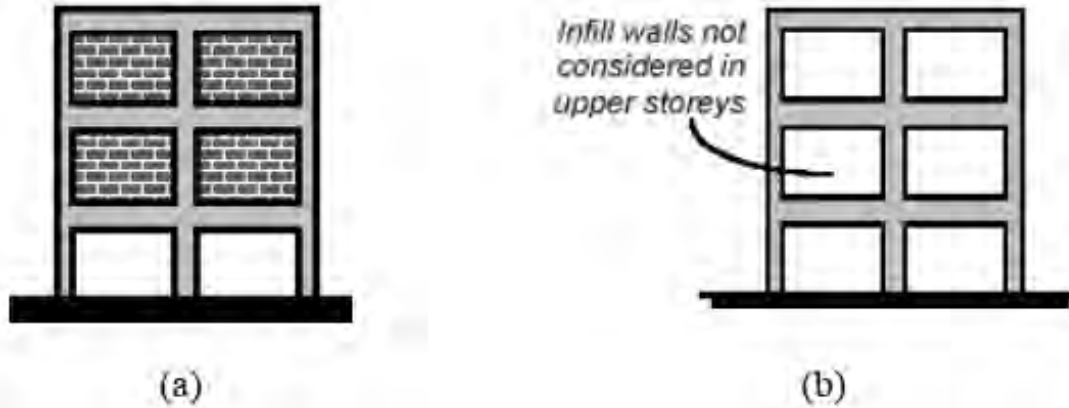


Figure 2.10: Buildings with open ground story (a) actual building (b) building being assumed in current design practice (Zerin, 2018).

Generally, a short column is stiffer than a tall column and comparatively a short column attracts more earthquake force. For this consequence, if a short column is not designed to resist such a heavy load, it will be undergone significant damage. The overall phenomenon is called as ‘short column effect’. According to Yadollahi et al. (2016), the short column effect mostly occurs when a partial-height wall is constructed to fit a window over the remaining height. During an earthquake, the floor slab and columns move horizontally. The stiff walls prevent the horizontal movement of a short column's lower portion and deform fully across its short height near the window opening. Regular columns distort along with their height. Since a short column's effective bending height is modest, it resists horizontal motion and attracts a bigger force than a conventional column. The incident is presented in Figure 2.11. They also explained some other reasons for the short column effect. It can also occur when a structure stands on the sloping ground containing columns of different heights. Additionally, this effect may be found in columns that endorse mezzanine floors or loft slabs that are attached in between two regular floors.

The behavior of a full infilled frame wall system and the interaction between infill & frame are explained by many other researchers. Among them, Fiorato et al. (1970), Mehrabi et al. (1994), Fardis et al., (1999), Zarnic et al. (2001), Al-Chaar et al. (2003), Calvi et al. (2004), Hashemi and Mosalam (2006), Centeno et al. (2008) are significant.

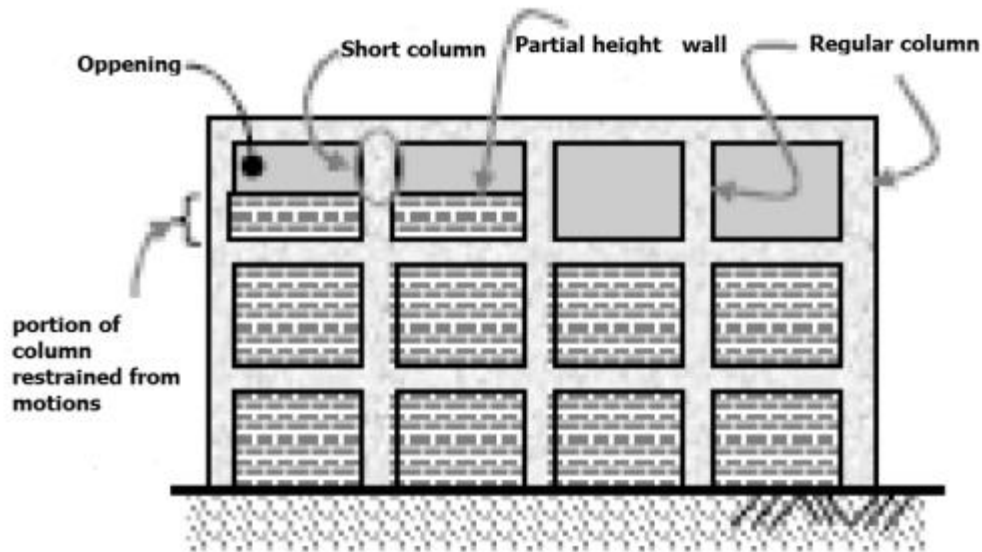


Figure 2.11: Formation of Short columns due to partial height of brick masonry infill wall (Yadollahi et al., 2016)

2.3 Different Failure Modes of Masonry Infilled RC Frame Structures

The cracking pattern and the failure modes of masonry infilled RC frame structures are related to the contribution of the infills to the cyclic resistance and the composite frame-infill behavior. Furthermore, the shear strength of the wall and the deformability of the frame supporting it both have a significant impact on how the full system behaves under cyclic action. Since the frame and infill are intended to function as a composite element, the ratio of strength and stiffness between the wall and the frame will ultimately determine how the structure fails. According to Gomez (2012), three main problems are primarily responsible for different types of failures of infilled frame walls. Firstly, the rotation of structures is due to the irregularity of the walls in plan. This causes eccentricity in the structure's rigidity. The overall structure's rotation deforms the distant columns greatly. Secondly, the short column effect means discontinuous infill walls throughout all the heights of the frame. Because the segments of the column that are not within the infill are more flexible, they must deform in tandem with the bigger columns that are not within the infill. Being short and stiff, these columns are prone to shear collapse due to strong shear forces. Thirdly, soft-story due to the irregularity of the stiffness along with the height of the column. Buildings with no lower-story walls and unfilled facades for commercial,

parking, or pedestrian usage are prevalent. So, the story seems to have the least rigid structure. Most of the failures were primarily brought on by the weak structural systems and substandard infill materials. A multitude of potential failure modes, including the crushing and cracking of the infill walls and the shear failure of the columns, can occur when an RC frame interacts with masonry infill. An infilled frame's ability to withstand lateral loads heavily depends on the failure mechanism that forms (Shing et al., 2009)

Smith and Coull (1991) showed different failure modes for both wall and frame individually. For the wall, they illustrated three types of failure (shear failure, diagonal cracking failure, and corner crushing failure) as shown in Figure 2.12(a). Firstly, shear failure descends through the masonry bond and is triggered by horizontal shear forces in the bed joint. Secondly, diagonal cracking failure is caused by the tensile stresses perpendicular to the leading diagonal and it creates along the leading diagonal of the wall. Thirdly, corner crushing failure occurs when there is the formation of high compressive stresses in corners. For the frame, they presented two types of failure (shear failure and tensile failure) as shown in Figure 2.12(b). When a frame is subjected to lateral cyclic excitation, the beam-column joint tends to fail in shear whereas the column receiving the excitation first tends to fail in tension at the base.

Mehrabi et al. (1994) observed three major types of failure mechanisms (horizontal sliding failure, diagonal cracking failure, and panel crushing failure) as shown in Figure 2.13. Firstly, the sliding of the masonry bed joints throughout the height of the wall typically exhibited a somewhat ductile behavior in frames with weak infill panels, which was dominant. This could occasionally result in masonry crushing at the compression corners and flexural yielding or shear cracks in the concrete columns. The whole phenomenon is termed a horizontal sliding failure. Secondly, a shear failure of the adjacent column was caused by a diagonal crack that started in the infill near the top windward corner. In non-ductile frames with robust infills, this procedure took place. Such brittle behavior was linked to a sharp decline in the loading carrying capacity. Thirdly, the panel crushing failure befalls when both the frame and the infill are adequately strong.

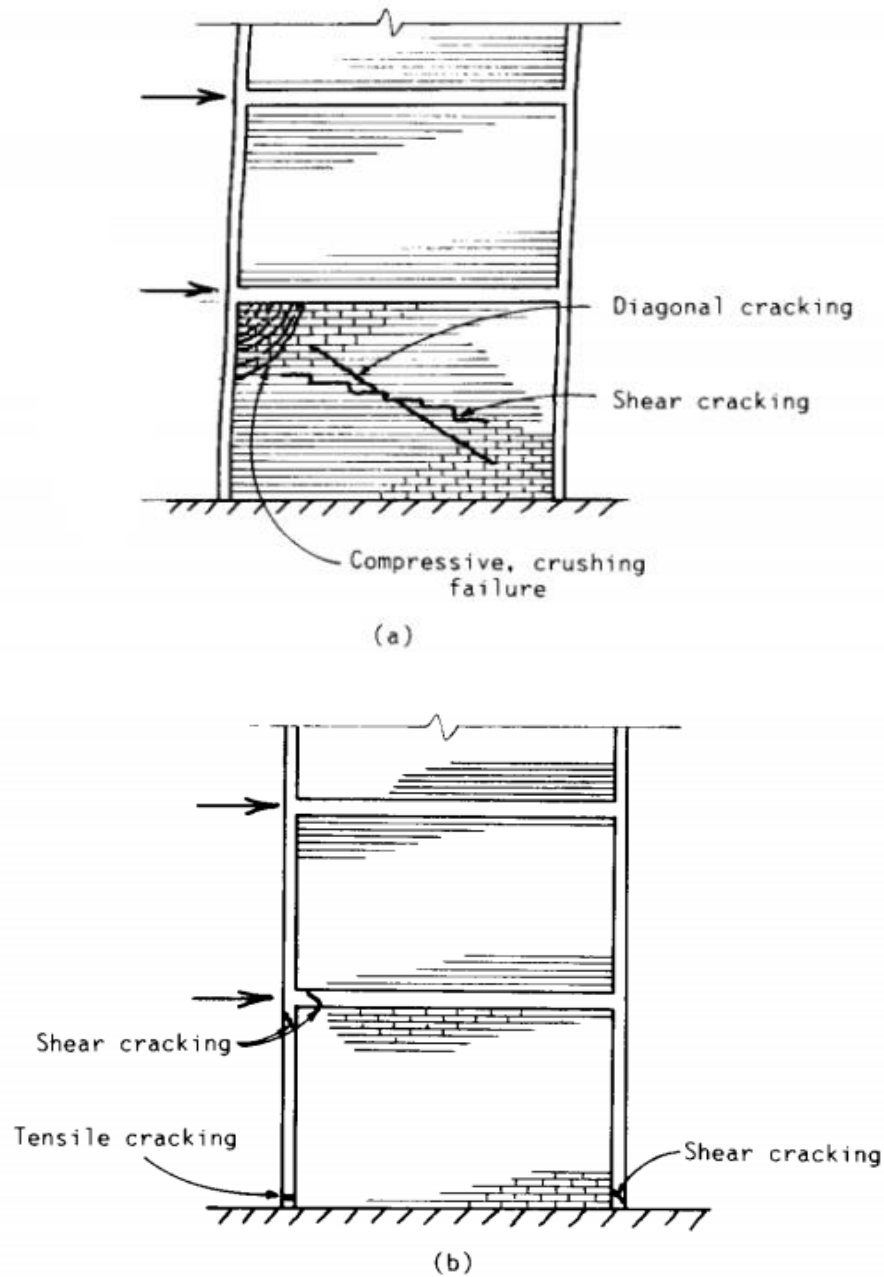







Figure 2.12: (a) Mode of infill failures (b) mode of frame failures (Smith and Coull, 1991).

In FEMA 306 (1998), four basic types of failures (bed joint sliding, corner crushing, diagonal tension cracking, and cracking due to both corner crushing and diagonal cracking) have been described. The expansive description of the aforementioned failure modes is illustrated in Figure 2.14, 2.15, 2.16, and 2.17 respectively.

Failure mechanisms

- (a) Horizontal sliding
- (b) Diagonal crack
- (c) Panel crushing

-  Plastic hinge
-  Shear crack
-  Crack in infill
-  Crushing
-  Slip at mortar joint

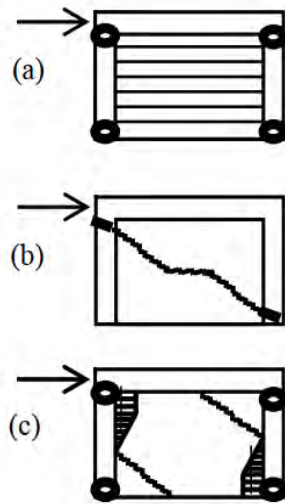
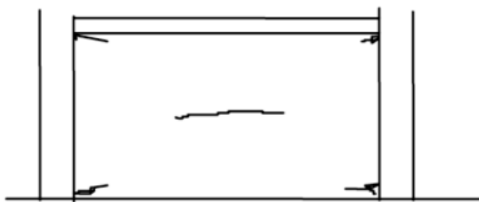
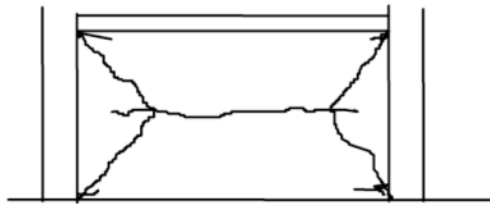


Figure 2.13: Failure mechanisms of infilled frames (Mehrabi et al., 1994).



Crushing of mortar around perimeter of frame. This is particularly noticeable adjacent to the columns near the corners of the infill panels.

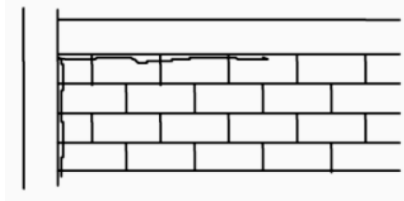


Crushing of mortar and cracking of bricks extend over larger zones adjacent to beam and column

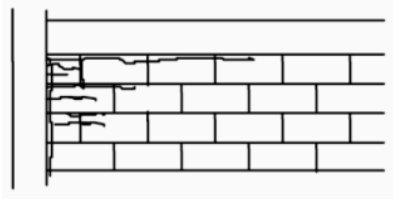


Significant crushing of mortar and bricks extends around most of the perimeter frame, particularly along the height of the column.

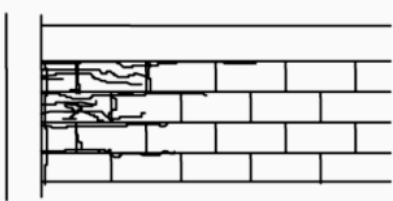
Figure 2.14: Typical degree of damage for bed joint sliding (FEMA 306, 1998).



Separation of mortar around perimeter of panel and some crushing or mortar near corners of infill panel

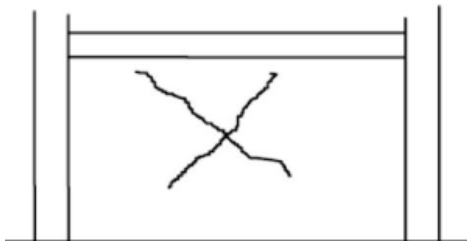


Crushing of mortar, cracking of blocks including lateral movement of face shells.

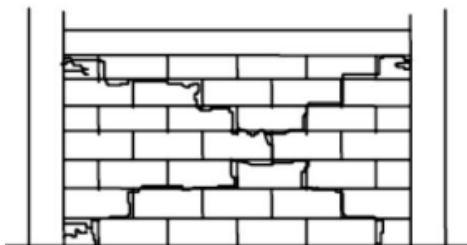


Loss of corner blocks through complete spalling of face shells. Diagonal (stairstep) cracking and/or bed joint sliding may also be evident.

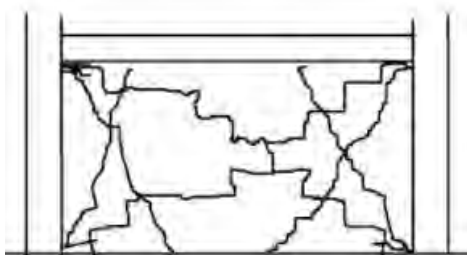
Figure 2.15: Typical degree of damage for corner crushing (FEMA 306, 1998).



Initial hairline cracking occur on diagonals in masonry. This is mostly associated with breaking of the bond between mortar and bricks. Cracking mostly concentrated within center region of panel



Hairline cracks fully extend along diagonals following the mortar courses in a stairstep fashion, but sometimes propagate through bricks. Some crushing and/or "walking-out" of the mortar may be observed. Cracks mostly closed due to confinement provided by frames.



Cracks widen to about 1/8", and are usually associated with corner crushing. Much loss of mortar is evident. More than one diagonal crack is generally evident. Crushing/cracking of the bricks is also evident. Portions of the entire infill may "walk" out-of-plane under cyclic loading.

Figure 2.16: Typical degree of damage for diagonal tension cracking (FEMA 306, 1998).

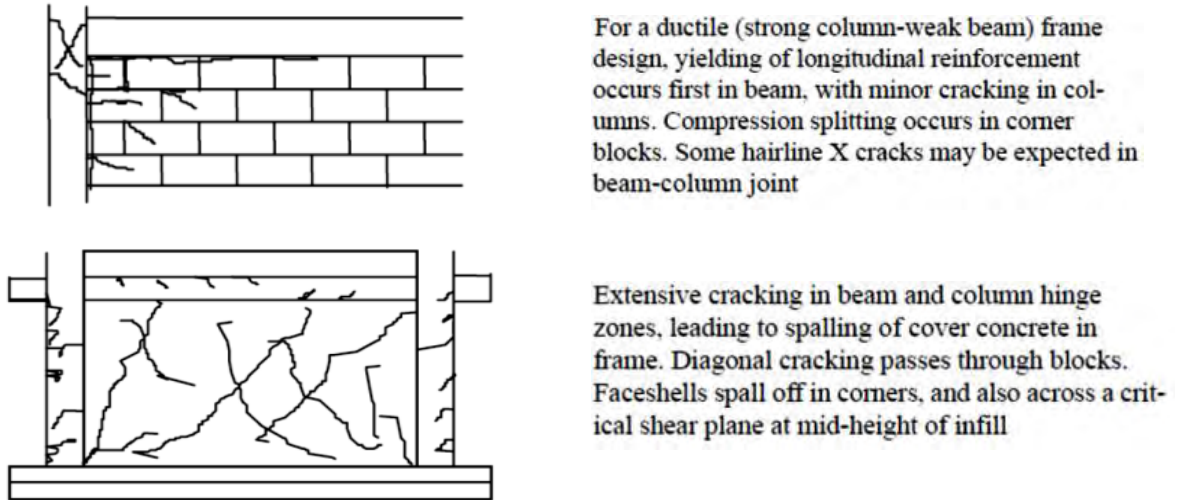


Figure 2.17: Typical degree of damage for both corner crushing and diagonal cracking (FEMA 306, 1998).

Shing and Mehrabi (2002) demonstrated the impact of the infill wall on the implosion process both in-plane and out-of-plane. It was demonstrated that the strength of the reinforced concrete and masonry infill totally determines the process of collapse. The full mechanism is illustrated in Figure 2.18.

According to Asteris et al. (2011), the failure of the infilled frame occurs as a confluence of the distinctive modes. Those individual modes described by him are presented in Figure 2.19. An experimental project was conducted to determine the relationship between the fracture pattern, the decrease in infill strength, and the extent and placement of the openings by him. Later, he identified various patterns and failure modes associated with very particular types of apertures and discovered a very sophisticated behavior that was distinct from the strut model.

According to Alam (2014), the probable modes of the collapse of masonry-infilled frame structures result from the interplay between the infill walls and the frame. He mentioned several failure patterns such as tension failure of tensioning column due to overturning moments, flexure or shear failure of the columns, compression failure of the diagonal strut, diagonal tension cracking of the panel, and sliding shear failure of the masonry along horizontal mortar beds.

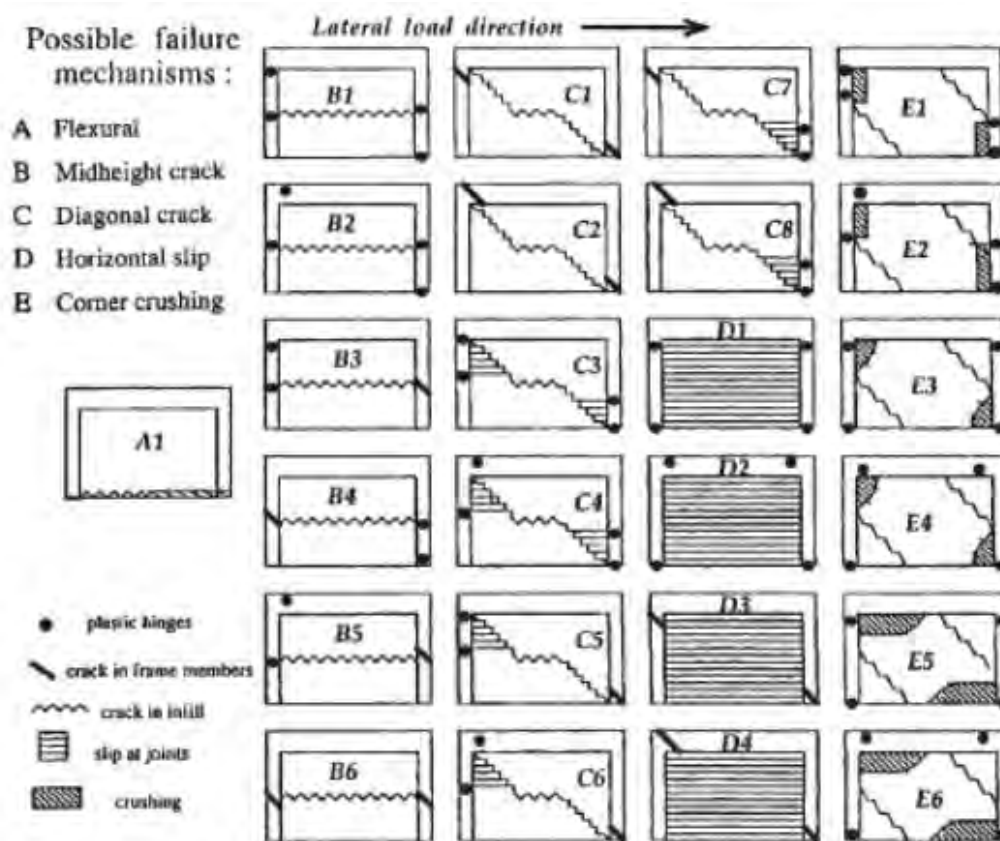


Figure 2.18: Collapse mechanism of solid infill masonry with reinforced concrete frame (Shing and Mehrabi, 2002)

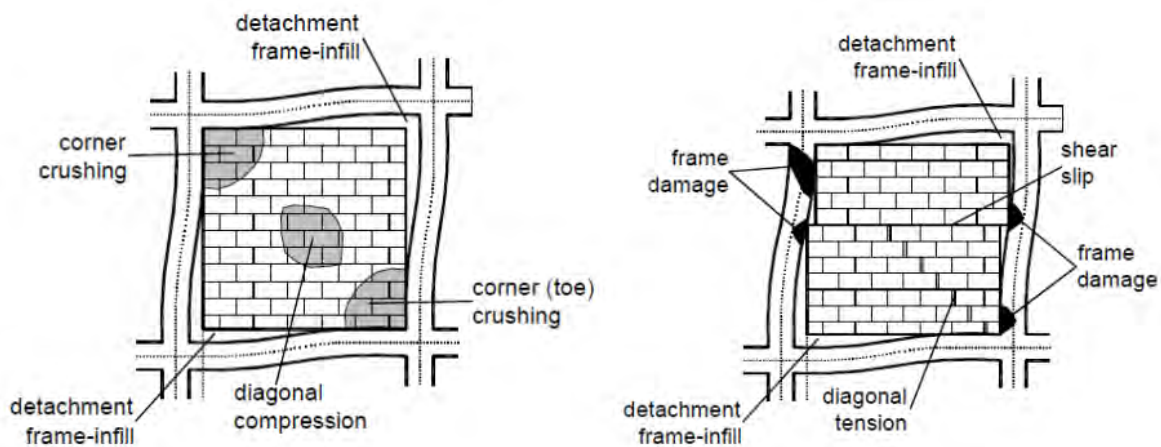


Figure 2.19: Modes of failure of infilled frames (Asteris et al., 2011)

Several real-life photos of different failure modes of masonry infilled RC frame structures under cyclic loading are presented in figure 2.20, Figure 2.21, Figure 2.22, and Figure 2.23.



Figure 2.20: Samples of collapses occurred for irregular distribution of infills over the height (Trapani et al., 2015).



(a)



(b)



Figure 2.21: Frame-infill interaction effects: local collapse due to the different infill–column height: (a) short column double plastic hinge mechanism; (b) short column shear failure (Trapani et al., 2015).



Figure 2.22: Effects of local infill–frame interaction: Sample of the local shear collapse of column ends and joints due to the interaction with the infills (Trapani et al., 2015).

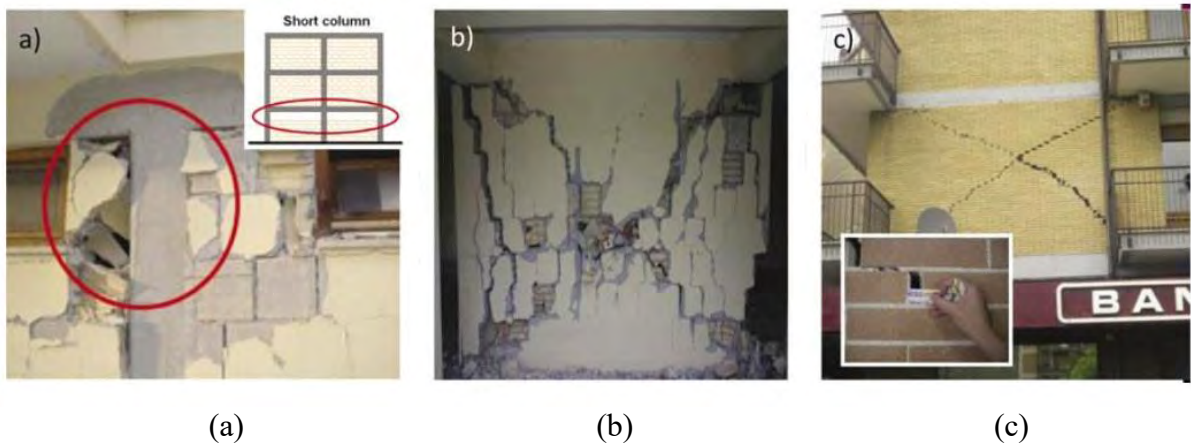


Figure 2.23: (a) Corner crushing of the infill; (b) in-plane cracking and crushing of masonry wall (c) horizontal bed joint sliding (Vicente et al., 2012).

2.4 Disasters and Cyclic Loads on Masonry infilled RC frame Structures

Masonry infilled RC frame constructions are one of the most ubiquitous types of structures worldwide. These types of structures are vulnerable especially when they are exposed to different natural or man-made disasters. During natural disasters like earthquakes and cyclones, these structures behave detrimentally in most of the cases. When these structures go through disasters, they experience intense dynamic and cyclic loads. If the structures are not adequately designed to resist such types of excitation, they tend to suffer from severe damage or complete structural failure.

Earthquake is one of the most terrible natural disasters in the world. It possesses the ability to demolish a whole civilization with a single ground motion. Tectonic movements are the main reasons for this dreadful catastrophe. To explain this tectonic movement, a theory termed ‘continental drift’ was proposed in 1912. According to this theory, the continents had been gradually shifting apart ever since they had once nestled together. However, questions aroused about the process of movement of continents. Later, evidence of the spreading of the Atlantic Ocean's sea floor was discovered in the 1960s. It was discovered that the crust itself is in motion rather than the continents moving over it. The contemporary theory of ‘plate tectonics’ was developed in this way. The Earth's upper mantle and solid crust collectively make up the lithosphere. It glides on the convective, free-flowing, and plastic components of the mantle. Convective currents in the mantle induce the motion of massive crustal plates (burro.case.edu., 2002). The crustal plate boundaries of the world are shown in Figure 2.24.

In past years, earthquakes have caused a tremendous loss of life and extensive damage to numerous structures, including residential, industrial buildings, and infrastructural systems. The forces of ground motion became devastating for poorly constructed infilled frame structures, which account for the majority of the buildings in different portions of the world. Among multitudinous earthquakes in history, some were highly fearful such as El Centro (1940), San Fernando (1971), Los Angeles (1994), Kobe (1995), Turkey (1999), Taiwan (1999), Bhuj (2001), Morocco (2003), Algeria (2003), Iran (2004), L'Aquila (2009), Nepal (2015), Mexico (2017), Palu (2018), Afghanistan (2022) Earthquake, etc.

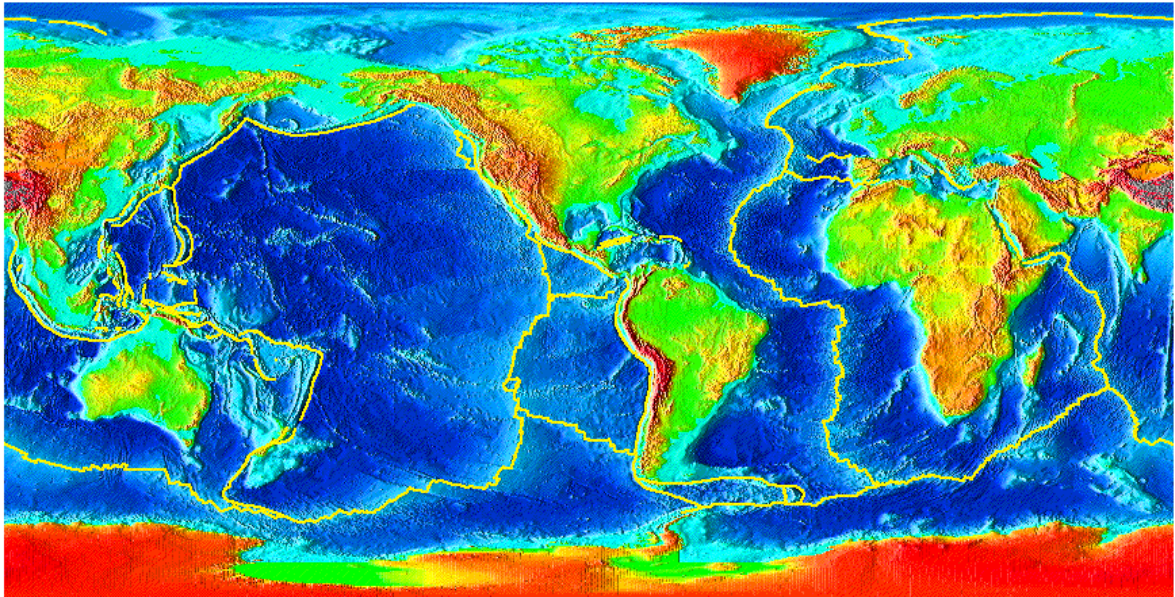


Figure 2.24: Crustal plate boundaries (burro.case.edu., 2002).

Bangladesh is one of the most natural disaster-prone countries in the world which is affected almost every year by multitudinous natural disasters. Among them, Earthquakes represent one of the most harmful and fatal natural disasters for humans (Rodrigues et al., 2018). The historical trend of seismicity and some recent tremors that occurred in Bangladesh and adjoining areas indicate that the country is also at high risk of earthquakes. Mainly, the geological formation, geomorphological landforms, and geophysical environment of this country are responsible for it (Biswas et al., 2018). The dynamic behavior of the earth's interior plays an important role in the formation of an earthquake (Khan, 2018). Bangladesh sits at the edge of the Indian Plate, the Eurasian Plate, and the Burmese Plate where the Indian Plate is moving north-east and slowly colliding with the Eurasian Plate (Hossain and Hossain, 2020). It makes Bangladesh one of the most tectonically active regions in the world. Moreover, five major faults are significant for the occurrences of devastating earthquakes in this country named Bogra Fault Zone, Tripura Fault Zone, Shilong Plateau, Dauki Fault Zone, and Assam Fault Zone (Al-Zaman and Monira, 2017). Two major active seismic belts, the Arakan system in the east and the Himalayan system in the north, are also accountable for destructive earthquakes in

Bangladesh and the surrounding area (Ansary and Arefin, 2020). The tectonic setup of Bangladesh is presented in Figure 2.25.



Figure 2.25: Tectonic setup of Bangladesh and plate boundaries (Akhter, 2010).

In this subcontinent, previous major earthquakes have resulted in significant structural damages and fatalities. Total of over 70000 people were severely affected due to five major earthquakes in this subcontinent. Those were Bihar (Magnitude: 8.1, Date: January 15, 1934), Gujarat (Magnitude: 7.7, Date: January 26, 2001), Maharashtra (Magnitude: 6.4, Date: September 30, 1993), Assam (Magnitude: 8.6, Date: August 15, 1950), and Uttarkashi (Magnitude 6.1, Date: October 20, 1991) Earthquakes (Hindustan times, 2015). Bangladesh was adversely influenced by these earthquakes. Due to its location in an earthquake-prone area (Figure 2.26), Bangladesh is at high risk. Long-term historical evidence suggests that Bangladesh experiences earthquakes frequently, with an average Richter scale magnitude of approximately 5 (Wikipedia: List of earthquakes in Bangladesh, 2022). Impairment from these earthquakes includes the collapse of reinforced concrete buildings in the port city of Chittagong (November 1997), serious structural damage to cyclone shelters in the Chittagong neighborhood of Moheshkhali (July 1999), significant cracking in masonry buildings, and malfunction of electric transformers in Chittagong (July 2003), and significant cracks in approximately 25 buildings in Chittagong

Division (November 2007), along with other tragedies (Zerin, 2018). In all of these earthquakes, a significant degree of damage was observed in the infilled frame structures.



Figure 2.26: Seismic zoning map of Bangladesh (BNBC, 2020).

Cyclones are one of the most destructive natural disasters in the world. The tropical cyclone is the generic scientific word for these events, depending on where they occur. Typhoons, cyclones, severe tropical cyclones, and severe cyclonic storms are some of the other names they are known by. It doesn't matter what name is given to them; the same forces and conditions are at work creating these massive storms, and every one of them has the potential to cause significant damage or destruction if it moves near populated areas (SciJinks, 2022). The formation and pathways of storms over the world are demonstrated in Figure 2.27.

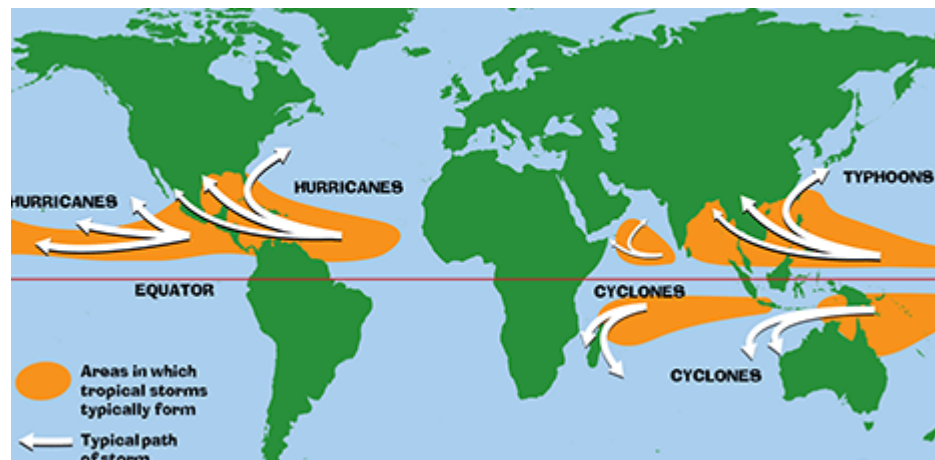


Figure 2.27: Formation and pathways of storms (SciJinks, 2022)

In past years, cyclones and storms were highly responsible for a lot of deaths and substantial structural damage to infrastructures. The masonry infilled RC frame structures were adversely susceptible to cyclones and storms. Among numerous storms in history, several were highly destructive such as Hakata Bay (1281), Backerganj (1584), Hooghly River (1737), Nagasaki (1828), Haiphong (1881), Tacloban (1912), Swatlow (1922), Great Bholá (1970), 02B (1991) cyclones (Weather Underground, 1999), etc.

Bangladesh is located between two diverse conditions, with the Bay of Bengal to the south and the Himalayas to the north (Rahman and Rahman, 2015). Low and nearly flat topography, an abundance of rivers, and a monsoon climate render the land vulnerable to the severe effects of natural disasters (Islam et al., 2010). Almost one-sixth of tropical storms that form in the Bay of Bengal make landfall on the coast of Bangladesh, causing

significant loss of life, and property and compromising development efforts (Asif et al., 2019). Although most of the worst affected areas are near coastal areas (Ali et al, 2017), most of the places (Basic wind speed of different districts of Bangladesh is presented in Figure 2.28) of the country are victims of this disaster.

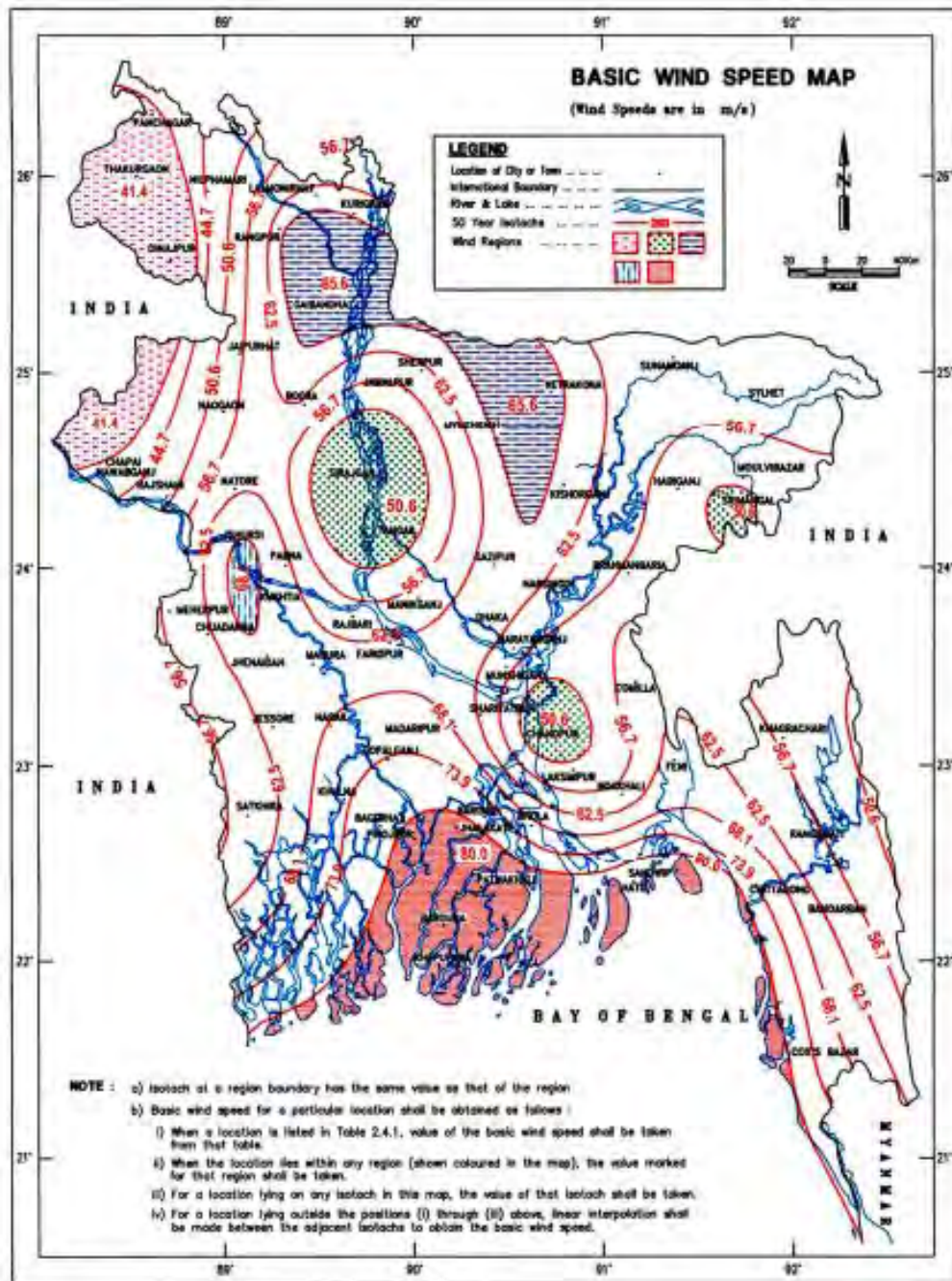


Figure 2.28: Basic wind speed (V, m/s) map of Bangladesh (BNBC, 2020).

In Bangladesh Bay of Bengal is the primary source of most of the cyclones. Wind and warm water work as the fuel to originate these cyclones. Cyclones in the Bay of Bengal often move first to the northwest before curving eastward. However, this pattern is not uniform, as evidenced by the paths of distinct cyclones. During storm, surges are accompanied by high rainfall and sea swells. If this occurs during high tide, the resulting storm surge can reach heights of up to 12 meters. This destructive wall of water causes the majority of the loss of lives and property (Banglapedia, 2021). Cyclone storm track in Bangladesh is shown in Figure 2.29.

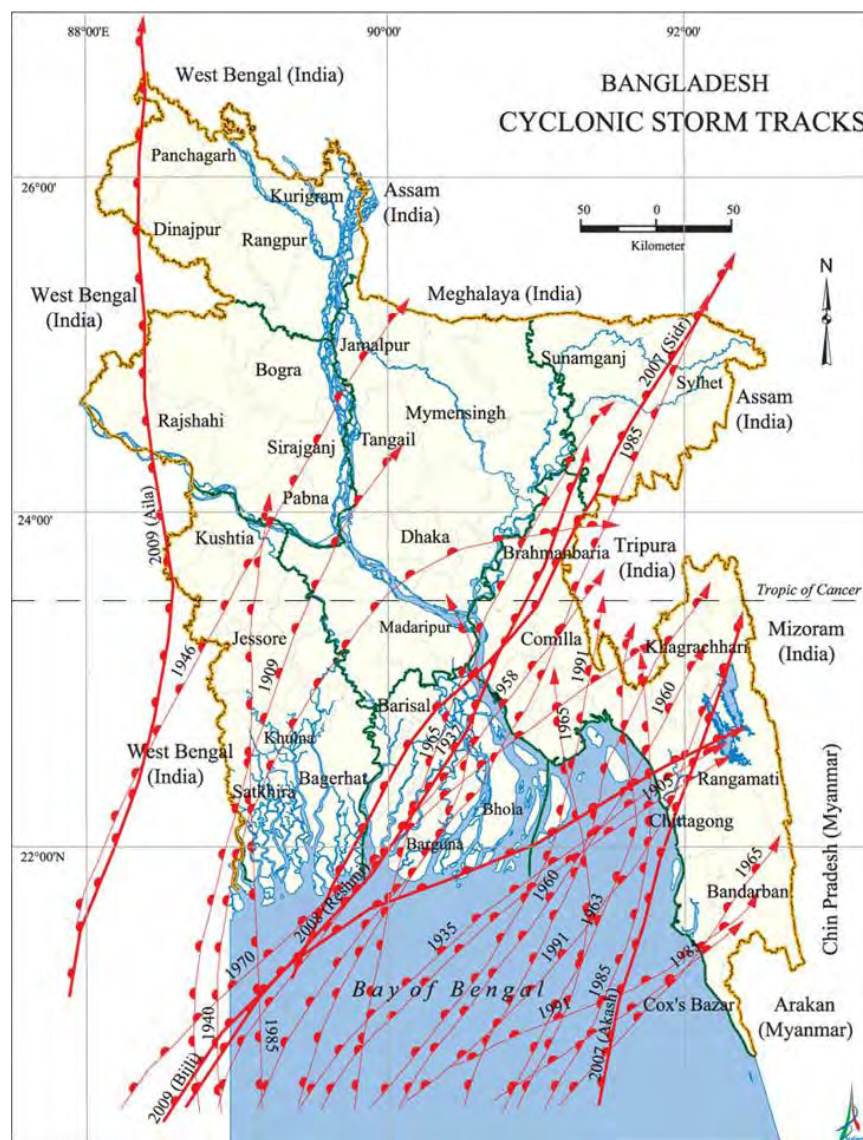


Figure 2.29: Cyclone storm tracks in Bangladesh (Banglapedia, 2021).

In Bangladesh, non-reinforced masonry walls used for peripheral and interior partition walls that fit snugly between structural columns and beams are deemed non-structural, despite interacting with the structural parts constraining it. However, these structures behaved profoundly poorly when they were exposed to disasters and experienced cyclic loading. In past, many researches have been conducted regarding masonry infilled RC frame structures. Nevertheless, it will be interesting to investigate the behavior of MIRCF structures built with locally available materials under cyclic loading.

2.5 Solid Clay Brick and Perforated Clay Brick

A masonry wall is a vital element of MIRCF structures, although they are non-structural elements and their contribution is mostly ignored in design. In general, it is common practice to use solid clay brick and it has been used traditionally for a long time. However, the perforated clay brick can be a viable alternative solution to be used in MIRCF structures for multitudinous advantages. According to ‘Go Smart Bricks’ (2022), perforated brick could be more beneficial for the following reasons:

2.5.1 Energy conservation

Due to their thermal insulation capabilities, perforated bricks can lessen the necessity of cooling and heating systems depending on the season. This lowers energy usage, conserving resources and money.

2.5.2 Cost-effective and low maintenance

Compared to solid bricks, perforated bricks are significantly lighter. The overall structural cost is decreased as a result. Masons are able to work more quickly, which results in lower labor expenses. Low maintenance expenses since perforated bricks tend to have less efflorescence than solid bricks have on their surface.

2.5.3 Time-saving

As perforated bricks are far lighter than solid bricks, the convenience of working with them expedites construction and accelerates project completion.

2.5.4 Less dead load

The use of perforated bricks will minimize a dead load of buildings, hence reducing the cost of building structures. Moreover, perforated bricks lessen the total weight of structures leading to more seismic efficient infrastructures.

2.5.5 Environment-friendly construction

Fewer natural resources are required to manufacture perforated clay bricks in comparison with solid clay bricks.

2.5.6 Easy electrical installation

The inclusion of holes in perforated bricks makes it easier to put electrical lines and plumbing fittings through it, which is one of its key advantages.

2.6 Lintel

The Lintel is a horizontal element placed directly above the openings of doors, windows, etc., to sustain the weight of the masonry work above it. It may be comprised of reinforced brick masonry, brick masonry arches, precast concrete, reinforced concrete, timber, or structural steel shapes. Numerous buildings in Greece appeared to have incorporated steel lintels and, more crucially, have made this integration obvious on their external elevations. From the 1910s to the 1930s, a large number of I-beams were incorporated into the stone architecture of Greece, particularly in public buildings. They are not a component of a steel structural system, but rather serve to span enormous openings in a typical stone structure. While timber lintels and arches continued to fulfill the needs of residential construction, new schools and stores benefited from wider openings that could only be accommodated by steel. Even when the openings had flat arches, they were supported structurally by concealed steel parts. Now in the modern era, the reinforced concrete lintel is globally used in most of the cases (Stavroulaki and Liarakos 2012). According to ‘Daily Civil’ (2022) and ‘Civilclick’ (2020), the lintel possesses the following advantages:

2.6.1 Withstanding load above the opening

When an opening is set on a wall, the masonry units above the opening tend to collapse. Lintel is profoundly beneficial in this case which does the task to take care of the load above the opening.

2.6.2 Resisting deflection

Lintel resists the deflection that ensued on the upper portion of the opening. It also counteracts the induced deflection on that particular place.

2.6.3 Transferring loads

Lintel follows a particular load-transfer mechanism. It transfers the loads to the side walls on which the lintel rests. The load on the lintel comes from the portion of the wall resting on that specific lintel.

2.6.4 Structural Contribution

A Lintel is a vital flexural component that must be built to withstand the tension, compression, and shear forces operating on it.

2.7 Previous Investigation of MIRCF Structures under Cyclic Loading

In past, several studies have been conducted regarding masonry infilled RC frame structures under cyclic loading.

Mehrabi et al. (1996) investigated the impact of masonry infill panels on the seismic performance of reinforced concrete (RC) frames created in compliance with current code requirements. Two different kinds of frames were explored: One was built to withstand wind loads, while the other was to withstand powerful seismic forces. Twelve single-story, single-bay frame examples at a 1/2 scale were put to the test. The parameters examined included the infill panels' strength in relation to the surrounding frame's integrity, the panel aspect ratio, the distribution of vertical loads, and the chronology of lateral loads.

According to the experimental findings, infill panels can greatly raise the efficiency (especially under lateral loads) of RC frames.

Mehrabi and Shing (1997) conducted experimental and computational investigations on masonry-filled RC frames under in-plane lateral excitation. This work summarized experimental results and presented a constitutive model for simulating mortar joints and cementitious surfaces. Typically, RC frames and masonry components were modeled using a smeared-crack finite element model. Finite element models can replicate the failure mechanisms of infilled frames, including crushing and cracking of concrete frames and masonry panels and sliding and separation of mortar joints. The models' lateral strength matches the tests' well.

Ghosh and Amde (2002), explained that the methods recommended by earlier authors work when designing infilled frames to resist lateral loads on structures in terms of their failure modes, failure loads, and baseline stiffnesses. This verification was carried out by contrasting the outcomes of the analytical techniques used by the previous authors with those of a novel finite element model for infilled frames, which was supported by experimental findings. Using the existing test data on masonry joints, a non-associated interface model was created to simulate the interface between the frame and the infill and the mortar joints encircling the masonry blocks. The von Mises criterion for the plane stress condition for uncracked masonry assembly and a smeared crack model were two examples of masonry failure criteria. The failure dynamics of the infilled frames were also properly understood owing to the finite element model.

Colangelo (2005) presented pseudo-dynamic tests on the in-plane seismic behavior of infilled frames. Thirteen half-size, single-bay, reinforced concrete-frame specimens with one story each were evaluated. The majority of these specimens had non-structural masonry constructed of perforated bricks and cement mortar. The strength, features, level of reinforcement, and aspect ratio of the frames were varied. The seismic input was applied to the specimens twice, once when they were brand new and once when they had been damaged by a prior test. Initial virgin infilled specimens had a significantly different global

seismic response than bare specimens. Following a significant alteration in the characteristics, the peak strength was found more than doubled and the baseline stiffness increased by an order of magnitude when compared to a bare frame. Peak drift declined, but the demand for displacement ductility did not.

Almusallam and Al-Salloum (2007) determined the efficiency of FRP for reinforcing and/or repairing unreinforced masonry infill walls in reinforced concrete frames that were exposed to in-plane seismic/cyclic loads. A complete presentation of specimen geometry, test setup, instrumentation, and a loading process that simulates earthquake loading was provided. Overall, the test findings showed that using glass FRP GFRP sheets as strengthening materials improved the infill wall's deformation capacity and allowed the wall to function as a single unit. These findings indicated a significant improvement and strengthening potential for the infill walls under in-plane seismic loads for externally bonded GFRP sheets.

Kakaletsis (2010) was encouraged to assess the modern retrofitting and repairing techniques for the existing structures (masonry walls of bare and infilled RC frames) which had already been damaged by cyclic loading. Under cyclic horizontal loading up to a drift level of 4 percent, four 1-story, 1-bay, 1/3-scale frame specimens were tested: two bare frames with spirals or stirrups as shear reinforcement, and two infilled frames with weak infills and spirals or stirrups as shear reinforcement, respectively. He used several techniques such as epoxy resin, CFRP plates, and polymer-modified cement mortar. Based on the maximum cycle load, loading stiffness, and hysteretic energy absorption capacities of the tested specimens, conclusions were reached regarding the comparison of the effectiveness of conventional and CFRP seismic retrofitting applied procedures.

Zovkic et al. (2013) discussed how different forms of masonry infill affect the response of reinforced concrete frames when subjected to lateral loads. Ten one-bay, one-story reinforced concrete frames for the larger project were constructed at a scale of 1:2.5, filled with masonry, and tested under constant vertical and cyclic lateral loads. The masonry wall had a range of strengths, including lightweight autoclaved aerated concrete blocks with

low strength, high strength hollow clay brick blocks, and medium strength hollow clay brick blocks. The findings demonstrated that compared to a bare frame construction, the composite "framed wall" structure had significantly higher stiffness, damping, and starting strength. When the frame took control, the masonry infill closed the load capacity gap, which had previously been very minimal. By taking into account the contribution of a common masonry that lowers the drift levels to reduce projected damages, improvement of the "infill provisions" in the codes may be attempted.

Essa et al. (2013) studied the behavior and ductility of H.S.R.C. frames with infill walls under the influence of cyclic load. On four samples, the experimental program was carried out (frames). The factors that affect the switch from a non-infill frame panel to infill were the thickness and bricks' composition. The size of the frames is chosen to simulate half-scale frames that were put to cyclic loading. Eventually, the lateral resistance and the ductility factor of infilled frame were found more and less respectively than the bare frame.

Misir (2014) examined how a novel infill technique, termed locked brick infill adopting horizontal sliding joints, impacted the creation of soft stories in reinforced concrete (RC) frames with seismic details that complied with building codes. He had conducted half-scale RC infilled frame tests on a single-story, single-bay frames that were stuffed with standard and locked bricks. These tests provided the specifications of the frame and infill elements that were employed in the numerical simulations. The numerical simulations demonstrated that, even in buildings with non-infilled first stories, the use of locked bricks to form infill walls had the capability to minimize the soft-story/weak-story formation in relation to conventional bricks due to its shear sliding mechanism and reduced upper-story/first-story stiffness.

Moretti et al. (2014) intended to evaluate the diagonal strut model, which is already widely utilized as a design tool in the case of masonry-infilled reinforced concrete (RC) frames. The strut model provisions in codes were examined together with the underlying presumptions. The response of eight 1/3-scale RC infilled frames to quasi-static cyclic horizontal displacements was the focus of experimental research; some of the results were

presented in parallel. Investigations had been conducted using two distinct aspect ratios and various infill-to-frame connections. To explain the behavior of the specimens tested in terms of stiffness, ultimate strength, and expected mode of failure, design provisions for infilled frames provided in codes were used.

Chiou and Hwang (2015) presented the findings of four specimens that were subjected to cyclic loading testing on reinforced concrete frames with brick infill walls. The RC columns and beams were cast in place after the pre-laid brick infill. The mortar compressive strength and the height-to-length ratio of the brick infill wall were core experimental parameters. The in-plane lateral strength of a brick infill wall was correlated with the fracture path, according to test data. Brick infill walls with significant height-to-length ratios typically fractured along bed joints, cross joints, and vertical brick splitting paths. Consequently, this kind of brick infill wall had more lateral strength. In contrast, brick infill walls with short height-to-length ratios only had joints as the fracture path, which resulted in decreased lateral strength. The lateral strength of a brick infill wall was enhanced with stronger mortar.

Huang et al. (2016) experimentally investigated the seismic performance of a class of reinforced concrete (RC) frames with weak infill panels and the complex interaction between the bounding frame and infill panel at various loading periods. Under reversed cyclic stress, large-scale infilled RC frame specimens that were made to replicate those in as-built RC frame structures developed in compliance with the Chinese seismic code (GB50011-2001) were evaluated. There were three different kinds of masonry infill used: hollow concrete blocks (HCB), aerated concrete blocks, and solid clay bricks (SCB) (ACB). According to the test results, infilled frame specimens' bounding frames failed using the same mechanism as bare frames. These infilled frames outperformed the bare frame in terms of strength and energy dissipation during earthquakes.

Zhang et al. (2017) proposed and tested a novel low seismic damage detailing technique that employed steel wire connections in mortar layers fastened to columns to isolate the infill panel from surrounding columns with finite width vertical gaps during the infill panel

building project. Six one-third scale, single-story, single-bay RC frames with various infill configurations and variable connection details were meticulously created and tested on a shake table. As input signals, three real earthquake records were chosen, scaled to increasing severity levels, and employed. Dynamic properties, hysteretic behavior, failure mechanisms, out-of-plane vulnerabilities, the impact of various gap filling materials, and load transfer methods were all thoroughly investigated. The experimental findings showed that the proposed minimal seismic damage detailing idea greatly reduced the undesired interaction between infill panels and the bounding frame. In general, infilled RC frames can be significantly enhanced in terms of structural stability, integrity, and deflection.

Preti and Bolis (2017) described the setup and testing of an inventive construction method for masonry infill. This methodology can offer a flexible and predictable in-plane reaction to the infill inside the frame, as well as a stable and reliable out-of-plane response. Because the masonry's in-plane stiffness has been drastically reduced, the design technique aims to reduce the infill reaction inside the structural frame. Vertical planks (or analogous beams) divide the infill into sub-panels that can move and rock reasonably freely. The planar stability is supplied by the planks attached to the beams. Construction specifics are given and the solution has been tested for use in both new and old infills. Additionally, a comparison of the performance of two infills—one continuous and the other with horizontal subpanels—that were previously evaluated under the same circumstances is provided. The infill-frame interaction and the post-earthquake masonry damage are almost minimal due to the observed infill decline.

Climent et al. (2018) experimentally investigated the seismic behavior of reinforced concrete (RC) frames that have been rebuilt with masonry infill walls after being damaged by earthquakes. In order to achieve this, a 2/5 scale one-bay, a one-story RC frame structure that was solely designed for gravity loads (without taking into account seismic design implications) was constructed in a lab. After that, the RC frame structure underwent four uniaxial seismic simulations after being retrofitted with two masonry infill walls that were facing the direction of motion. Without showing any signs of massive

failure, the structure with infills was subjected to drift ratios of up to around 5% and was able to continue dissipating energy after the walls reached their maximum strength. Given how brittle masonry is, the highest drift achieved was unexpected. The test's findings reveal a wide range of options for infill walls as seismic retrofit solutions.

Dautaj et al. (2018) investigated the behavior of masonry-infilled reinforced concrete (RC) frames with diverse lateral strengths. Eight RC frame specimens with a single bay and a single story were examined at a 2/3 scale. One was filled with solid clay bricks, one had no infill, and six were filled with hollow clay block masonry units and combined with RC frameworks of varying strengths (bare frame). The test findings demonstrated that the failure mechanism of the RC frames filled with masonry was affected by the type of masonry unit. Further analysis of the results revealed that shear failure of the masonry infill, failure of the beam-column connection, and creation of bending hinges were the primary failure mechanisms of the masonry-filled RC frames filled with hollow clay blocks. In contrast, shear failure of the column and the masonry infill was the primary form of failure for RC frames with masonry infills made of solid clay bricks.

Kareem and Guneyisi (2018) employed the equivalent diagonal strut model. This strut's corresponding width serves as its fundamental characteristic. In the initial phase of the investigation, a number of equations for calculating the width of the compressed diagonal strut that was previously published in the literature were compared. Next, the sensitive analysis of 2-, 4-, 6-, and 8-storey RC bare frames and those with infill walls were conducted. Infill wall frame configurations for four different wall types, including fully infilled, fully infilled-except for the first story, interior bay infilled, and interior bay infilled-except for the first story were used. In all infilled frames, wall panels were simulated using single-strut and three-strut models. In order to assess the impact of infill walls on the overall performance of the case study frame buildings, a total of 36 distinct RC frame models were examined using the nonlinear pushover analysis. The examination of the data revealed that the performance of structures was significantly influenced by the placement of the infill panels relative to the elevation of the frame.

Li et al. (2019) investigated the cumulative collapse behavior of RC infilled frames experimentally and statistically under quasi-static loading utilizing macro (strut) and micro (finite-element) models to predict the damage distribution within infill walls. A three-strut model was suggested to mimic the behavioral pattern of infill walls based on the finding that corner portions of infill walls played a significant role even after the diagonal zone of infill walls had cracked. In order to test the precision of the proposed method, experimental data were compared with the simulated responses of detailed finite-element models and simplified strut models. And the modified three-strut model is compared to other widely utilized strut models. The comparison demonstrated that the proposed three-strut model accurately predicted the maximum resistance force.

Alwashali et al. (2019) examined three 1/2-scale single-story reinforced concrete frames with masonry infill that were subjected to static cyclic lateral loads for their in-plane seismic capability. The strength of the encircling reinforced concrete (RC) columns, the strength of the RC beams, and the mortar strength of the masonry infill were the three key factors assessed. The infill shear strength significantly increased with the enclosing frame strength, as per experimental observations. The onset stiffness was not considerably impacted by the tested characteristics. The specimen, which was a masonry panel constructed with weak mortar, had considerably greater ductility and relatively less damage to the surrounding frame and masonry infill panel.

Soulis (2019) stated that the influence of the peripheral mortar joint, which created the contact boundary between the masonry infill and the surrounding frame, was generally disregarded. A thorough experimental and numerical analysis was done to show the importance of such a contact boundary.

Wararuksajja (2020) studied the interaction between infill walls and frames. They assessed two full-scale intermediate RC moment-resisting frame specimens with infill concrete block walls. To evaluate the reaction, particularly with regard to the interactions between the infill and the frame, finite element analysis was used. A design technique to eliminate local failure in the surrounding frame was suggested in light of the findings. The

suggested approach was based on a local plastic mechanism analysis of the column that takes into account the variation in column shear capacity and demand at various response states as the frame deforms. The bearing force from the infill wall's magnitude and direction determine the shear demand. Depending on how the infill wall was constraining the column, it is classified as either a captive or slender column, which had an impact on the shear capacity of the column. The suggested strategy can be quickly implemented without significantly altering accepted design standards and practices.

2.8 Codes

The purpose of building codes is to protect structures from catastrophic structural failure and the general public from death and injury. These parameters are based on prior seismic experience and expert opinion. Due to variances in earthquake magnitude, geological formations, styles of building, and other considerations, the seismic design philosophies of engineers from different countries varied in various respects.

Only a few codes explicitly propose segregating the masonry infills from the RC frames such that the stiffness of the infills has no influence on the stiffness of the total system (NZS-3101 1995, SNIP-II-7-81 1996). This deduction is beneficial in some ways because the negative effect of infill is also deducted simultaneously.

A different set of national codes favors utilizing the high initial lateral stiffness, affordability, and simplicity of construction of masonry infill walls. The favorable advantages of masonry infill must be correctly included in the study and design process, and the negative effects must be minimized, according to these rules. Eurocode 8 (2004) posits addressing infills in models when their contribution has the potential to significantly impact lateral stiffness and strength. In order to account for potential planar irregularities, it is recommended to include infill walls in models that conduct a sensitivity analysis on their position and attributes. If more precise models are not employed, Eurocode 8 advises that amplification of seismic activity should be taken into consideration by the magnification factor η (This is in reference to a potential non-uniform distribution of infills over the structural height):

$$\eta = 1 + \frac{\Delta W_{Rw}}{\Delta W_{Sd}} \quad (2.1)$$

where, ΔW_{Rw} is the strength reduction of the current story with respect to the upper infilled one while ΔW_{Sd} is the sum of the seismic shear forces acting at the top of considered story.

Several national standards indicate that basic and regular structures perform well during earthquakes, and the unsymmetrical placement of masonry infill walls might induce irregularities. These codes allow static analysis for short buildings in low-seismic areas. For other buildings, dynamic assessments are proposed, in which all mass- and stiffness-adding components should be modeled. Most codes restrict the use of seismic design force generated from dynamic analysis to a minimum value based on an empirical estimate of the natural period. This constraint inhibits building design for unnecessarily low forces resulting from dynamic analysis uncertainty.

Italian technical code (DM (Ministerial Decree), 2008) explained the soft story effects. It suggested enhancing forces in possibly soft stories by a constant term of 1.4 augmentation. The code does not contain any modeling criteria for more complicated studies.

Costa Rican Code (1986) stipulates that all structural-resisting systems must be continuous from the foundation to the top of structures and that a story's stiffness cannot be less than fifty percent of that of the story below it.

Some national standards punish beams and/or columns of irregular stories because they must be designed for higher seismic stresses to make up for lack of infills. The Indian seismic code (IS-1893 2002) enables components of the soft story to be designed for 2.5 times the seismic story shears and moments, without evaluating masonry infills in any story. The empirical method specifies a factor of 2.5 for all soft-story buildings, regardless of irregularity. The next option is to construct homogeneous RC shear walls, intended for 1.5 times the design story shear force in both orientations of the building.

A key factor in the building code formulae for calculating the design earthquake force using any analogous static force approach is the natural period of vibration. Buildings' natural lifespans are influenced by their mass and lateral stiffness. Buildings' mass and stiffness both rise when non-isolated masonry infill walls are present, but the stiffness effect is more substantial. As a result, a masonry infilled reinforced concrete frame (MIRCF) structure's natural period is often shorter than that of the corresponding bare frame. As a result, brick infilled frames typically have seismic design forces that are higher than those of bare frames. Only a few national regulations specifically give empirical formulae for MIRCF frames, despite the fact that all national codes explicitly specify empirical formulae for the fundamental natural period computations of bare RC frames. Some of the codes—IS-1893 (2002); NBC-105 (1995); NSR-98 (1998); Egyptian code (1988); Venezuelan code (1988); Algerian code (1988) recommend utilizing an empirical equation:

$$T_a = \frac{0.09h}{\sqrt{d}} \quad (2.2)$$

Where T_a is the natural period of MIRCF, h is the height of the building (meter) and d is the base dimension of the building (meter) at the plinth level along the considered direction of the lateral force.

However, the French code (AFPS-90 1990) suggests Eqn. 2.2 as the most unacceptable and the following equation that specified for masonry buildings:

$$T = 0.06 \frac{h}{\sqrt{d}} \sqrt{\frac{h}{2d+h}} \quad (2.3)$$

According to FEMA 356 (2000), the elastic in-plane stiffness of a solid unreinforced masonry infill panel prior to cracking shall be represented with an equivalent diagonal compression strut of width, a , given by Eqn. 2.4. The equivalent strut shall have the same thickness and modulus of elasticity as the infill panel it represents.

$$a = 0.175(\lambda_1 h_{col})^{-0.4} r_{inf} \quad (2.4)$$

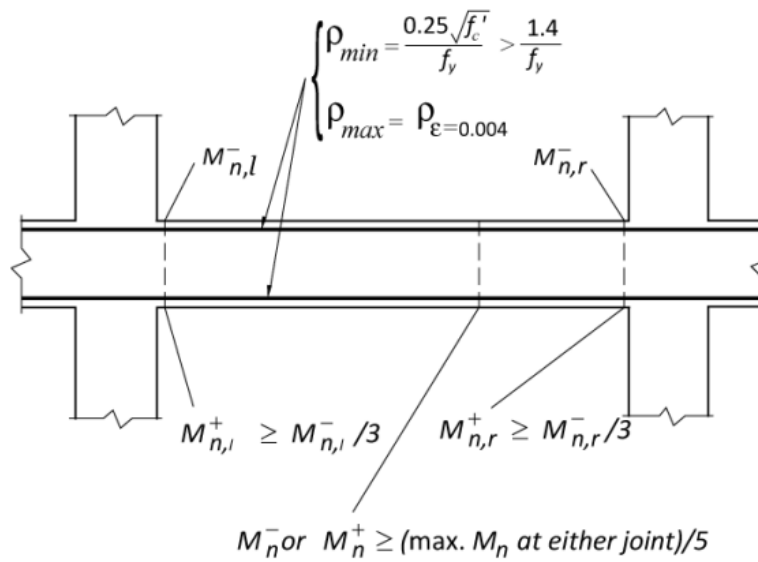
Where, λ_1 is represented by Eqn. 2.5:

$$\lambda_1 = \left[\frac{E_{me} t_{inf} \sin 2\theta}{4E_{fe} I_{col} h_{inf}} \right]^{\frac{1}{4}} \quad (2.5)$$

Here, h_{col} is column height between centerlines of beams (inch), h_{inf} is the height of the infill panel (inch), E_{fe} is expected modulus of elasticity of frame material (ksi), E_{me} is expected modulus of elasticity of infill material (ksi), I_{col} is moment of inertia of column, in^4 , L_{inf} is length of infill panel (inch), r_{inf} is diagonal length of infill panel (inch), t_{inf} is thickness of infill panel and equivalent strut (inch), θ is angle whose tangent is the infill height-to length aspect ratio (radians), λ_1 is Coefficient used to determine equivalent width of infill strut.

BNBC (2020) published reinforcement provisions for the intermediate moment frame (IMF). The following provisions have been provided for beam (IMF):

- I. The positive moment strength at the face of the joint shall not be less than one-third the negative moment strength provided at that face (Figure 2.30). Neither the negative nor positive moment strength at any section along the length of the member shall be less than one-fifth of the maximum moment strength provided at the face of either joint.
- II. At both ends of the member, stirrups shall be provided over lengths equal to twice the member depth measured from the face of the supporting member toward mid-span (Figure 2.31). The first stirrup shall be located not more than 50 mm from the face of the supporting member. Maximum stirrup spacing shall not exceed (a) $d/4$ (b) 8 times the diameter of the smallest longitudinal bar enclosed, (c) 24 times the diameter of the stirrup bar, and (d) 300 mm.
- III. Stirrups shall be placed at not more than $d/4$ throughout the length of the member.



Note: Transverse reinforcement not shown for clarity

Figure 2.30: Flexural requirements for beams (IMF) (BNBC, 2020)

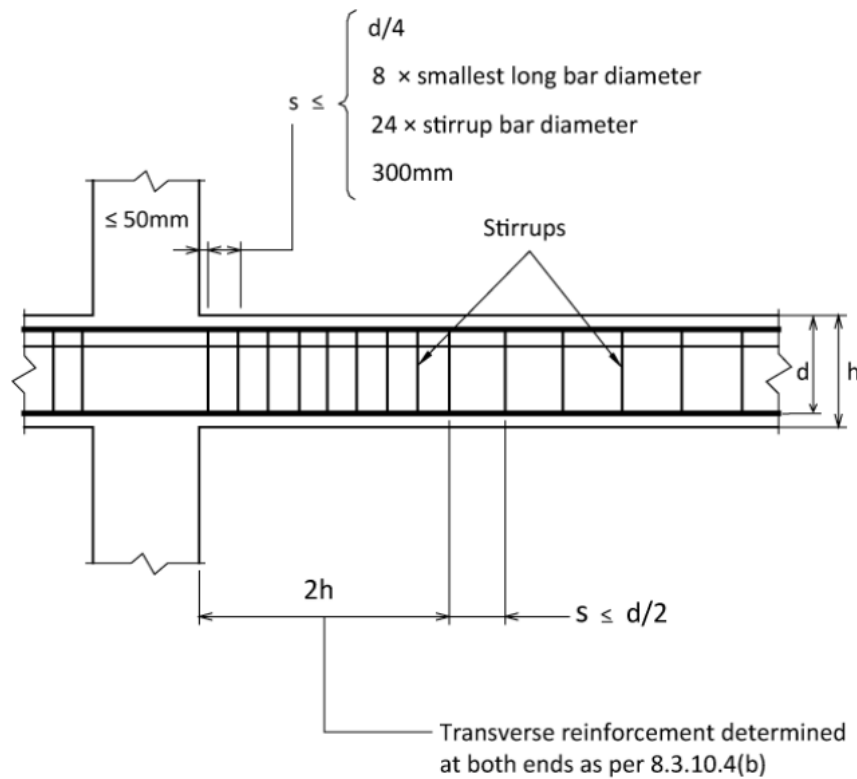


Figure 2.31: Transverse reinforcement requirements for beams (IMF) (BNBC, 2020)

The following provisions have been provided for beam (IMF):

- I. Maximum tie spacing shall not exceed s_0 over a length l_0 measured from the joint face. The spacing s_0 shall not exceed (i) 8 times the diameter of the smallest longitudinal bar enclosed, (ii) 24 times the diameter of the tie bar, (iii) one-half of the smallest cross-sectional dimension of the frame member, and (iv) 300 mm. The length l_0 shall not be less than (i) one-sixth of the clear span of the member, (ii) maximum cross sectional dimension of the member, and (iii) 450 mm (Figure 2.32)
- II. The first tie shall be located not more than $s_0/2$ from the joint face.
- III. Joint reinforcement shall conform to Sec 6.4.9.
- IV. Tie spacing shall not exceed $2s_0$ throughout the length of the member.

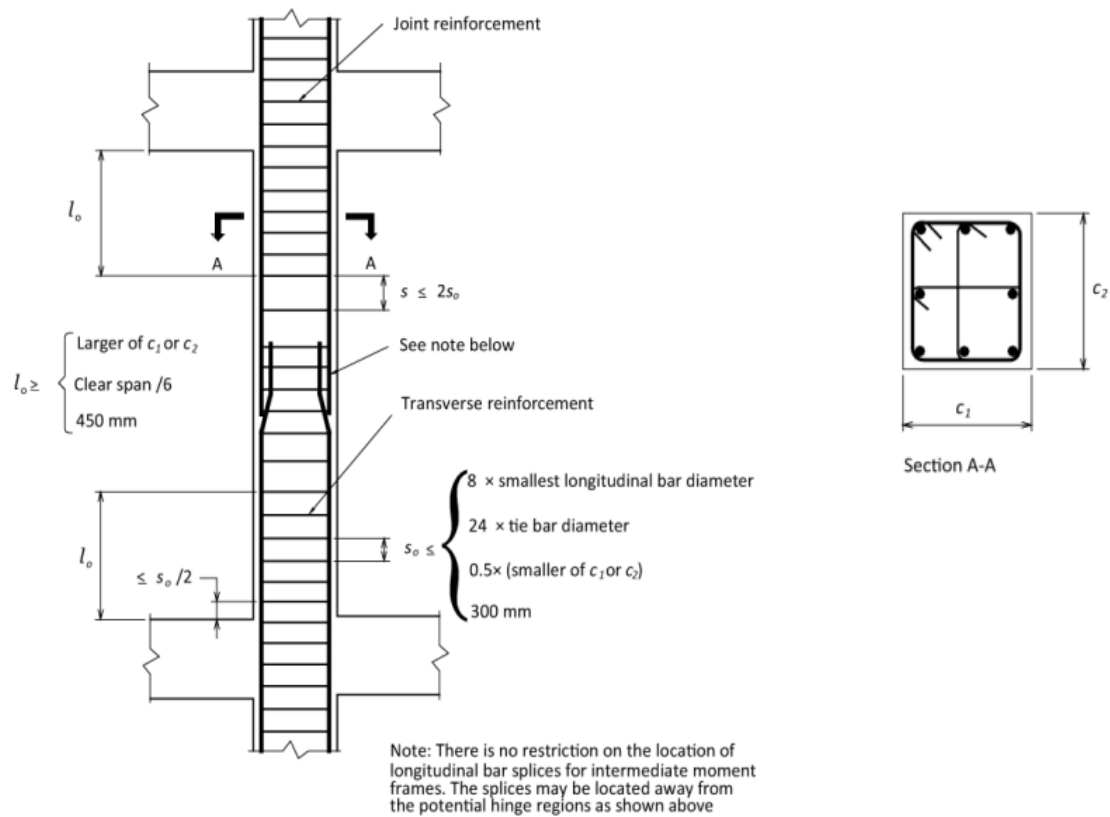


Figure 2.32: Transverse reinforcement requirements for columns (IMF) (BNBC, 2020).

Chapter 3

EXPERIMENTAL SCHEME

3.1 Introduction

The purpose of this experiment is to determine the effect of lintel and perforated clay brick on MIRCF structures under cyclic loading. In this chapter, the details of material properties, specimens, preparation of specimens, experimental setup, and test procedure will be presented and discussed.

3.2 Material Properties

Cement, fine aggregate, coarse aggregate, reinforcement, clay bricks, and water were used as basic materials in this experiment. Later, by combining basic materials, mortar, and concrete were cast.

3.2.1 Cement

Ordinary portland cement (CEM I) was used as binding material (Conforming to BDS EN 197-1, 2003).

3.2.2 Fine aggregate

Fine aggregate (Sand) was clean, strong, and free of organic impurities and deleterious substances (conforming to ASTM C33, 2020). It was collected from a credible source. Two types of fine aggregates were used in this study such as sylhet sand (FM: 2.7) and local sand (FM: 1.5).

3.2.3 Coarse aggregate

Coarse aggregate was clean, strong, and free of organic impurities and deleterious substances (conforming to ASTM C33, 2020). 12.5 mm and downgraded coarse aggregates were used.

3.2.4 Reinforcement

Two types of reinforcement were used in this investigation such as 8 mm diameter B420DWR rebars and 12 mm diameter B420DWR rebars. The results of tension tests of these rebars are shown in Table 3.1. Details of the results of reinforcement testing are illustrated in Appendix-A.

Table 3.1: Results of rebar testing

Bar Dia (mm)	Average Yield Strength (MPa)	Average Ultimate Strength (MPa)
8	472	686
12	465	637

3.2.5 Clay brick

Solid clay brick and perforated clay brick were used in this experiment.

A full-scale solid clay brick (240 mm × 115 mm × 67 mm) was cut along the dashed lines as shown in Figure 3.1 to convert it to eight half-scale solid clay bricks. Each half-scale solid clay brick was 120 mm × 57.5 mm × 33.5 mm in dimension.

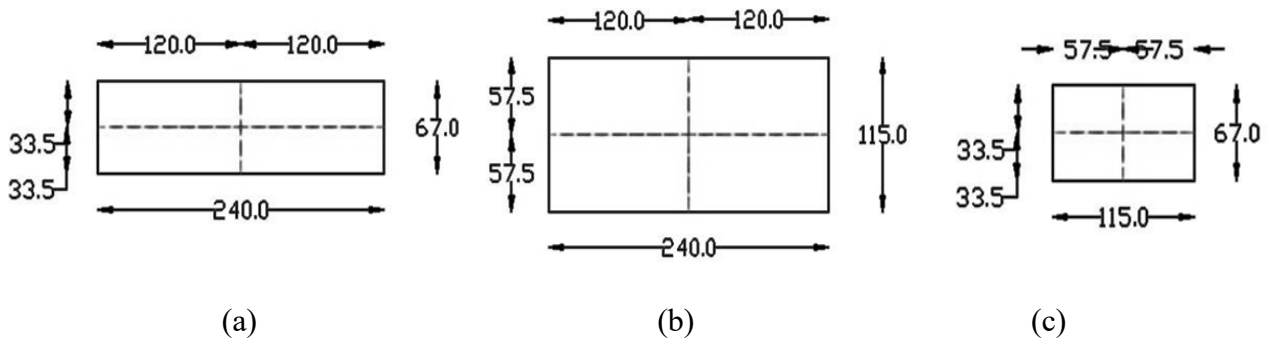


Figure 3.1: (a) Front / back elevation, (b) plan view, (c) side elevation of a full-scale solid clay brick (Every unit is in mm).

A full-scale perforated clay brick contained 10 holes (each hole was 23 mm in diameter) in it. It (240 mm × 115 mm × 67 mm) was cut along the dashed lines as illustrated in Figure 3.2 to convert it to eight half-scale perforated clay bricks. The middle hatched portion was deducted from the usage. Each half-scale perforated clay brick contained 2 holes (each hole was 23 mm in diameter) in it and was 104 mm × 57.5 mm × 33.5 mm in dimension.

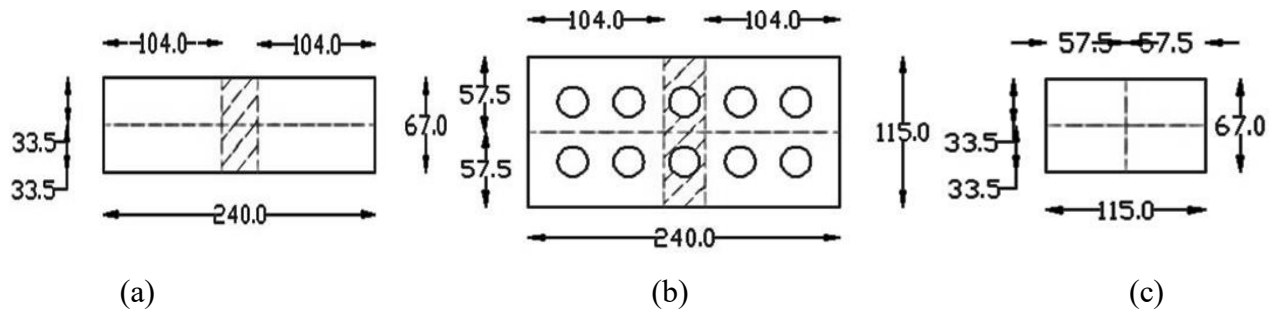


Figure 3.2: (a) Front / back elevation, (b) plan view, (c) side elevation of a full scale perforated clay brick (Every unit is in mm).

The results of compressive strength tests of bricks are shown in Table 3.2 (conforming to ASTM C67, 2020). Details of the results of compressive strength tests of bricks are illustrated in Appendix-B.

Table 3.2: Compressive strength of brick

Brick Type	Average Compressive Strength (MPa)
Solid	40.39
Perforated	26.80

The results of absorption capacity tests of bricks are shown in Table 3.3 (conforming to ASTM C67, 2020). Details of the results are illustrated in Appendix-C.

Table 3.3: Water absorption capacity of brick

Brick Type	Average Absorption Capacity (%)
Solid	14.67
Perforated	12.84

3.2.6 Water

Water used for specimens was fresh, clean, and free from organic matter and salt.

3.2.7 Mortar

Cement and local sand were mixed at 1:4 ratio to cast mortar (M2 grade related to BNBC, 2020). The water/cement ratio was kept as 0.45 in this case. The compressive strengths of

the mortar cube on different days are presented in Figure 3.3. Details of the test results (conforming to ASTM C109, 2020) of reinforcement are illustrated in Appendix-D.

3.2.8 Concrete

Cement, sylhet sand and Coarse aggregate were mixed at 1:1.5:3 ratio to cast concrete. The water/cement ratio was kept as 0.45 in this case. The compressive strengths of concrete cylinder on different days are presented in Figure 3.4. Details of the test results (conforming to ASTM C39, 2020) of reinforcement are illustrated in Appendix-E.

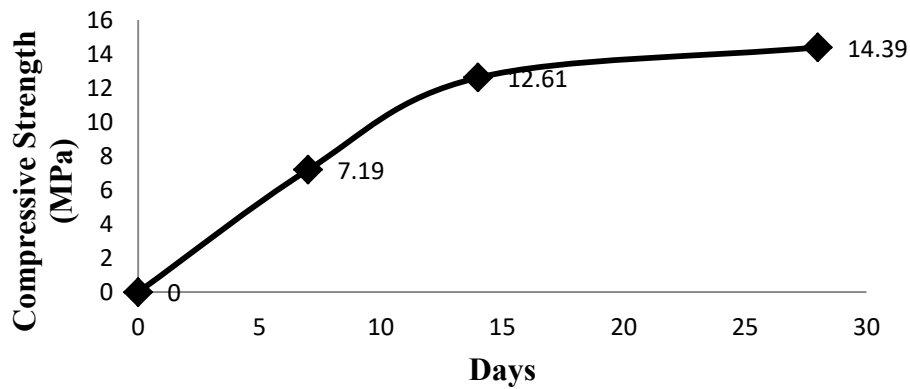


Figure 3.3: Compressive strength of mortar cube

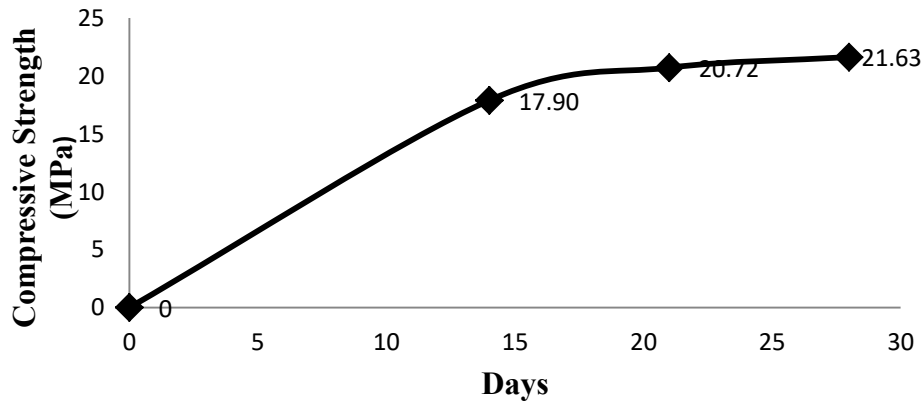


Figure 3.4: Compressive strength of concrete cylinder

3.2.9 Prism Test

The masonry prism was prepared with clay bricks and mortar. In a set of solid masonry prism and perforated masonry prism, ten solid bricks and perforated bricks were used

respectively and they were connected by mortar. The test results of compressive strength of brick prisms are shown in Table 3.4 (conforming to ASTM C1314, 2020). Details of the test results are illustrated in Appendix-F.

Table 3.4: Compressive strength of brick prism

Brick Type	Average Compressive Strength (MPa)
Solid	11.08
Perforated	4.50

3.3 Details of Specimens

In this experiment, four single bay single-story half-scale MIRCFC structures were constructed and they were tested under in-plane lateral cyclic loading. Among four specimens, the core variation was introduced in masonry materials and the existence of lintel. Two of the specimens contained lintel and the rest two were constructed without lintel. Again, solid clay bricks were used in two specimens and the masonry work of the rest two structures were built with perforated clay bricks. The detail of the frame was adopted from Zerín (2018). Each frame consisted of two columns (150 mm × 150 cross-sectional area) and one beam (150 mm × 150 cross-sectional area). In both the beam and columns, 12 mm dia and 8 mm dia bar were used as main bar and shear reinforcement respectively. The main frame was the same in all four specimens. The cross-sectional dimension of the lintel was 125 mm × 100 mm and it contained 8 mm dia reinforcement both as the main bar and stirrup. The details of the specimens are illustrated in Table 3.5. The schematic drawings of the specimens are presented in Figures 3.5 to 3.8.

Table 3.5: Details of the specimens

Specimen No.	Specimen Name	Masonry Type	Existence of Lintel
1	SB	Solid Clay Brick	No
2	SBL	Solid Clay Brick	Yes
3	PB	Perforated Clay Brick	No
4	PBL	Perforated Clay Brick	Yes

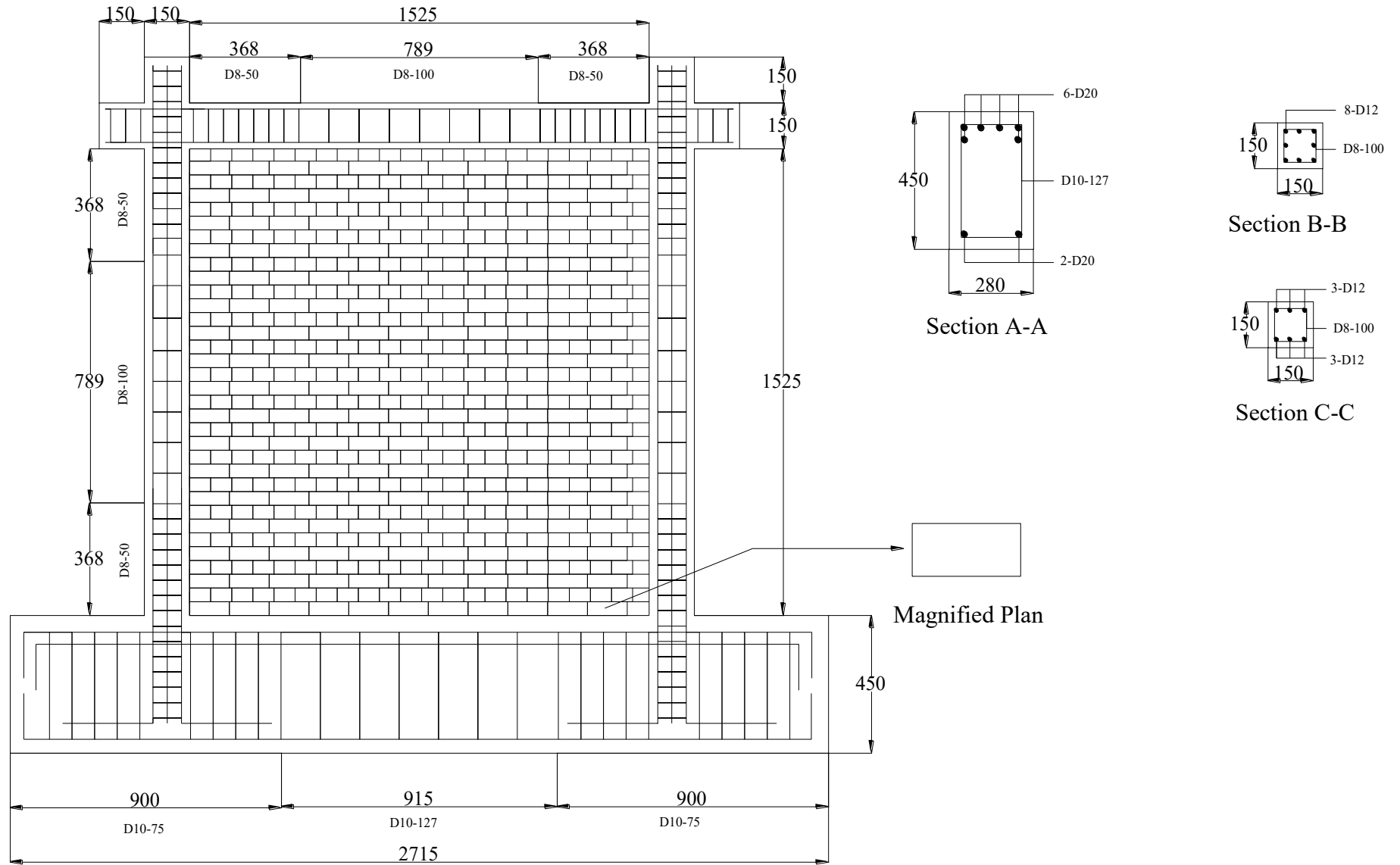


Figure 3.5: Schematic drawing of SB (Every unit is in mm) [Note: Section A-A, B-B and C-C are the midsection of base, column and beam respectively].

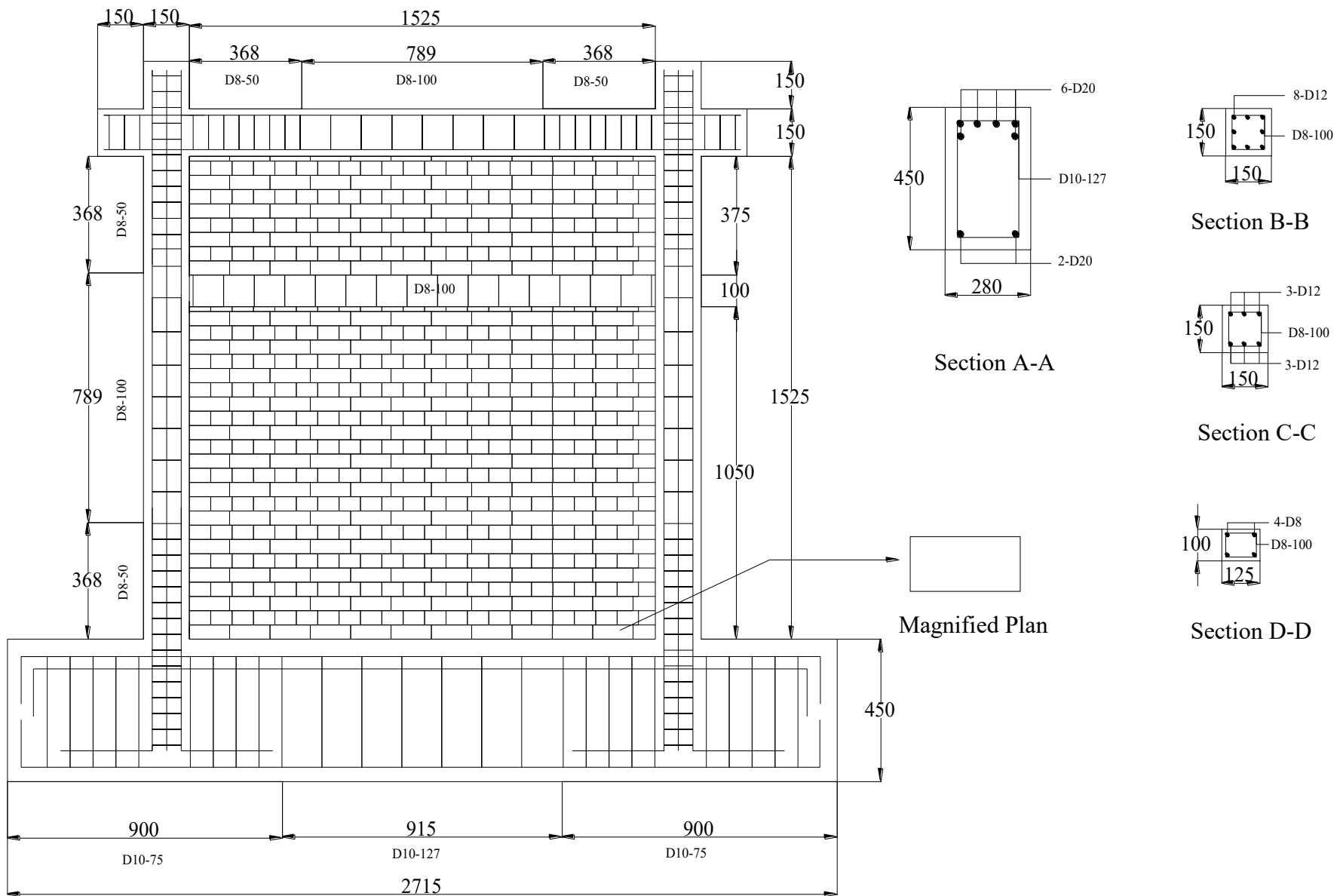


Figure 3.6: Schematic drawing of SBL (Every unit is in mm) [Note: Section A-A, B-B, C-C and D-D are the midsection of base, column, beam and lintel respectively].

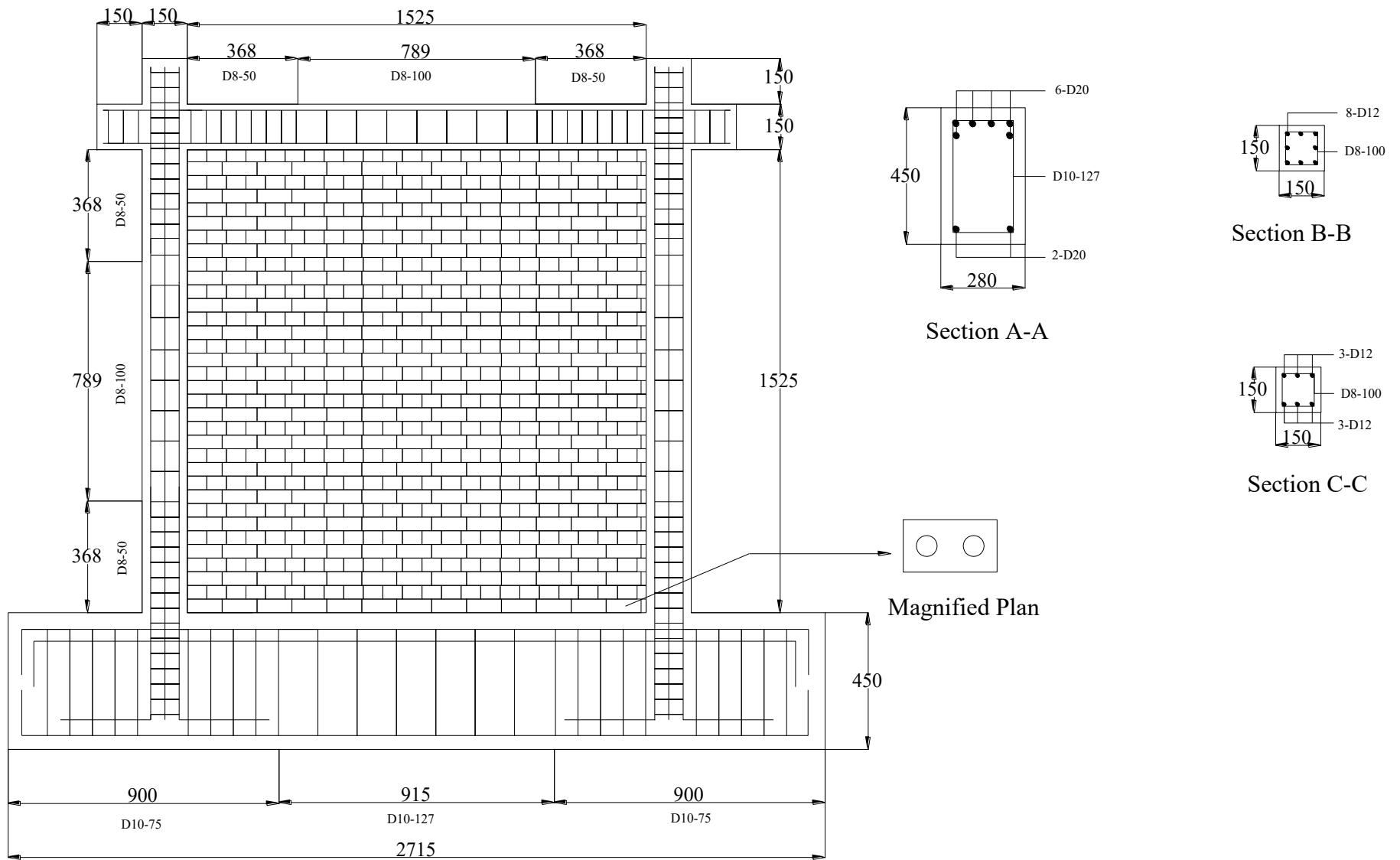


Figure 3.7: Schematic drawing of PB (Every unit is in mm) [Note: Section A-A, B-B and C-C are the midsection of base, column and beam respectively].

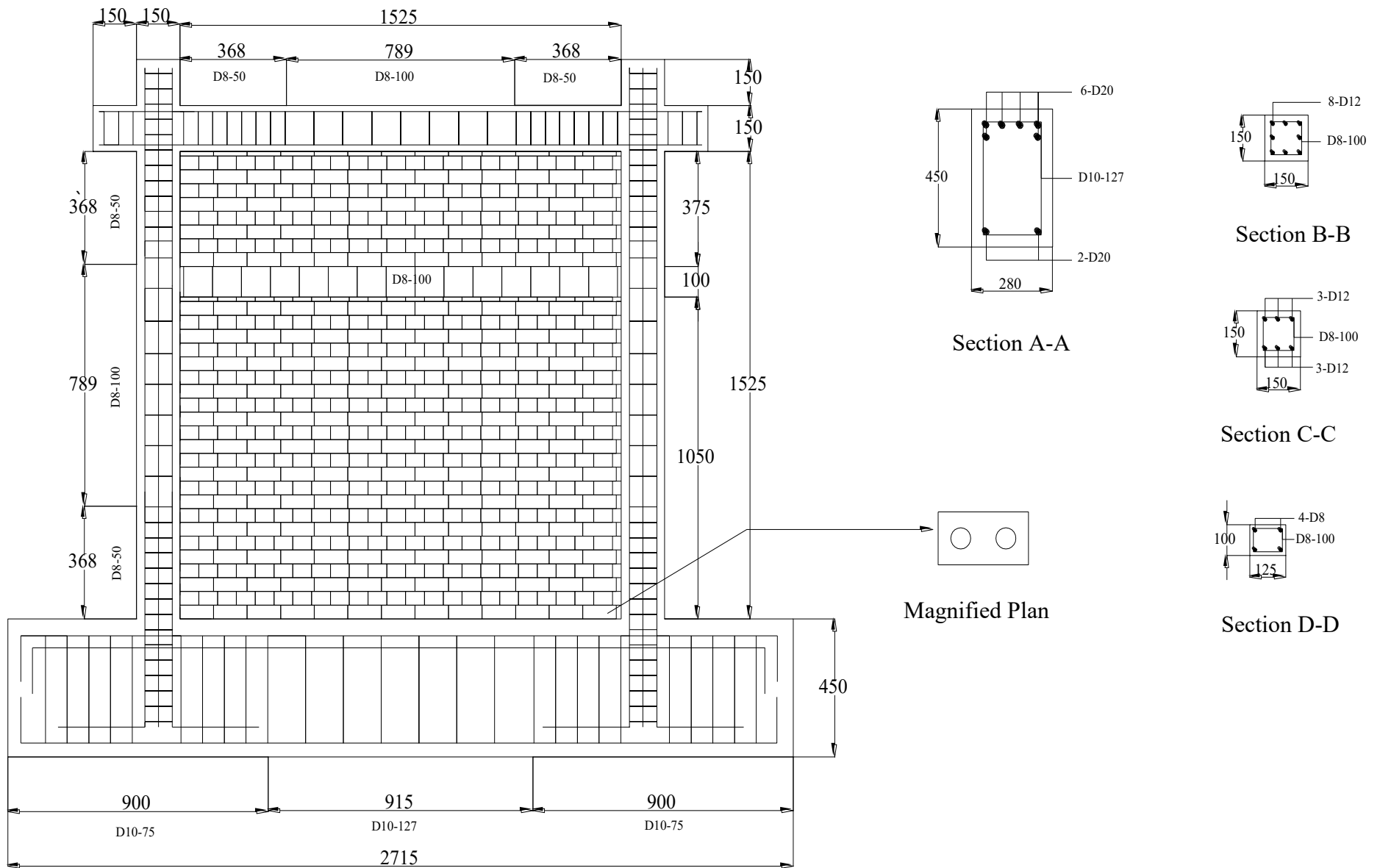


Figure 3.8: Schematic drawing of PBL (Every unit is in mm) [Note: Section A-A, B-B, C-C and D-D are the midsection of base, column, beam and lintel respectively].

3.4 Preparation of Specimens

To obtain satisfactory experimental results, it is essential to prepare the specimens with maximum precision. In this study, all four specimens were formed in meticulous care through various vital steps:

In step 1, reinforcements were bent and fastened to form a reinforced structure. Mainly, 8 mm and 12 mm dia rebars were used in the frame and lintel. Only 8 mm bars were used in lintel in all cases. However, in the beam and columns, 12 mm bar and 8 mm bar were used as the longitudinal reinforcement and stirrup respectively. Different stages of these processes are presented in Figure 3.9.

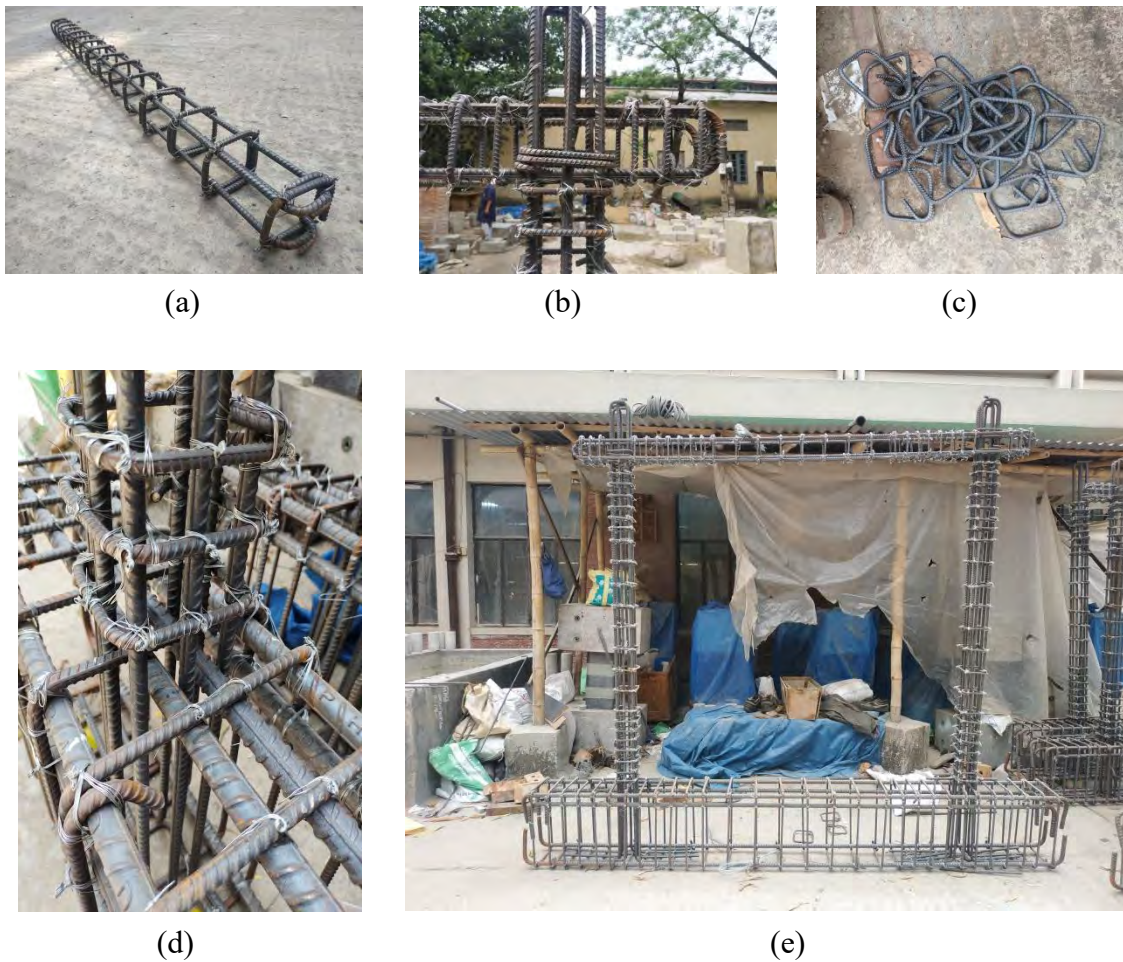


Figure 3.9: (a) lintel, (b) beam-column joint, (c) stirrups / ties, (d) column-base joint, (e) a full reinforced structure.

In step 2, a wooden formwork is constructed to facilitate the concrete casting. Afterward, the previously built reinforced structure was placed in the wooden formwork as shown in Figure 3.10.



Figure 3.10: Shuttering work.

In step 3, cement, sylhet sand, and coarse aggregate were mixed at 1:1.5:3 ratio by volume in a mixture machine to prepare concrete. The water/cement ratio was kept at 0.45. During casting slump was kept between the range of 75 mm to 100 mm. After preparing fresh concrete, they were poured carefully in the formwork and compacted cautiously with a vibrator. Different stages of these processes are presented in Figure 3.11.



Figure 3.11: Measuring slump and concrete casting.

In step 4, the concrete was led to curing for 28 days as shown in Figure 3.12 (a). Curing provided enough scope for hydration. Wet gunny bags were used for curing. After 28 days of casting, the concrete became strong enough for commencing the masonry work. The full concrete frame is shown in Figure 3.12 (b).



(a)



(b)

Figure 3.12: (a) curing, (b) a concrete frame after 28 days of casting.

In step 5, all clay bricks (both solid and perforated) were cut through predetermined lines so that a full-scale brick ($240 \text{ mm} \times 115 \text{ mm} \times 67 \text{ mm}$ in dimension each) can be converted to eight half-scale bricks (solid brick $120 \text{ mm} \times 57.5 \text{ mm} \times 33.5 \text{ mm}$ in dimension each and perforated brick $104 \text{ mm} \times 57.5 \text{ mm} \times 33.5 \text{ mm}$ in dimension each). Eight half-scale perforated clay bricks produced from a single full-scale perforated clay brick are shown in Figure 3.13.



Figure 3.13: Eight half-scale bricks produced from a single full-scale brick.

In step 6, bricks, cement, local sand, and water were prepared to commence masonry work. Cement and local sand were mixed at 1:4 ratio by volume for mortar and the water/cement

ratio was maintained at 0.45. After that, the whole $1525 \text{ mm} \times 1525 \text{ mm} \times 125 \text{ mm}$ wall of each specimen was filled up with bricks in two layers. Masonry units were joined using english bond. The lintel ($1525 \text{ mm} \times 125 \text{ mm} \times 100 \text{ mm}$) was connected both with masonry and column at two sides by mortar. After completing the masonry work, the specimens were kept 28 days more before testing. Different stages of masonry work are presented in Figure 3.14.



Figure 3.14: Masonry work.

In the last step, all the specimens were whitewashed such as in Figure 3.15 to identify the cracks properly during testing.



Figure 3.15: Whitewashing.

3.5 Experimental Setup

After completing the full construction of all four specimens, they were transported to the ‘Strength of Materials Laboratory’ of Bangladesh University of Engineering and Technology one by one and prepared for the experiment. The schematic diagram of the experimental setup is shown in Figure 3.16.

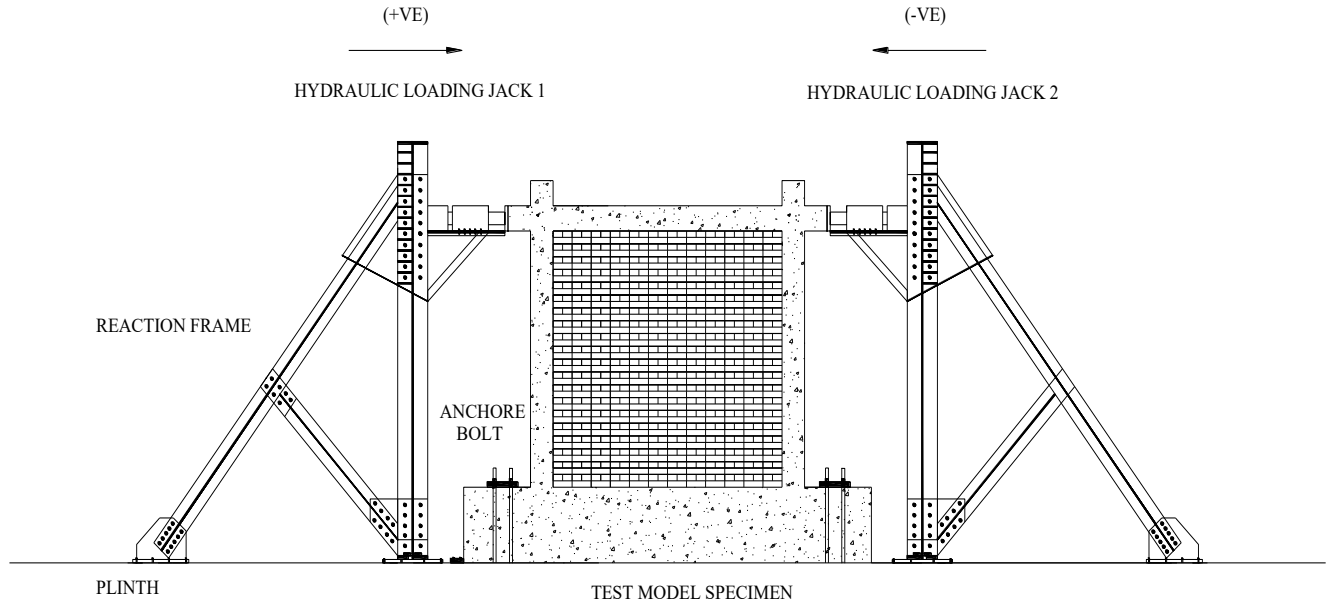


Figure 3.16: Schematic diagram of the experimental setup.

3.5.1 Firm base

A firm base was essentially needed to make the infilled frame stable on it. For this, a firm reinforced concrete base was prepared monolithically with the reinforced concrete frame. The base of each specimen was 2715 mm × 450 mm × 280 mm in dimension. In base, 20 mm rebar was used as the main bar and 10 mm rebar was used as shear reinforcement. During construction, the mixing ratio was 1:1.5:3 (cement: fine aggregate: coarse aggregate by volume). Moreover, the water-cement ratio of the base was maintained at 0.45. The base is shown in Figure 3.17.



Figure 3.17: Firm base.

3.5.2 Anchor bolt and steel plate

Four pairs of anchor bolts were used to fasten the base with the ground as shown in Figure 3.18. Each pair of anchor bolts was accompanied by a 475 mm × 75 mm × 50 mm steel plate. Each anchor bolt was 24 mm in dimension. Each side of the base was attached with two pairs of bolts. The bolts were strong enough to restrain the base from moving when the specimen is subjected to in-plane lateral loading.



Figure 3.18: Anchor bolt and steel plate.

3.5.3 Reaction frame

The test setup's structure consisted of two reaction frames, which are steel truss sections fastened to the sturdy foundation. Each reaction frame incorporated a hydraulic jack which was used to apply cyclic loading. One of the reaction frames is demonstrated in Figure 3.19 (a).

3.5.4 Tripod stands

To hold the dial gauges at predetermined places two tripod stands were used as shown in Figure 3.19 (b).



(a)



(b)

Figure 3.19: (a) Reaction frame, (b) tripod stand.

3.5.5 Dial gauges

Three dial gauges were used to measure the displacement of the specimens during the cyclic excitation. They were set on the specimens with the help of the tripod stands. One dial gauge was set at the top-left corner and the other was set at the top-right corner of the

specimens. The third dial gauge was set at the bottom right corner of the base to identify the base movement. All three dial gauges are shown in Figure 3.20.

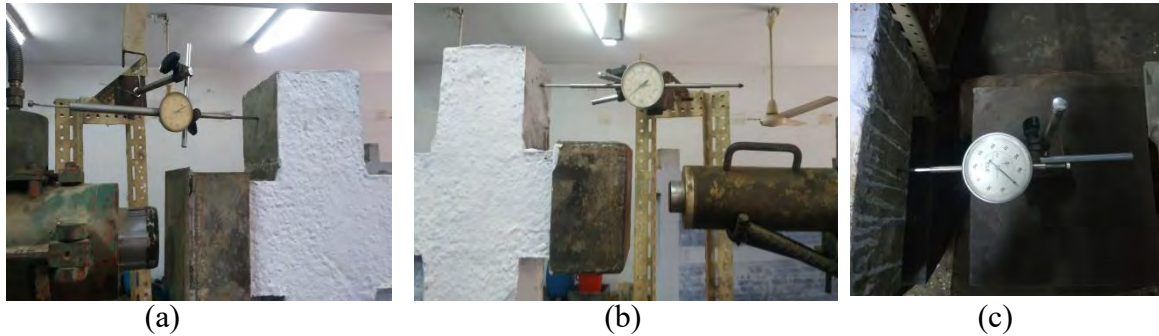


Figure 3.20: Dial gauges at (a) top-left corner at the specimen, (b) top-right corner of the specimen, (c) bottom-right corner of the base.

3.5.6 Hydraulic jack

Two Hydraulic jacks were utilized in this experiment for applying lateral load. Hydraulic jack 1 (Capacity : 50 ton) was attached to the left reaction frame and the Hydraulic jack 2 (Capacity : 30 ton) was attached to the right reaction frame. The jacks are shown in Figure 3.21. The deformation of the specimen due to the applied load by hydraulic jack 1 is assumed as positive direction. On the contrary, the deformation of the specimen due to the applied load by hydraulic jack 2 is assumed negative direction. Details of the hydraulic jacks are illustrated in Appendix-G.



Figure 3.21: (a) Hydraulic Jack 1, (b) hydraulic jack 2.

The full setup is demonstrated in Figure 3.22.

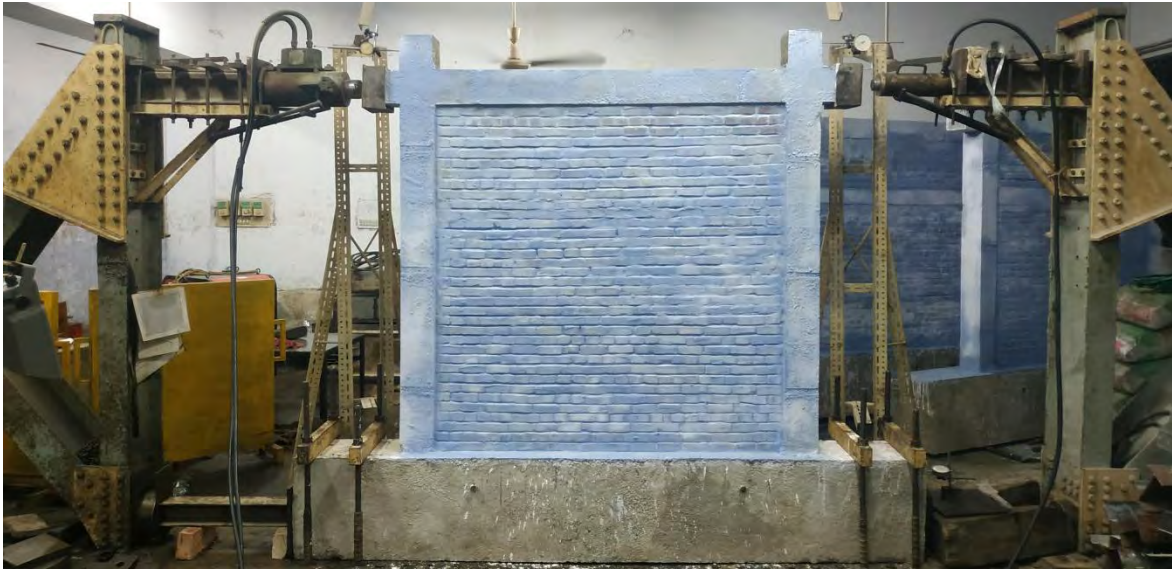


Figure 3.22: Full experimental setup.

3.6 Test Procedure

Cyclic lateral load was applied to the specimens to investigate performance of the MIRCFC structures. Each cycle contains both equal amounts of positive and negative portions. The positive portion occurred when the load was applied by the hydraulic jack 1 and the negative portion befell when the load was exerted by the hydraulic jack 2. The loading value in each cycle and the loading increment are shown in Figure 3.23.

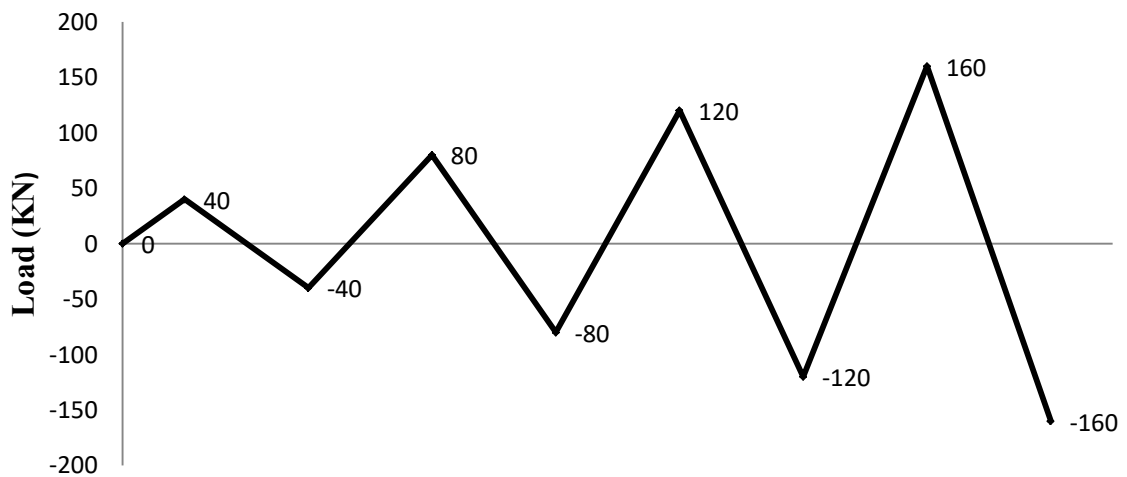


Figure 3.23: Applied loading pattern during testing.

Chapter 4

RESULTS AND DISCUSSION

4.1 Introduction

The goal of this experiment is to examine the influence of lintel and perforated clay brick under cyclic loads on MIRCF structures. In this chapter, initially, the damage and failure patterns are assessed. Later, extensive comparative studies are conducted to identify the behavior of the specimens (SB, SBL, PB, PBL). The individual effects and the combined effects of the parameters are carefully observed and carefully recorded.

4.2 Summary of The Experimental Results of The Specimens

The summary of the experimental results of all specimens (SB, SBL, PB, PBL) is provided in Table 4.1.

Table 4.1: Summary of The Experimental Results of The Specimens

Description	SB	SBL	PB	PBL
First cracking load at infill (KN)	80	80	80	80
Displacement at first infill cracking (mm)	5.17	5.29	5.7	6.14
Stiffness at first infill cracking (KN/mm)	15.47	15.12	14.04	13.03
First cracking load at frame (KN)	80	120	120	80
Displacement at first frame cracking (mm)	5.17	15.26	10	6.14
Stiffness at first frame cracking (KN/mm)	15.47	7.86	12	13.03
Ultimate load at specimen failure (KN)	150	160	130	160
Displacement at specimen failure (mm)	17.25	31.14	22.41	34.12
Stiffness at specimen failure (KN/mm)	8.70	5.14	5.80	4.69
Cumulative Energy Dissipation (KN-mm)	1549.6	2268.4	1676	8098

4.3 Damage Assessment and Failure Mode of the Specimens

The cracking pattern and the damage scenario of the specimens in individual cycles are extensively elucidated below:

4.3.1 SB (Solid Brick Infill)

The specimen SB was attached to the experimental setup and subjected to the cyclic load as described in Chapter 3. It experienced a total of three full cycles and failed in the 4th cycle. The total hysteretic graph of load vs. displacement is shown in Figure 4.1. Details of the values of loads and displacements are presented in Appendix-H.

At cycle 1, the load was applied maximum to 40 KN from each side of the specimen. No significant crack or change is identified on the specimen. Condition after the completion of cycle 1 is shown in Figure 4.2.

At cycle 2, the load was applied maximum to 80 KN from each direction of the specimen. At 80 KN (towards positive direction) load, a long horizontal crack was observed along the mortar (about 300 mm below from the bottom layer of the beam). It indicated that the mortar along that particular point was comparatively weak and there might be an alteration of mix ratio when the mortar was mixed. A mild shear crack was also identified at the beam-column (left) joint. At 40 KN (towards negative direction) load, the horizontal crack extended to the right and it stopped at the column. Consequently, a vertical crack was clearly spotted on the infill-column interface as the interface forms a continuous vertical joint. Moreover, At 80 KN (towards negative direction) load, the vertical crack enhanced to 0.05 mm and it traveled more to the down direction and formed a diagonal shear crack in the masonry wall. It ensued because the shear from the column contributed to the tensile stress of the wall. A tiny crack was also noticed at the base-column (right) joint. Status after the completion of cycle 2 is shown in Figure 4.3.

At cycle 3, the maximum load of was applied to 120 KN from each direction. At 60 KN (towards positive direction) load, the shear crack previously created in cycle 2 is further extended. The horizontal crack extended to the left in this cycle and befell a diagonal shear crack as the wall received more tension. Many microcracks were identified in mortar.

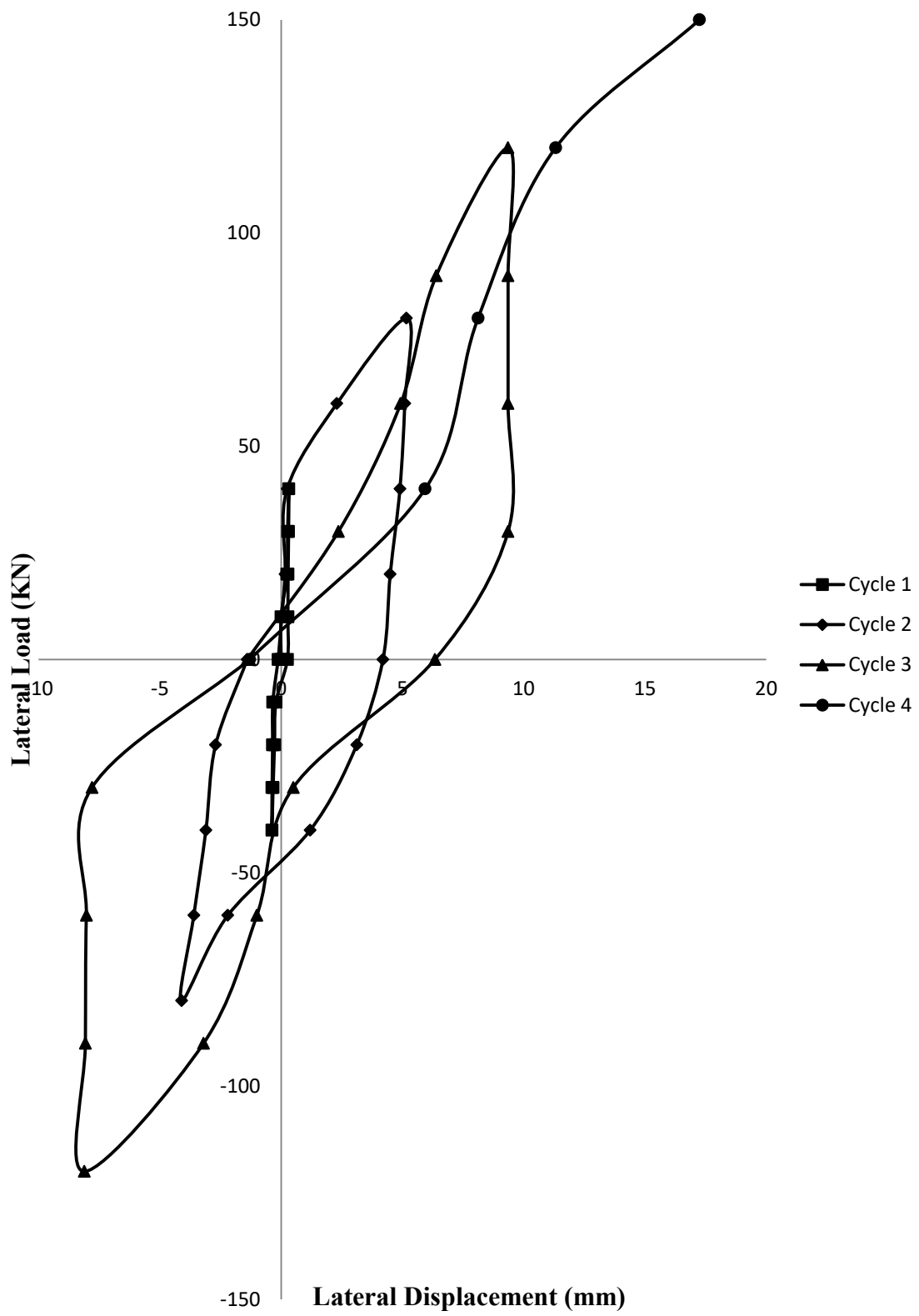


Figure 4.1: Hysteretic load-displacement curve for SB.

For the first time, a 1 mm crack in the masonry unit was noticed. At 80 KN (towards negative direction) load, some new wide cracks, some as wide as 4 mm, were spotted in bricks. It indicated that the masonry units started receiving stress beyond their compressive strength. At 120 KN (towards negative direction) load, a new vertical shear crack was produced from the previously formed horizontal crack. Furthermore, the diagonal shear crack created at the beginning of this cycle extended further and it turned into a long diagonal shear crack which covered almost the primary diagonal of the full masonry wall. It indicated that the frame transferred the maximum amount of shear it was receiving from lateral load and this shear exerted diagonal tensile stress on the wall. Additionally, a plethora of flexural cracks were recognized on both of the columns. It expressed that the infill wall intended to receive less amount of stress and it tried to transfer the stress on columns which eventually resulted in a multitude of flexural cracks in columns. Again, several cracks were noted on the beam-column (right) joints. The situation after the completion of cycle 3 is presented in Figure 4.4.

At cycle 4, the load intended to be applied was 160 KN maximum from each direction but the specimen failed at 150 KN (Positive direction). At 60 KN (towards positive direction) load, the segregated hairline cracks formed in the previous cycle connected and created a long diagonal crack. More flexural cracks were identified on both of the columns. The previously formed diagonal tensile crack extended to the top upper-left corner and reached the beam-column (left) joint. Consequently, multiple shear cracks formed in the joint. At 120 KN (towards positive direction) load, some flexural cracks were spotted on the beam. Thus it was evident that the beam received a significant amount of moment from the applied lateral load. A new diagonal shear crack was observed along the secondary diagonal of the wall. At 150 KN (towards positive direction) load, some cracks, as wide as 5 mm, were generated in the wall. Some significant damages were spotted on the base-column (left) joint. All the previously generated cracks widened in size and extended in length. Eventually, the whole specimen failed at this load. State after failure (at cycle 4) is presented in Figure 4.5.

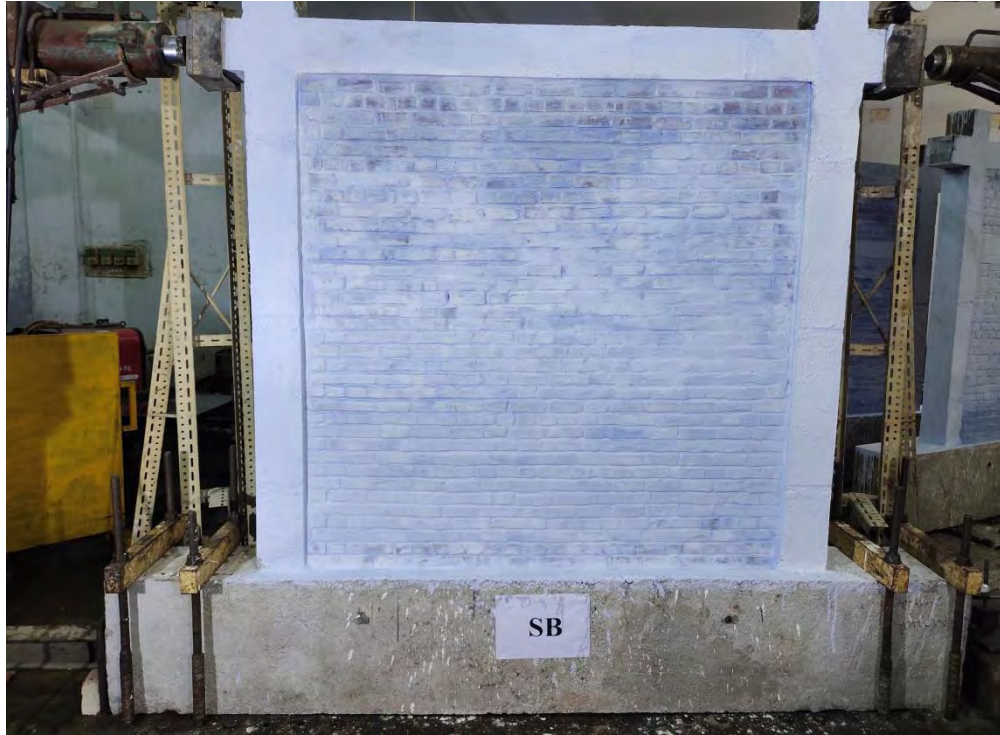


Figure 4.2: SB after the completion of cycle 1.

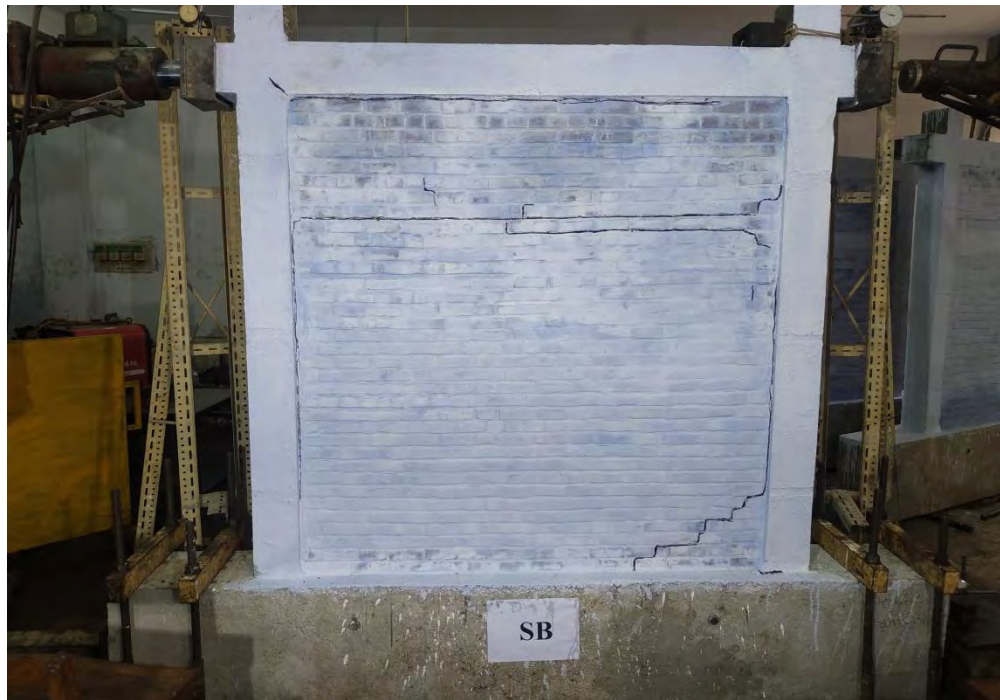


Figure 4.3: SB after the completion of cycle 2.

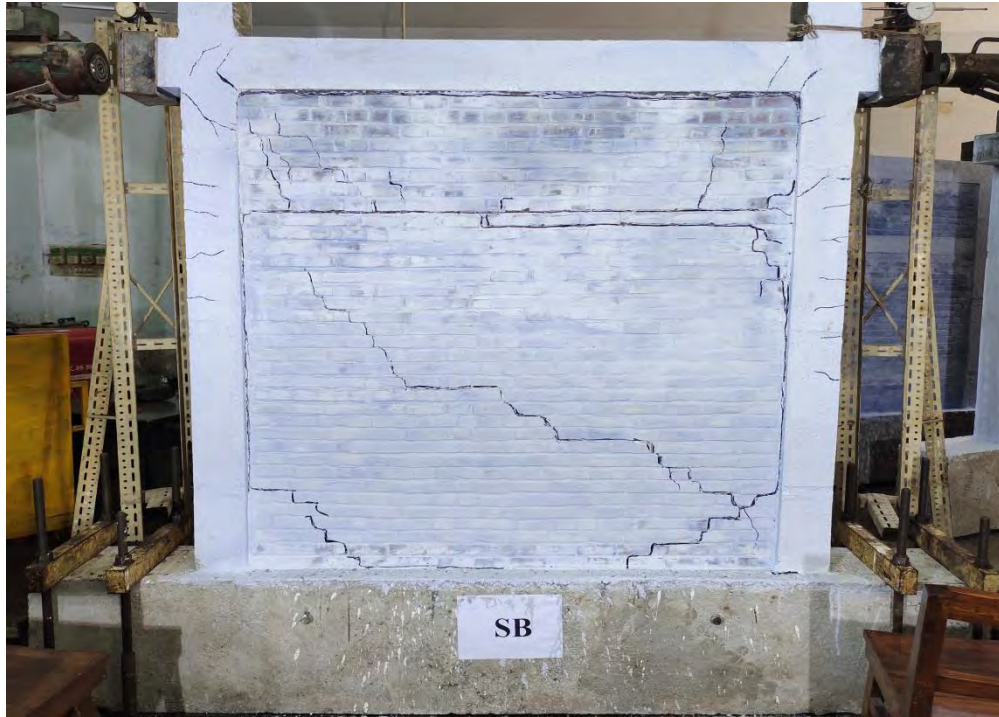


Figure 4.4: SB after the completion of cycle 3.

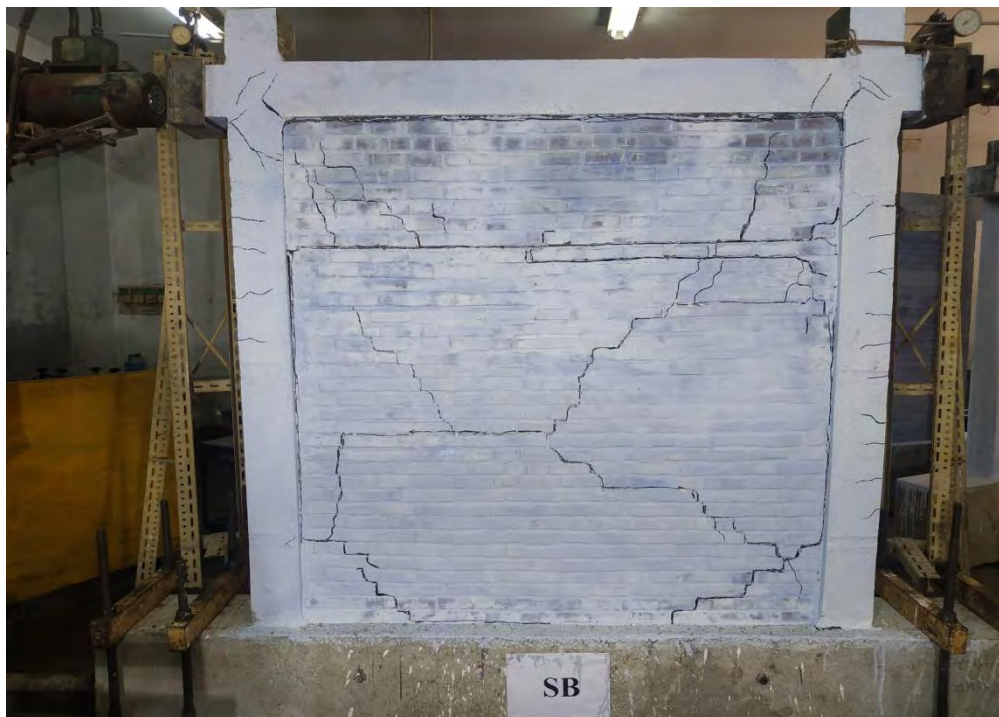


Figure 4.5: SB at complete failure (at cycle 4).

4.3.2 SBL (Solid Brick Infill with Lintel)

The specimen SBL was set in the experimental arrangement and cyclic load was subsequently applied. It experienced a total of three full cycles and failed in the 4th cycle. The total hysteretic graph of load vs. displacement is illustrated in Figure 4.6. Details of the values of loads and displacements are presented in Appendix-H.

At cycle 1, the load was exerted to a maximum of 40 KN from each direction of the specimen. No considerable crack or change is spotted on the specimen. Status after completion of the cycle 1 is shown in Figure 4.7.

At cycle 2, the load was applied to a maximum of 80 KN from each side of the specimen. At 80 KN (towards positive direction) load, the mortar joint of column (left) and wall showed distress and the masonry wall got slightly segregated from the column. This crack gradually extended downward along the mortar and suddenly changed its direction to the right. As a result, a long conspicuous horizontal crack was observed. It mainly occurred due to the weak joint of mortar between two layers of brick and the joint between column and wall. Excessive horizontal shear stress caused the cracks in the weak joints. At 80 KN (towards negative direction) load, a few mild shear cracks were visible which were generated from the previously created horizontal crack. For the first time, a tiny crack was noticed on the right portion of the lintel. The stress was distributed more to the right and it isolated the wall from the column (right). The weak mortar joint also played a major role here. Furthermore, slight damage was found on the mortar joint at the lower portion of the lintel and the masonry wall. The lintel was about to slide over the wall when the load was gradually increased. Condition after completion of the cycle 2 is shown in Figure 4.8.

At cycle 3, the load was applied to a maximum of 120 KN from each side of the specimen. At 120 KN (towards positive direction) load, no significant change was observed on the masonry wall. However, several cracks in the frame were spotted. As a portion of the wall in rectangular shape was isolated from the column of both sides and lintel, the load-carrying capacity of the wall suddenly dropped. Consequently, the frame received a considerable amount of stress which ended up having a visible shear crack at the beam-column (left) joint. At 120 KN (towards negative direction) load, some noticeable cracks

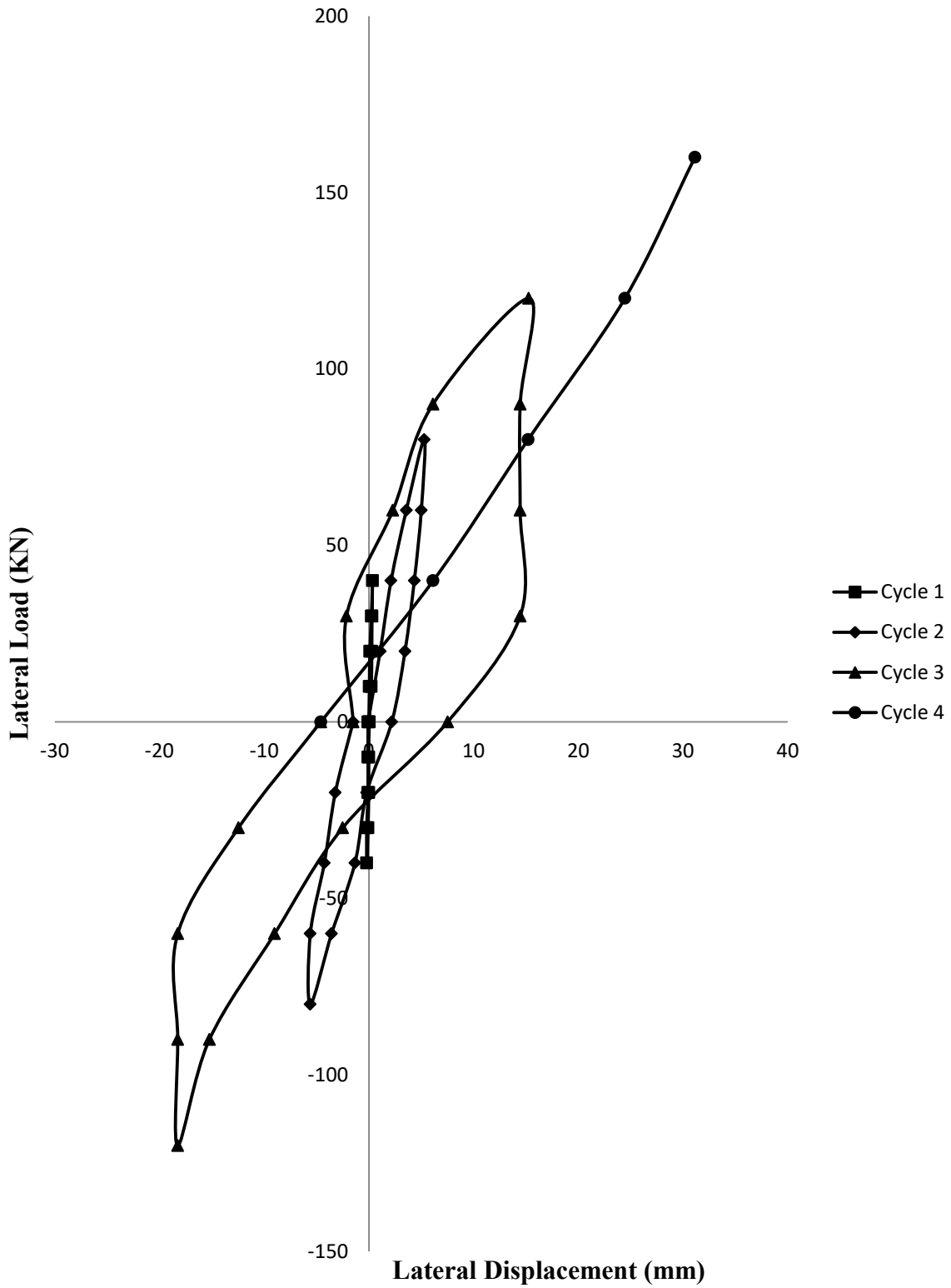


Figure 4.6: Hysteretic load-displacement curve for SBL.

were observed at the base column (right). It occurred due to excessive shear and short column effect. State of the specimen after completion of the cycle 3 is shown in Figure 4.9.

At cycle 4, a maximum of 160 KN load was supposed to be applied from each direction of the specimen. The specimen failed at the maximum load but during loading in the positive direction. At 160 KN (towards positive direction) load, a diagonal shear crack was clearly observed in the middle of the infill wall. It befall due to the diagonal tension in the wall. Not only the mortar but also a few bricks were also damaged due to excessive stress in comparison to their compressive strength. Moreover, a large number of flexural and shear cracks were identified on the left column. Some were also noticed on the right column. The bottom right corner of the wall was crushed due to excessive bearing stress. A multitude of horizontal, vertical, and inclined shear cracks was also observed on the wall situated at the upper portion of the lintel. Again, a few flexural cracks were seen on the beam due to the moment greater than it could resist. A few shear cracks were also visible on the beam-column (right) joint. Some cracks on the wall were about 30 mm wide. Moreover, the wall moved about 42 mm from the column due to the applied load and the total specimen failed at 160 KN load. The situation after failure (at cycle 4) is presented in Figure 4.10.

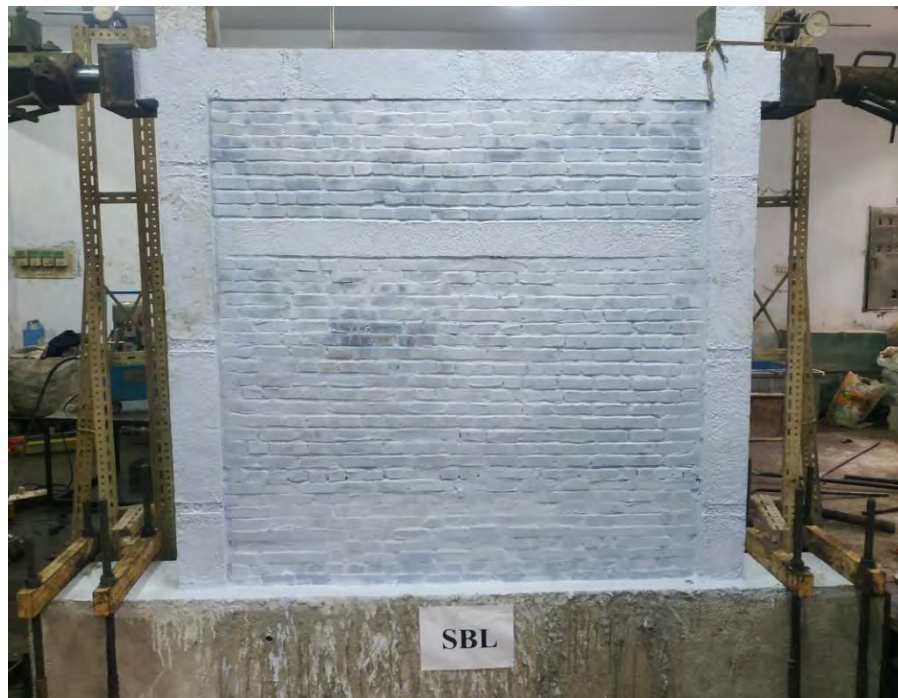


Figure 4.7: SBL after the completion of cycle 1.



Figure 4.8: SBL after the completion of cycle 2.



Figure 4.9: SBL after the completion of cycle 3.



Figure 4.10: SBL at complete failure (at cycle 4).

4.3.3 PB (Perforated Brick Infill)

The specimen PB was placed according to the experimental setup and the cyclic load was applied subsequently. It experienced a total of three full cycles and failed in the 4th cycle. The total hysteretic graph of load vs. displacement is illustrated in Figure 4.11. Details of the values of loads and displacements are presented in Appendix-H.

At cycle 1, a maximum of 40 KN load was applied from each side of the specimen. No noticeable crack or change is observed on the specimen. Condition after the completion of cycle 1 is shown in Figure 4.12.

At cycle 2, a maximum of 80 KN load was applied from each direction of the specimen. At 80 KN (towards positive direction) load, no significant changes were observed on the specimen. At 80 KN (towards negative direction) load, several mild cracks were identified on the infill wall. The wall was slightly segregated from the frame due to weak mortar strength in the wall-column joint. As a result, some cracks were spotted on those joints. State after completion of the cycle 2 is shown in Figure 4.13.

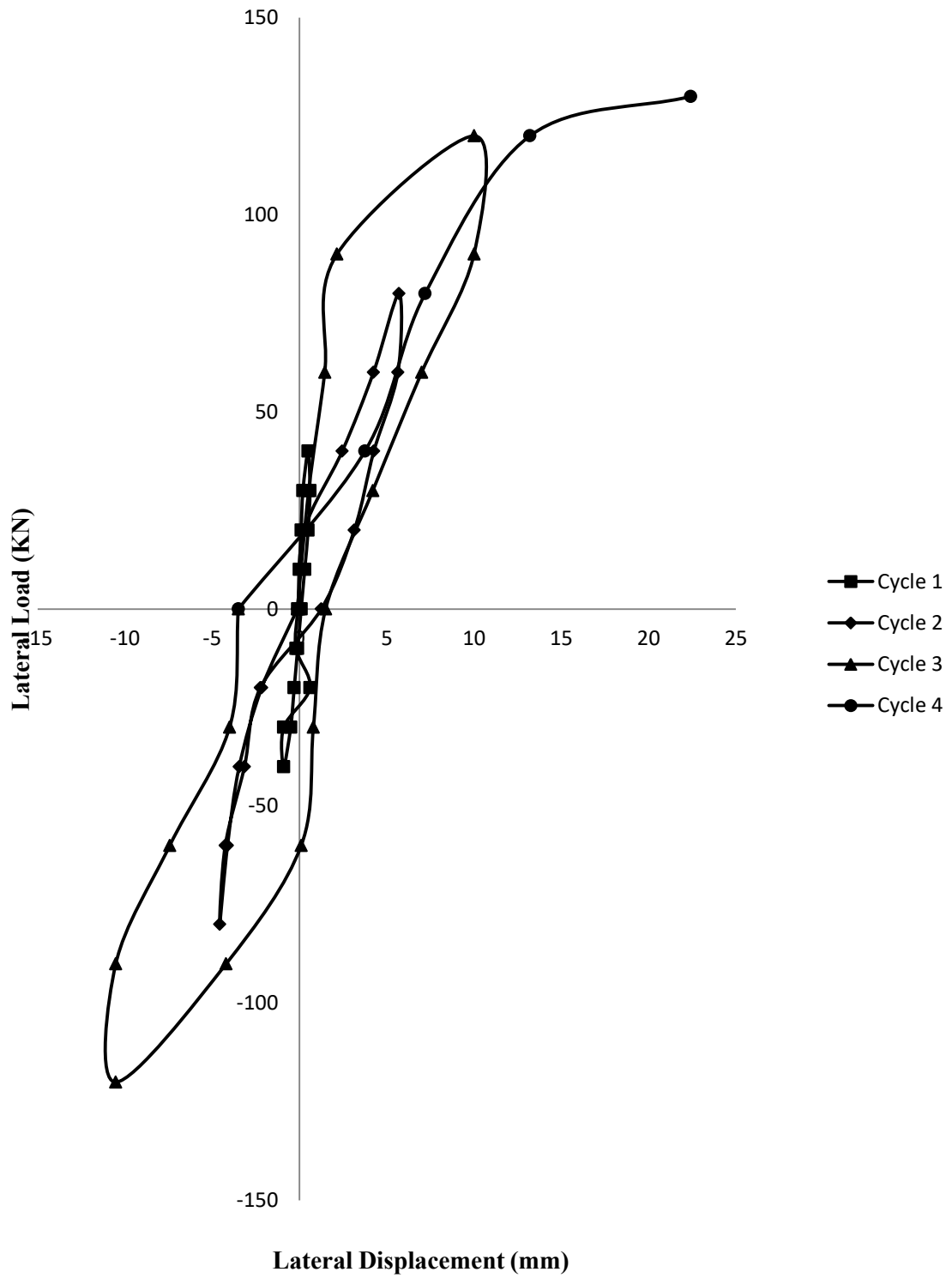


Figure 4.11: Hysteretic load-displacement curve for PB.

At cycle 3, a maximum of 120 KN load was applied from each direction of the specimen. At 120 KN (towards positive direction) load, a significant number of shear cracks were generated parallel to the primary diagonal of the wall. These cracks occurred because the applied load caused excessive diagonal tension on the wall. Cracks were vivid both in mortar and masonry units as the exerted load was higher than their resisting capacity. Bricks also experienced spalling. The wall gap between the wall and column increased. A bunch of flexural cracks were also spotted on the column (left) because the load-carrying capacity of the wall suddenly decreased and it transferred the load to the frame. Eventually, the diagonal shear crack extended to the top-left corner and it reached the joint. Consequently, a shear crack was observed on the beam-column(left) joint. At 120 KN (towards negative direction) load, diagonal shear cracks were visible along the secondary diagonal of the wall. Initially, the cracks were close to 1 mm and gradually increased in width with the increment of load. Additionally, a multitude of horizontal cracks were spotted in different locations of the wall where there were weak mortar joints. The shear cracks along the secondary diagonal extended and reached the top-right corner which resulted in shear crack at the beam-column (right) joint. At the end of this cycle, the segregated cracks combined which created a number of large cracks. Status after the completion of cycle 3 is shown in Figure 4.14.

At cycle 4, the load was intended to be applied to a maximum of 160 KN from each direction of the specimen but the specimen failed at 130 KN (Positive portion). At 130 KN (towards positive direction) load, a large number of flexural cracks were identified on the column (left). It happened because the wall was less capable of carrying load and that is why it transferred the load to the columns. Some cracks were also observed on the base-column (right) joint due to the short column effect. Both of the beam-column joints also went through significant shear cracks. Initially, at a low load, the stress was concentrated on corners. However, with the increment of loads, the normal stresses redistributed and the line of action of this stress shifted from corners which resulted in the increased bending moment on the frame. For these circumstances, some flexural cracks were seen on the frame. The cracks of the wall enhanced in width up to 8mm. Eventually, the specimen failed at 130 KN load. Situation after failure (at cycle 4) is presented in Figure 4.15.



Figure 4.12: PB after the completion of cycle 1.



Figure 4.13: PB after the completion of cycle 2.

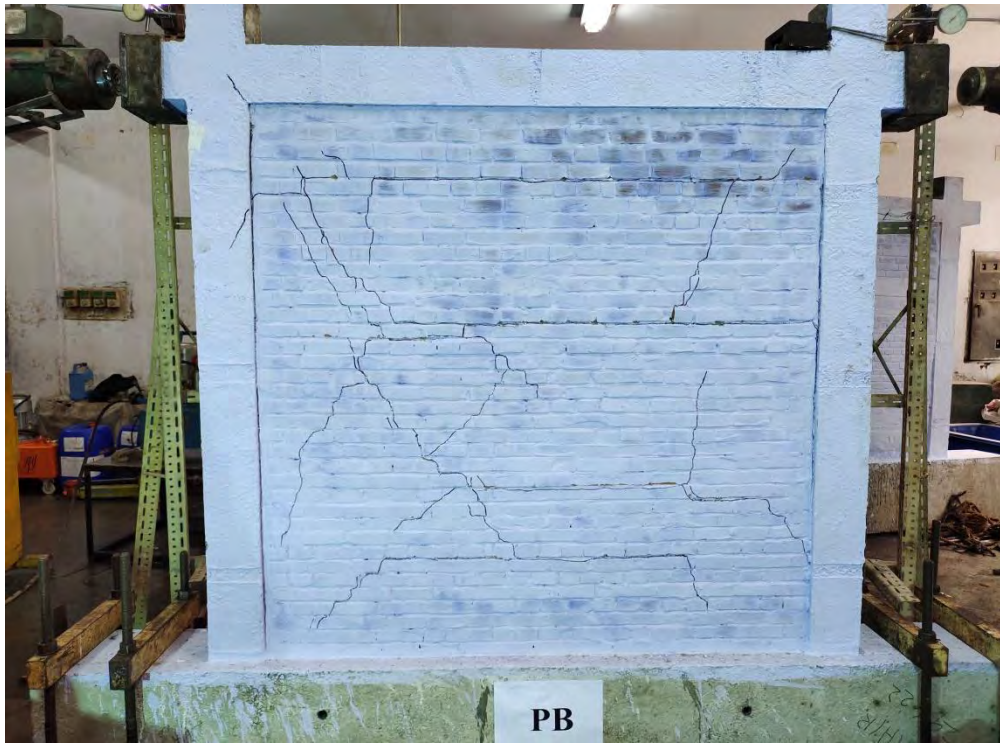


Figure 4.14: PB after the completion of cycle 3.

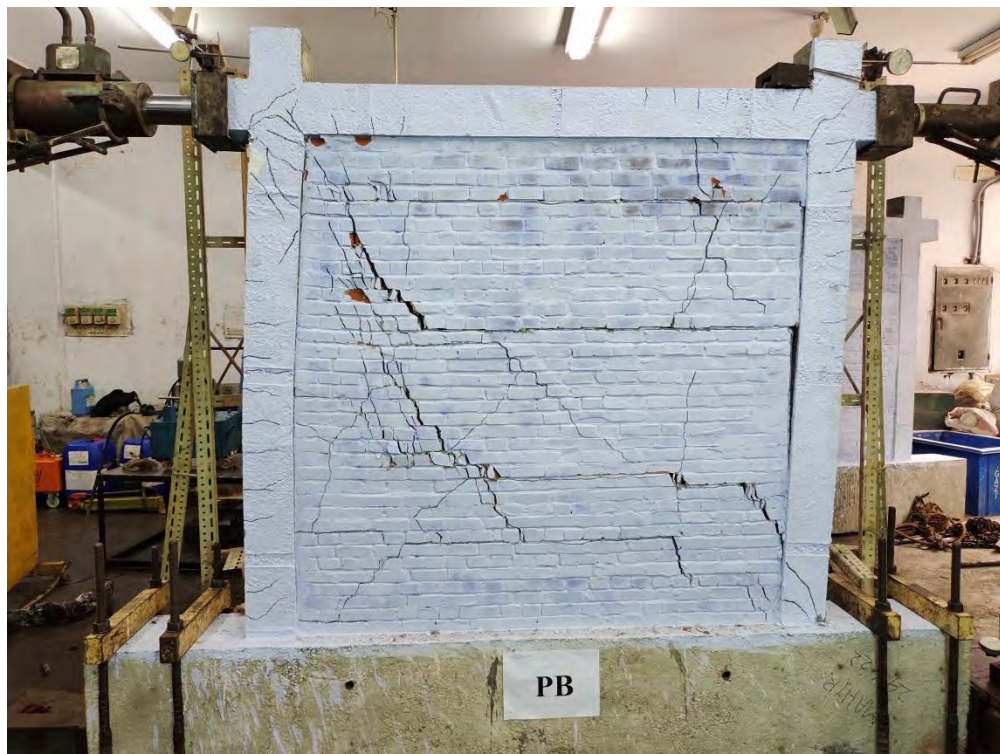


Figure 4.15: PB at complete failure (at cycle 4).

4.3.4 PBL (Perforated Brick Infill with Lintel)

The specimen PBL was placed in the experimental arrangement and the cyclic load was exerted subsequently. The specimen experienced a total of four full cycles and failed in the 5th cycle. The total hysteretic graph of load vs. displacement is illustrated in Figure 4.16. Details of the values of loads and displacements are presented in Appendix-H.

At cycle 1, the load was applied to a maximum of 40 KN from each side of the specimen. No significant crack or change is noticed on the specimen. Condition after the completion of cycle 1 is shown in Figure 4.17.

At cycle 2, load was applied to a maximum of 80 KN from each direction of the specimen. At 80 KN (towards positive direction) load, a significant portion of crack was observed at the wall-column (left) mortar joint as the mortar was the weakest point of the specimen. There was also a crack found at the lintel-column (left) mortar joint and it was about 3 mm wide. Moreover, a mild crack was also seen on the beam-column (left) joint due to the moment induced by the lateral load on the frame. At 80 KN (towards negative direction) load, cracks were visible both in the wall-column (right) joint and lintel-column (right) joint (2mm). Status after the completion of cycle 2 is shown in Figure 4.18.

At cycle 3, the load was applied to a maximum of 120 KN from each direction of the specimen. At 120 KN (towards positive direction) load, multiple shear and flexural cracks were found especially at the left column of the frame. It occurred as a significant portion of stress was carried by the frame. The short column effect might play an important role here. Additionally, the wall also carried some portion of the stresses as a diagonal shear crack as spotted on the wall along the primary diagonal and it extended further (1 mm wide) horizontally along a weak mortar joint between two brick layers. At 120 KN (towards negative direction) load, a bunch of wide horizontal and shear cracks measuring about 3 mm were notified on the infill wall. A major diagonal shear crack formed along the secondary diagonal of the brick as it received a huge amount of tension from the lateral load. Moreover, a few shear and flexural cracks were noticed on the column (right). Some shear cracks on the beam-column (right) joint were also observed. Furthermore, a few flexural cracks were recognized on the lower-right portion of the beam. The cracks of the

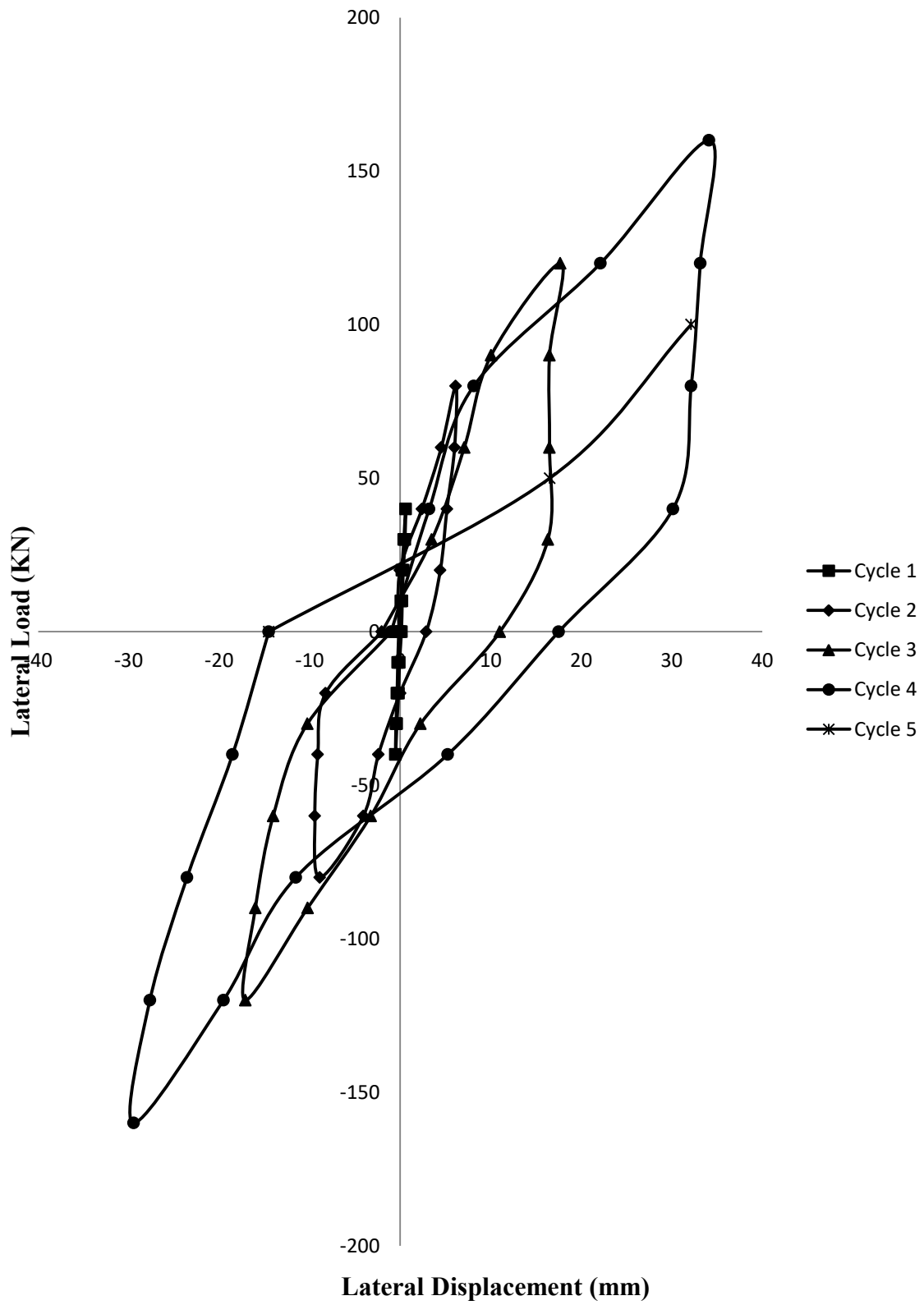


Figure 4.16: Hysteretic load-displacement curve for PBL.

Frame occurred because, with the escalation of loads, the normal stresses redistributed and the line of action of this stress changed which resulted in a higher bending moment on the frame. State after the completion of cycle 3 is shown in Figure 4.19.

At cycle 4, load was applied to a maximum of 160 KN from each direction of the specimen. At 160 KN (towards positive direction) load, a large number of horizontal, diagonal, and vertical cracks were observed at the portion of the wall which is located above the lintel. The cracks were caused because the masonry wall was about to lose its ultimate load-carrying capacity. Cracks were visible both at the mortar joints and bricks because the induced stress by the applied load exceeded their compressive strength. The cracks on the wall extended downward toward the lintel and generated some conspicuous cracks on the lintel too. Additionally, a lot of shear and flexural cracks were visible on both of the columns. Some shear cracks were also spotted on the beam-column(left) joint. Furthermore, several flexural cracks were noticed on the lower portion of the left side of the beam. These were due to excessive moments on the frame. At 160 KN (towards negative direction) load, some significant cracks were observed on both of the base-column joints due to the short column effect as some portion of the masonry wall tended to move away from the column. Some wide flexural cracks such as 20 mm were also spotted on the column. Moreover, a significant amount of spalling of bricks occurred and it created some considerable gaps between the brick layers. Situation after the completion of cycle 4 is presented in Figure 4.20.

At cycle 5, load was intended to be applied to a maximum of 200 KN from each direction of the specimen but the specimen failed at 100 KN (positive direction). At 100 KN (towards positive direction) load, an excessive spalling and crushing of the masonry units occurred. The damages were so extensive that a significant amount of gaps could easily be observed at different locations of the wall. The previously created cracks both in the frame and wall were further extended. More flexural cracks were noticed at the upper right portion of the frame as the amount of stresses on the frame was increasing strongly. A significant amount of sliding occurred at the interface between the lintel and masonry wall. Eventually, corners of the masonry wall were crushed, and total failure of the specimen occurred. Situation after failure (at cycle 5) is presented in Figure 4.21.

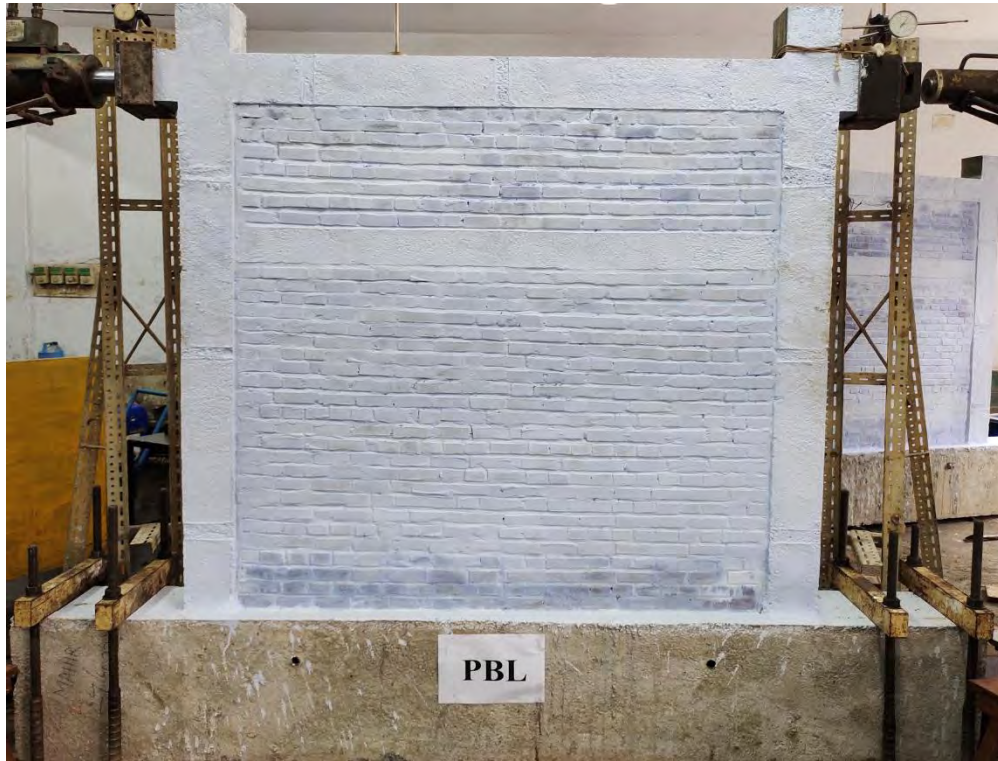


Figure 4.17: PBL after the completion of cycle 1.



Figure 4.18: PBL after the completion of cycle 2.

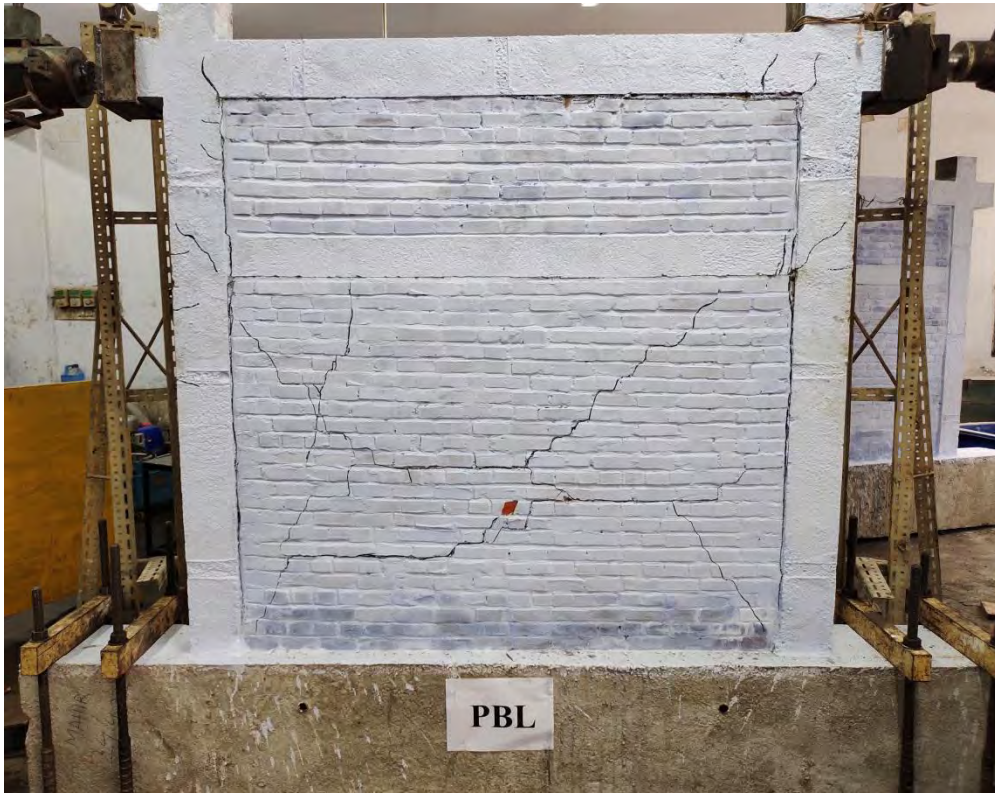


Figure 4.19: PBL after the completion of cycle 3.

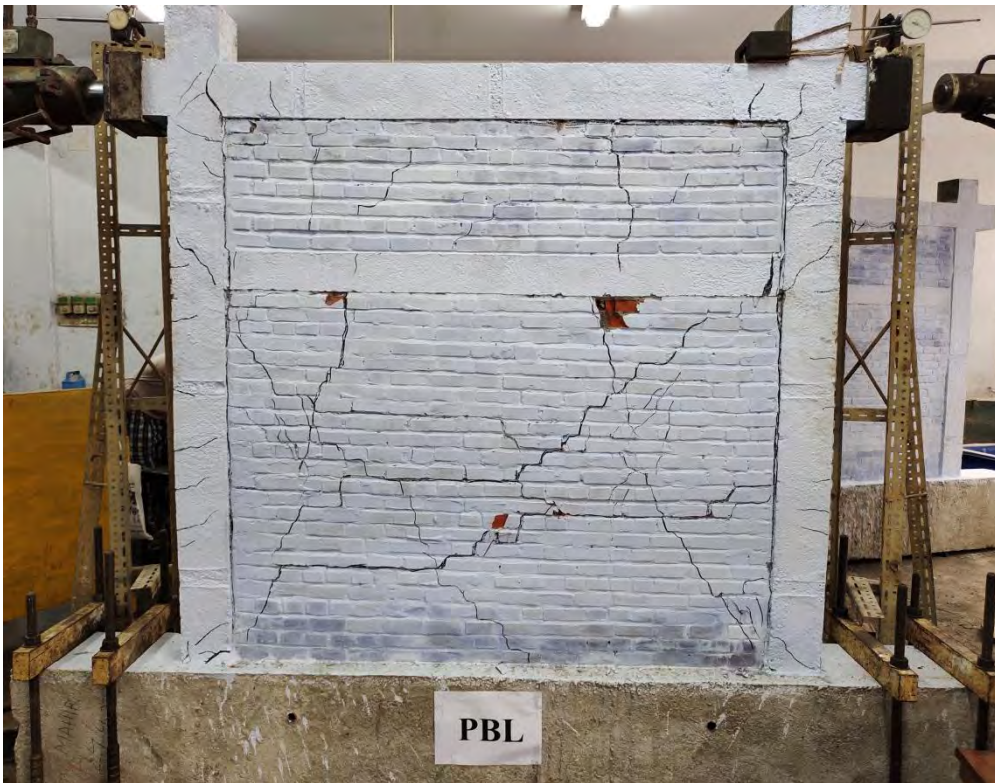


Figure 4.20: PBL after the completion of cycle 4.

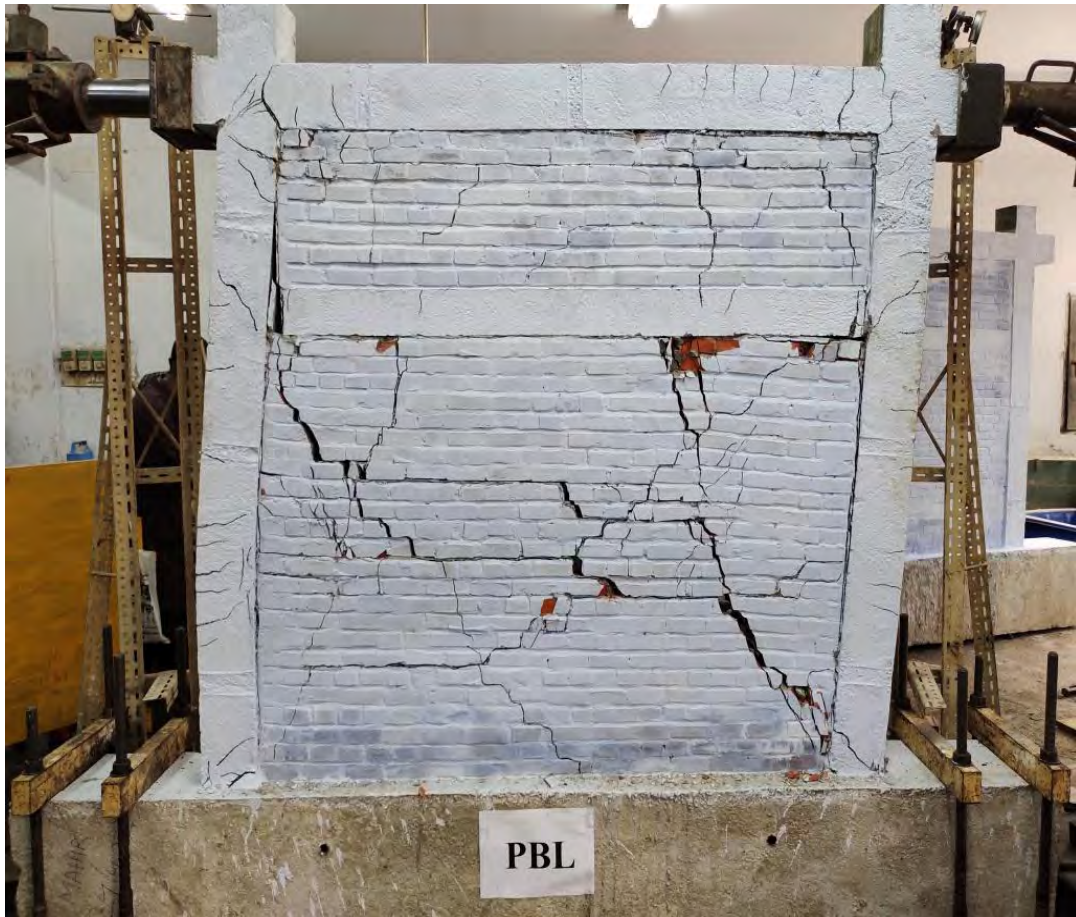


Figure 4.21: PBL at complete failure (at cycle 5).

4.4 Comparative Study

Comparative studies between two sets of specimens are conducted here. Extensive observations are made in relation to the individual effects of different parameters such as specimens having lintel and perforated clay brick.

4.4.1 Comparison between SB and SBL

The purpose of this comparison is to determine the effect of lintel when the masonry unit is solid clay brick.

A summary of the test results is given in Table 4.1. The frame of SBL carried 50% more load than the frame of SB before cracking although their infill cracked at the same load. At infill first cracking, SBL showed 2% more displacement and 2% less stiffness than SB.

On the other hand, at first cracking of the frame, SBL showed about 3 times more displacement and 49% less stiffness than SB. Eventually, the ultimate load-carrying capacity of SBL was found about 7% more than SB. At this point, SBL exhibited 81% more displacement and 41% less stiffness than SB. Furthermore, SBL dissipated 46% more energy than SB. On another note, story drift is the lateral displacement of one level relative to the level above or below. The relation of lateral load vs. story drift, stiffness vs. story drift, and cumulative energy dissipation vs. story drift of SB and SBL are illustrated in Figure 4.22, 4.23, and 4.24 respectively.

Maximum stiffness and stiffness at maximum displacement at each cycle of SB and SBL are presented in Figure 4.25 and 4.26. SBL demonstrated 9%, 2%, 63%, 81% more maximum displacement and 9%, 2%, 39%, 40% less stiffness at maximum displacement than SB in cycle 1, 2, 3, 4 respectively. SBL experienced comparatively more displacement before failure because lintel works as confinement and obstructs the extension of cracks.

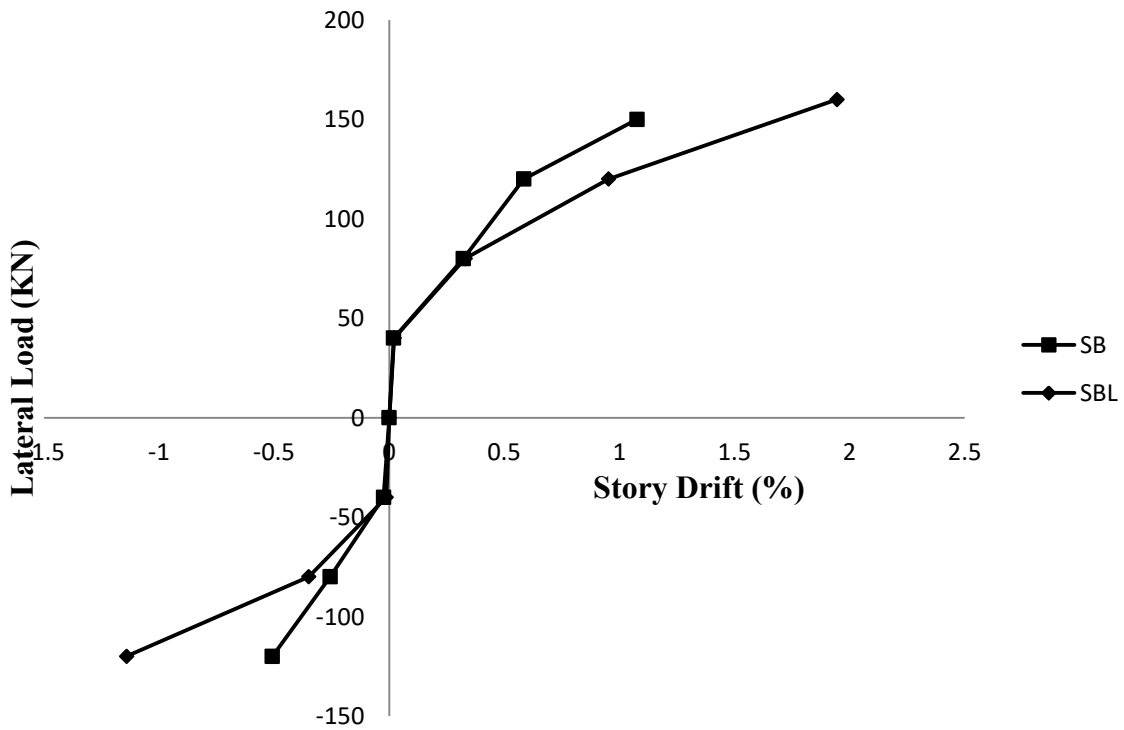


Figure 4.22: Relation between lateral load and story drift.

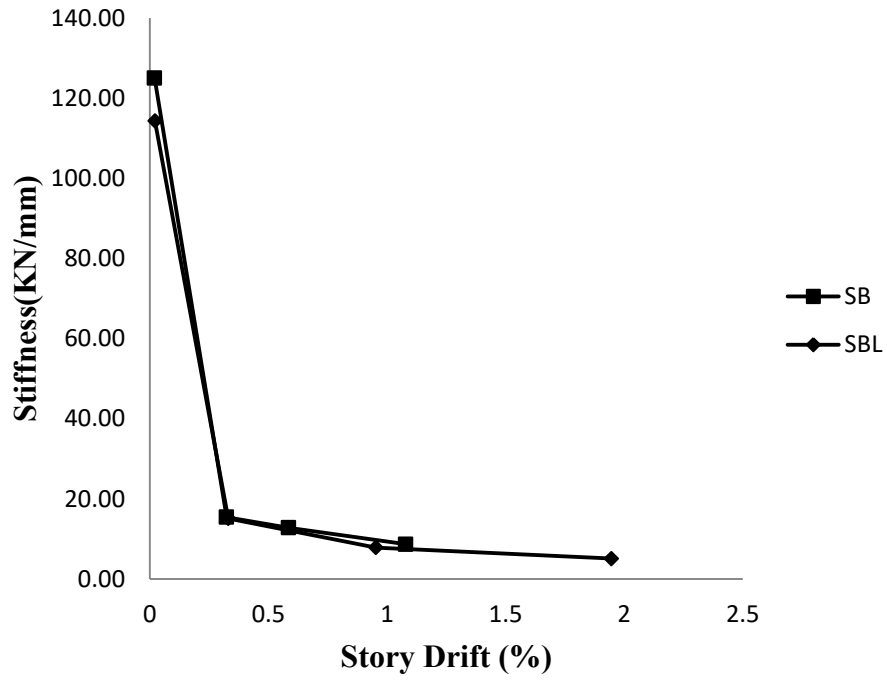


Figure 4.23: Relation between stiffness and story drift.

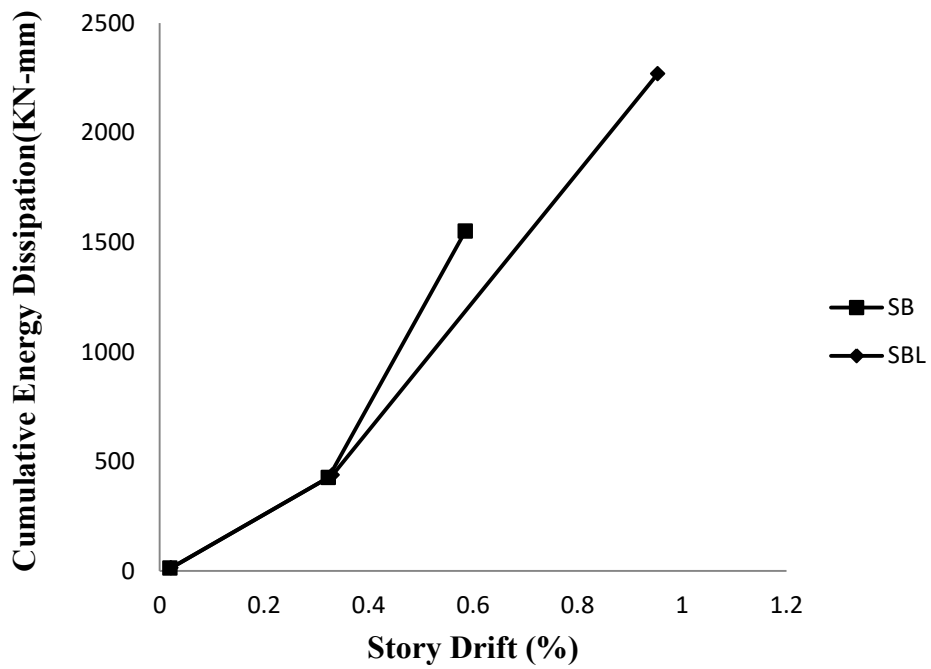


Figure 4.24: Relation between cumulative energy dissipation vs. story drift.

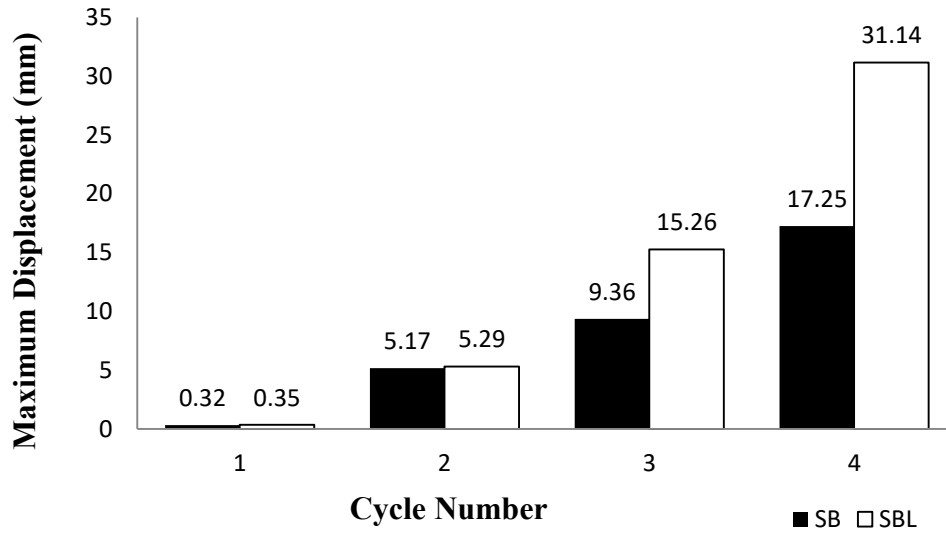


Figure 4.25: Maximum displacement at each cycle.

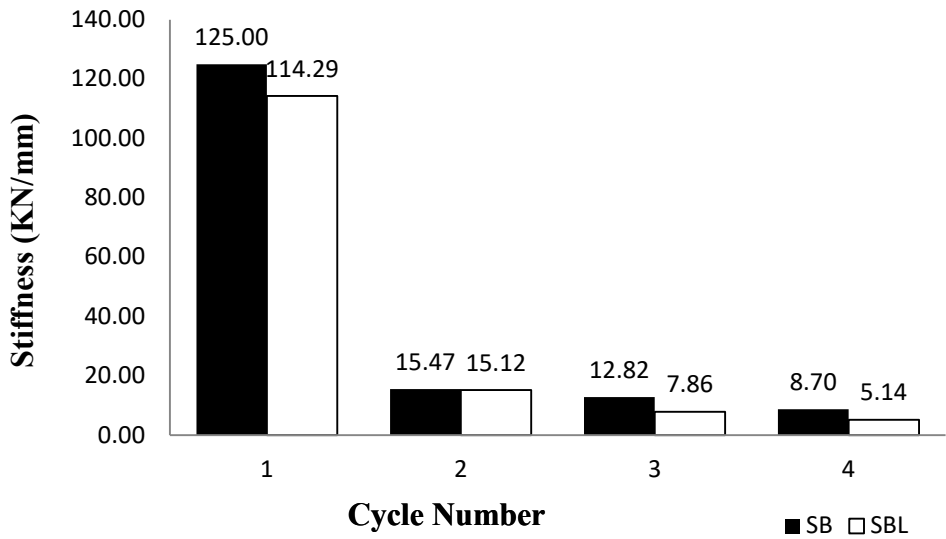


Figure 4.26: Stiffness at maximum displacement at each cycle.

4.4.2 Comparison between PB and PBL

The purpose of this comparison is to determine the effect of lintel when the masonry unit is perforated clay brick.

From Table 4.1 we can see the summary of the test results. The frame of PBL carried 33% less load than the frame of PB before cracking although their infill cracked at the same load. At first cracking of the infill, PBL showed 8% more displacement and 8% less

stiffness than PB. On the other hand, at first cracking of the frame, PBL showed 39% less displacement and 9% more stiffness than PB. Eventually, the ultimate load-carrying capacity of PBL was found about 23% more than PB. At this point, PBL exhibited 52% more displacement and 19% less stiffness than PB. Furthermore, PBL dissipated about 5 times more energy than PB. On another note, story drift is the lateral displacement of one level relative to the level above or below. The relation of lateral load vs. story drift, stiffness vs. story drift, and cumulative energy dissipation vs. story drift of PB and PBL are illustrated in Figure 4.27, 4.28, and 4.29 respectively.

Maximum stiffness and stiffness at maximum displacement per each cycle of PB and PBL are presented in Figure 4.30 and 4.31. PBL demonstrated 20%, 8%, 77%, 52% more maximum displacement and 17%, 7%, 44%, 20% less stiffness at maximum displacement than PB in cycle 1, 2, 3, 4 respectively. It should be noted that PBL experienced one more cycle before failure than PB. PBL exhibited considerably greater displacement before failure because the lintel acts as confinement and prevents fractures from extending.

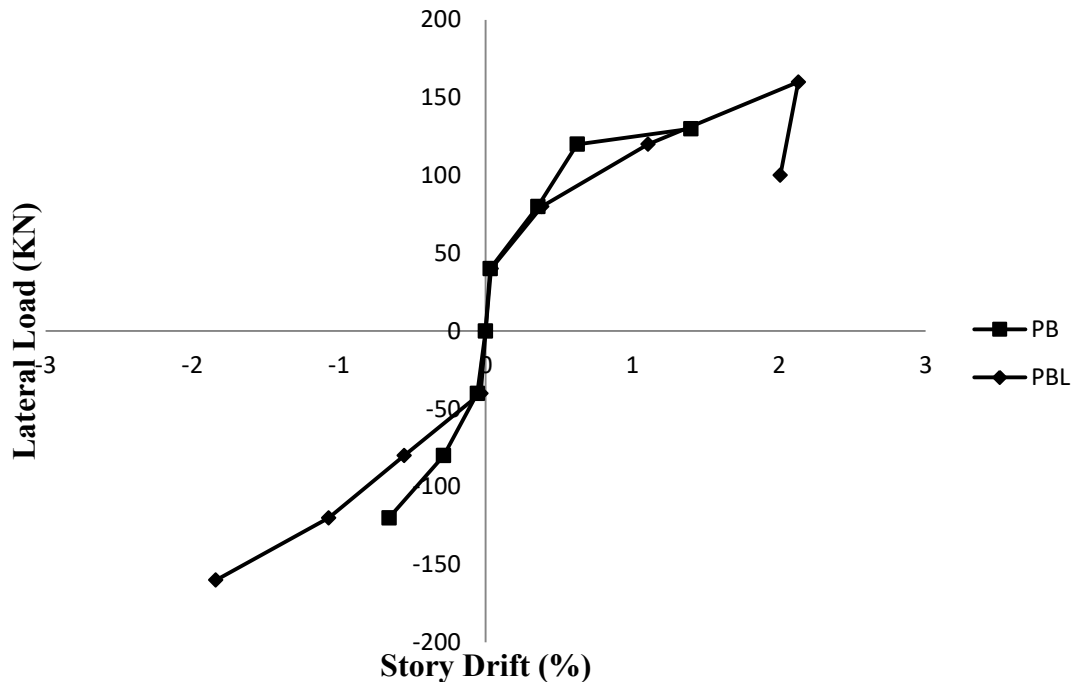


Figure 4.27: Relation between lateral load and story drift.

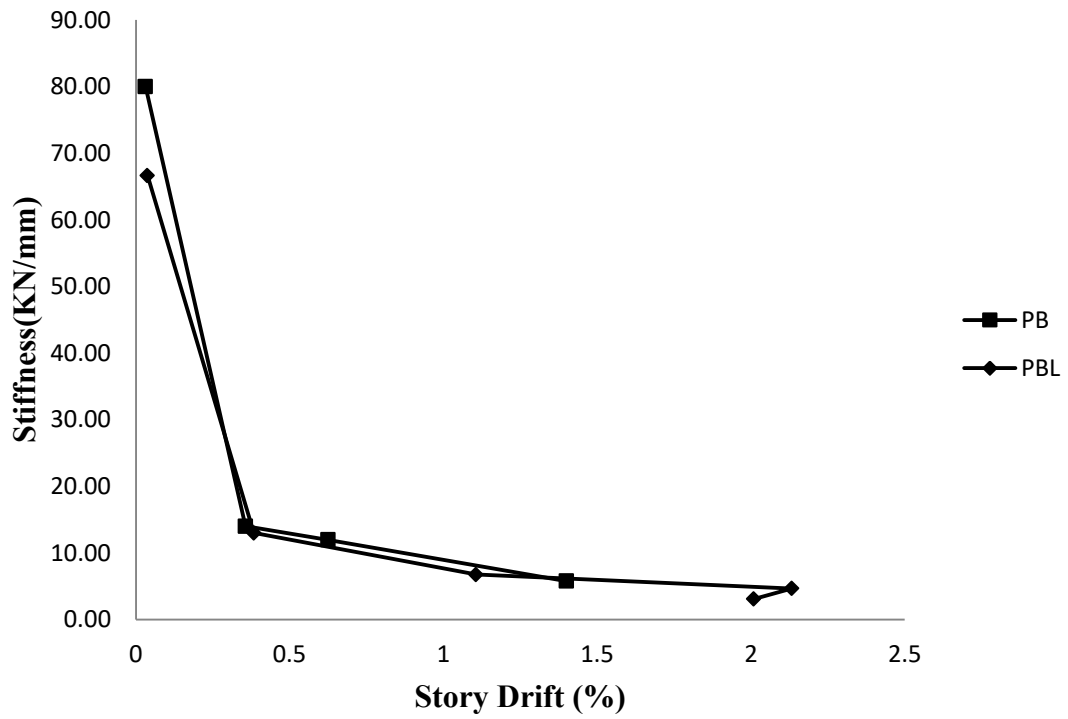


Figure 4.28: Relation between stiffness and story drift.

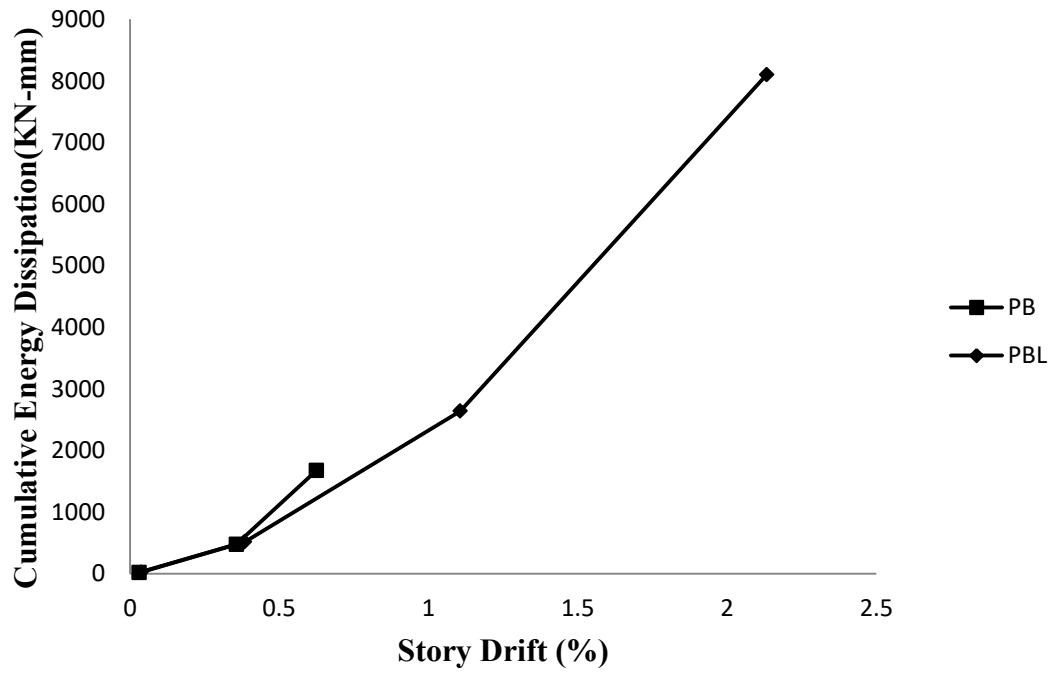


Figure 4.29: Relation between cumulative energy dissipation vs. story drift.

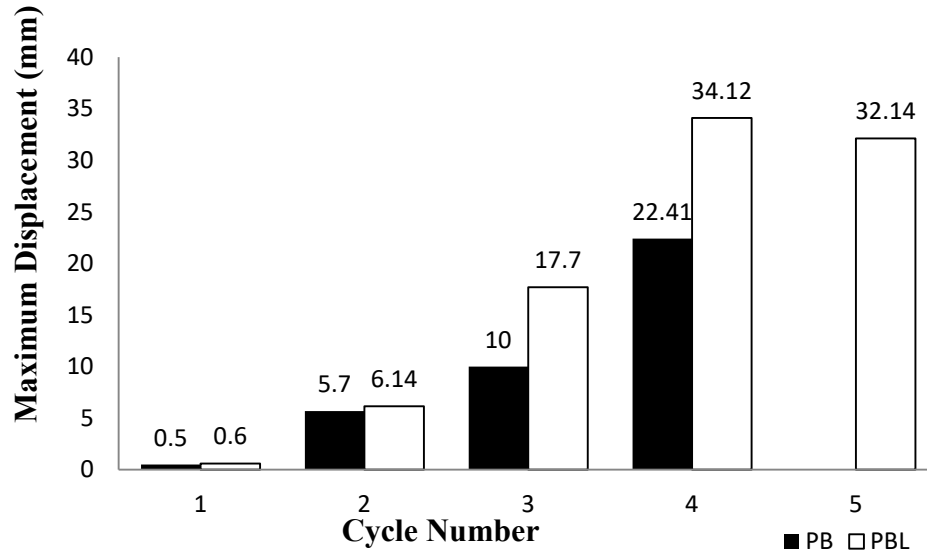


Figure 4.30: Maximum displacement at each cycle.

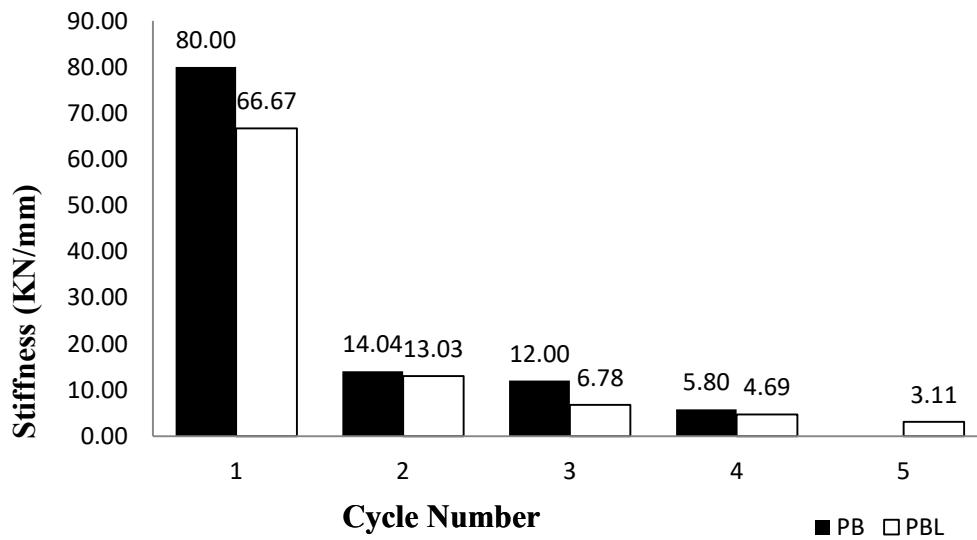


Figure 4.31: Stiffness at maximum displacement at each cycle.

4.4.3 Comparison between SB and PB

The purpose of this comparison is to determine the effect of perforated clay brick as an alternative of solid clay brick where both of the specimens do not contain a lintel.

A summary of the test results is given in Table 4.1. The frame of PB carried 50% more load than the frame of SB before cracking although their infill cracked at the same load. At infill first cracking, PB showed 10% more displacement and 9% less stiffness than SB.

On the other hand, at frame first cracking, PB showed 93% more displacement and 22% less stiffness than SB. Eventually, the ultimate load-carrying capacity of PB was found about 13% less than SB. At this point, PB exhibited 30% more displacement and 33% less stiffness than SB. Furthermore, PB dissipated 8% more cumulative energy than SB. On another note, story drift is the lateral displacement of one level relative to the level above or below. The relation of lateral load vs. story drift, stiffness vs. story drift, and cumulative energy dissipation vs. story drift of SB and PB are illustrated in Figure 4.32, 4.33, and 4.34 respectively.

Maximum stiffness and stiffness at maximum displacement per each cycle of SB and PB are presented in Figures 4.35 and 4.36. PB demonstrated 56%, 10%, 7%, 30% more maximum displacement and 36%, 9%, 6%, 33% less stiffness at maximum displacement than SB in cycle 1, 2, 3, 4 respectively.

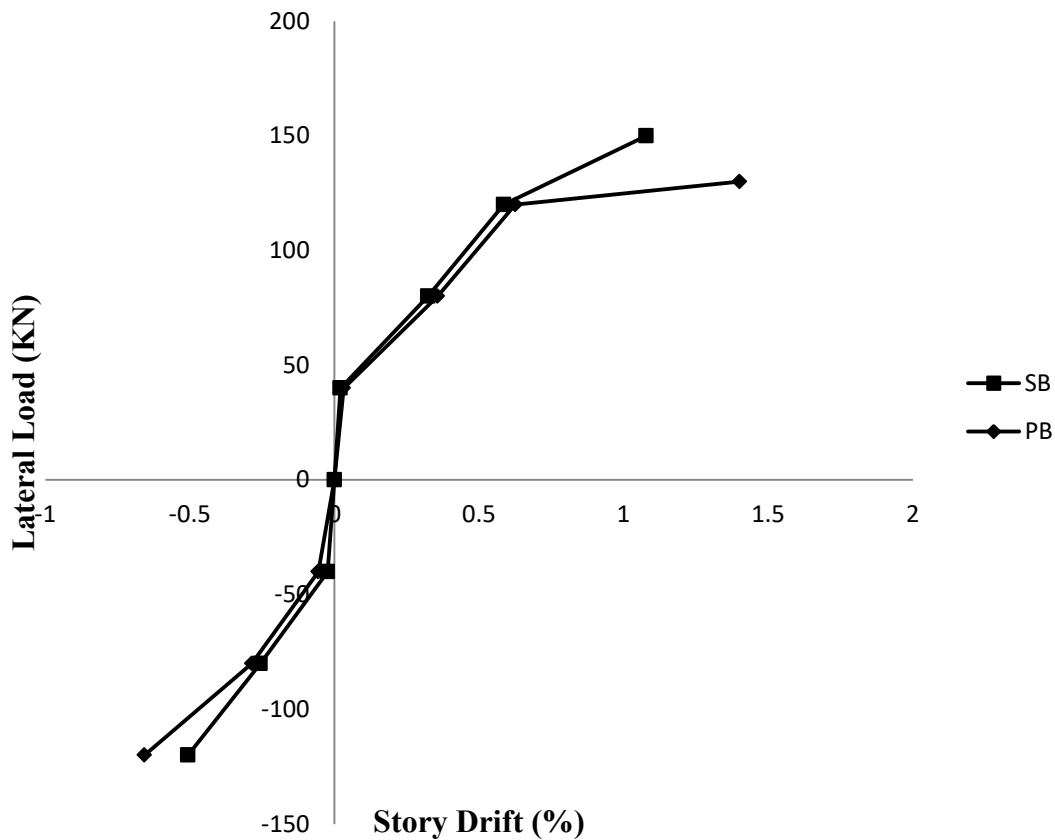


Figure 4.32: Relation between lateral load and story drift.

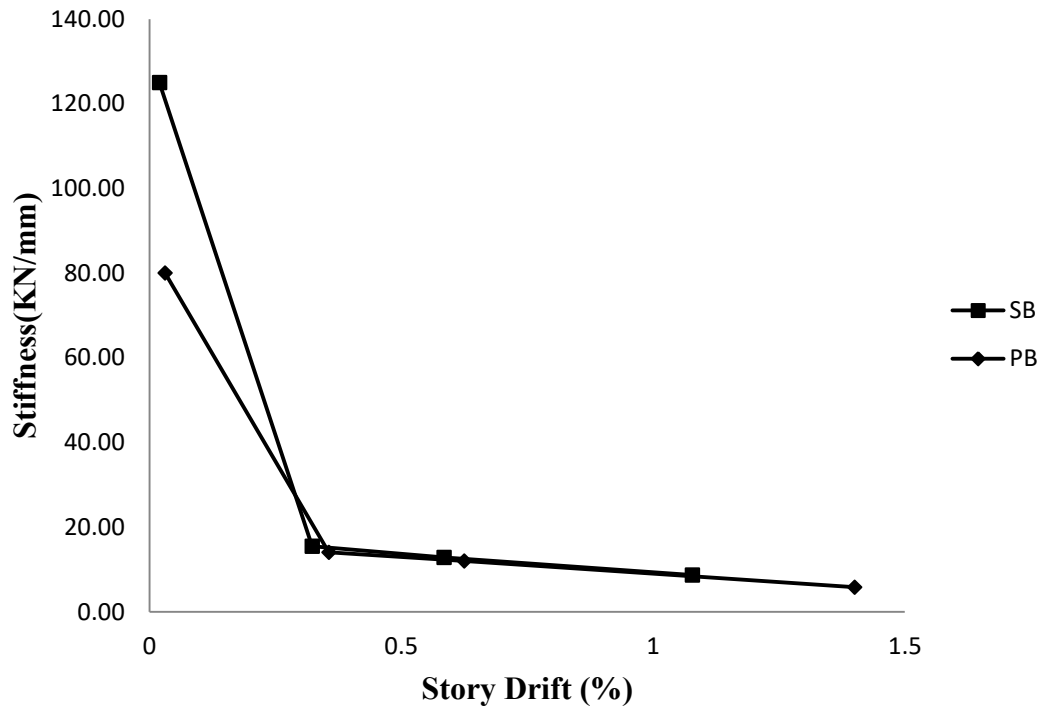


Figure 4.33: Relation between stiffness and story drift.

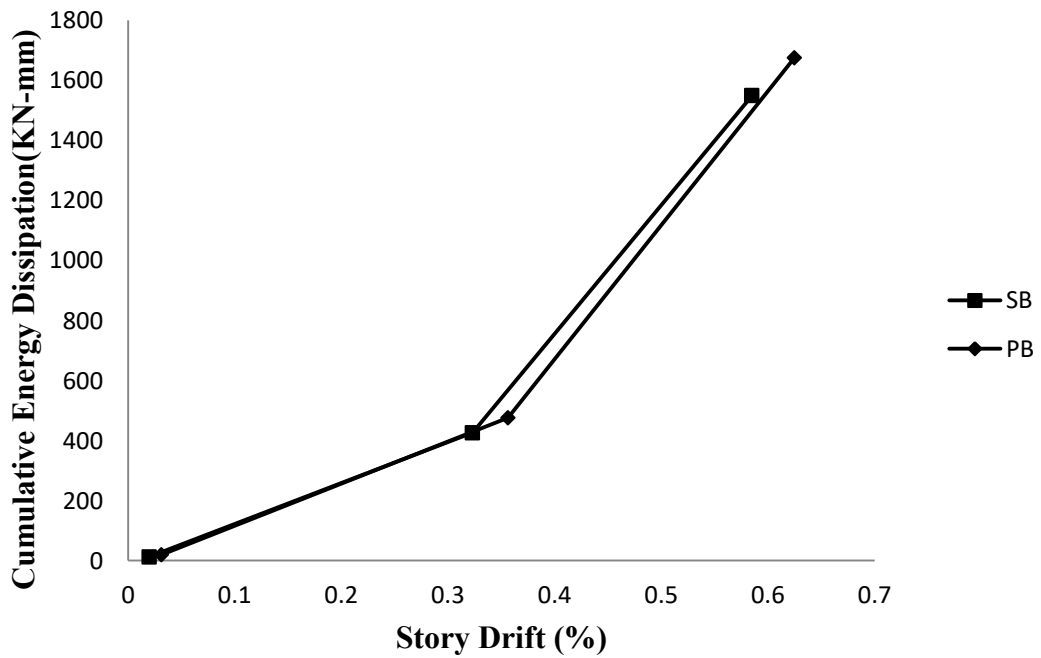


Figure 4.34: Relation between cumulative energy dissipation vs. story drift.

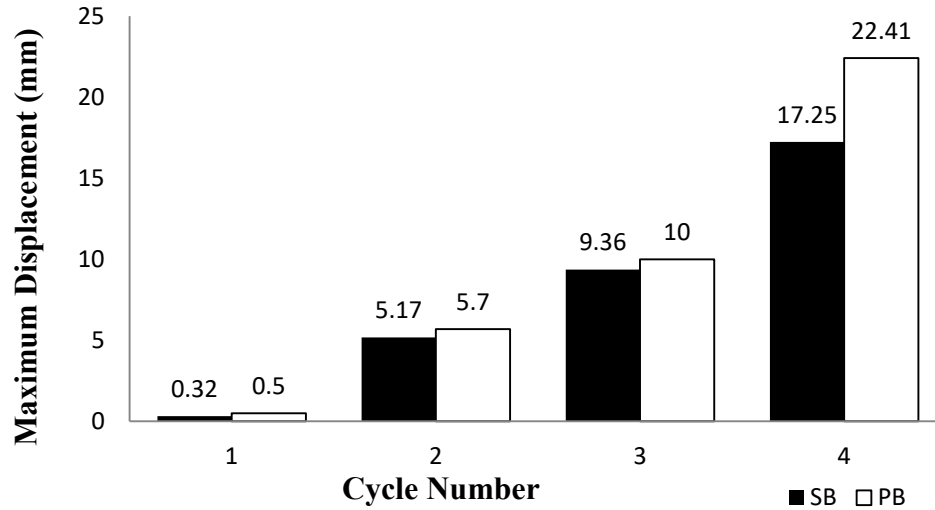


Figure 4.35: Maximum displacement at each cycle.

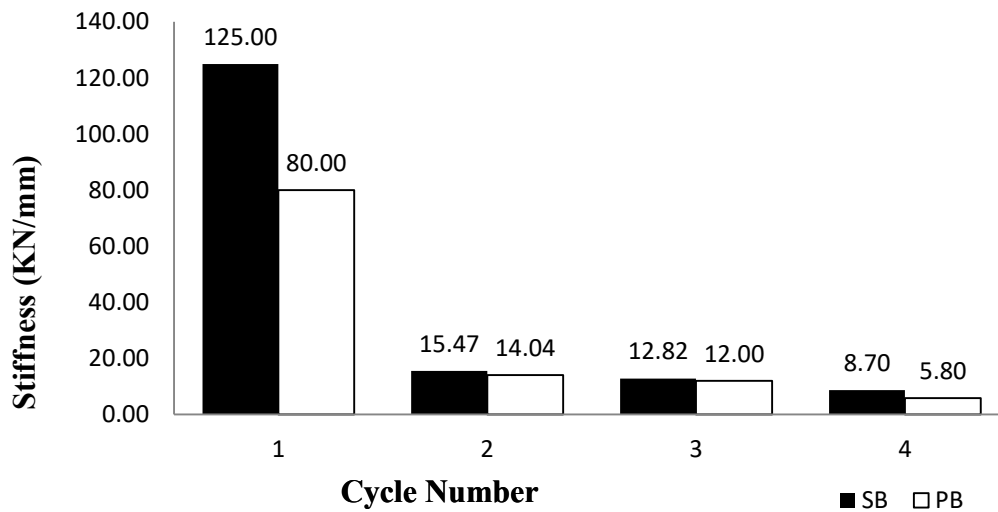


Figure 4.36: Stiffness at maximum displacement at each cycle.

4.4.4 Comparison between SBL and PBL

The purpose of this comparison is to determine the effect of perforated clay brick as an alternative of solid clay brick where both of the specimens contain a lintel.

A summary of the test results is given Table 4.1. The frame of PBL carried 33% less load than the frame of SBL before cracking although their infill cracked at the same load. At first cracking of the infill, PBL showed 16% more displacement and 14% less stiffness

than SBL. On the other hand, at first cracking of the frame, PBL showed 60% less displacement but 66% more stiffness than SBL. Eventually, they both displayed identical ultimate load-carrying capacity. At this point, PBL exhibited 10% more displacement and 9% less stiffness than SBL. Furthermore, PBL dissipated about 4 times more cumulative energy than SBL. On another note, story drift is the lateral displacement of one level relative to the level above or below. The relation of lateral load vs. story drift, stiffness vs. story drift, and cumulative energy dissipation vs. story drift of SBL and PBL are illustrated in Figure 4.37, 4.38, and 4.39 respectively.

Maximum stiffness and stiffness at maximum displacement per each cycle of SBL and PBL are presented in Figure 4.40 and 4.41. PBL demonstrated 71%, 16%, 16%, 10% more maximum displacement and 42%, 14%, 14%, 9% less stiffness at maximum displacement than SBL in cycle 1, 2, 3, 4 respectively. It should be noted that PBL experienced one more cycle before failure than SBL.

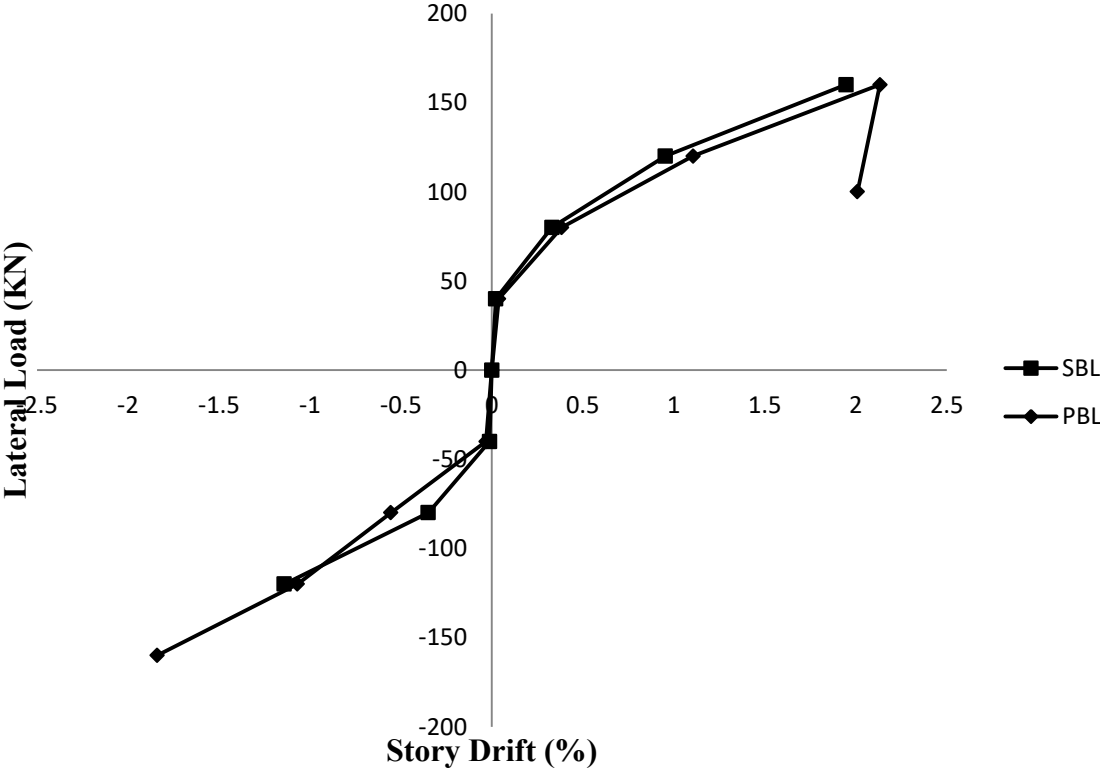


Figure 4.37: Relation between lateral load and story drift.

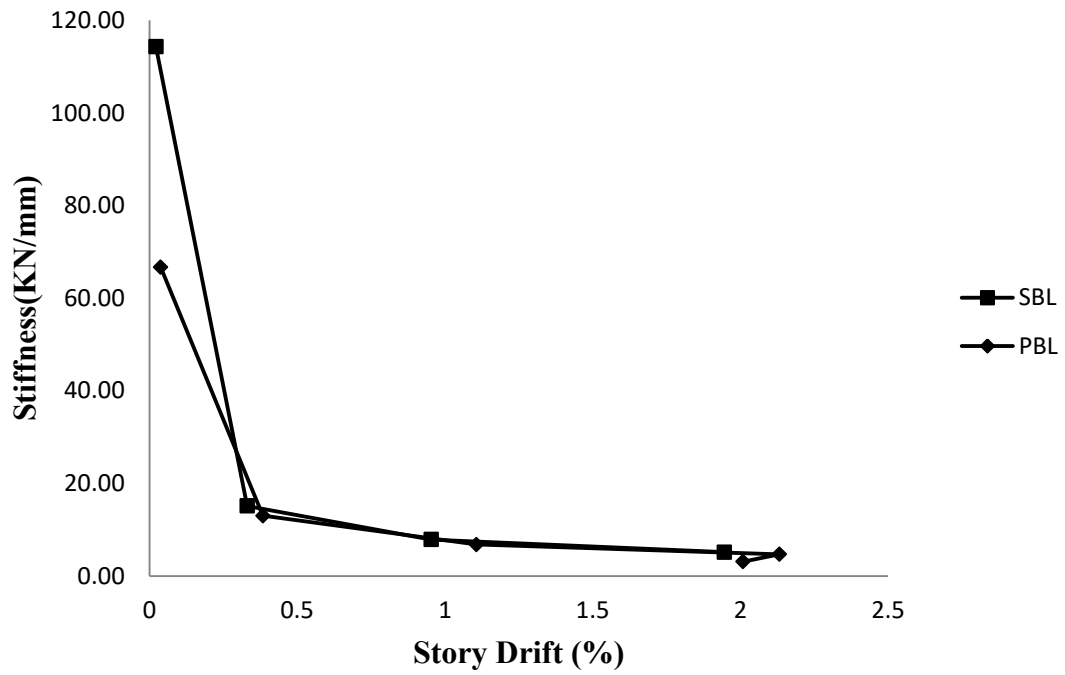


Figure 4.38: Relation between stiffness and story drift.

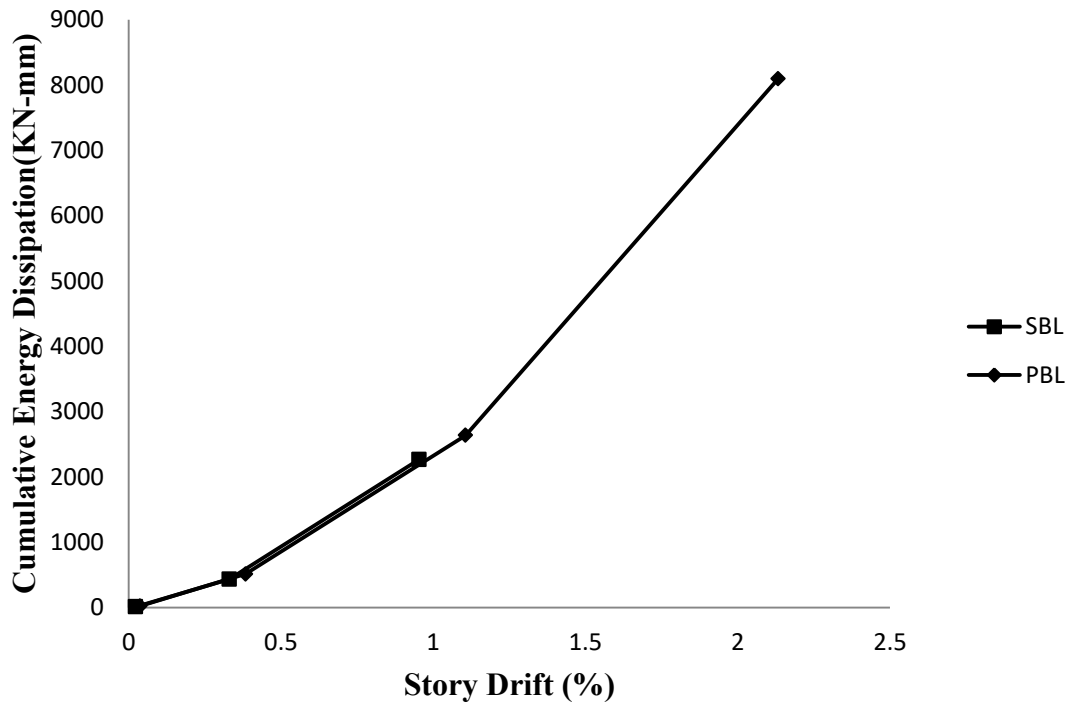


Figure 4.39: Relation between cumulative energy dissipation vs. story drift.

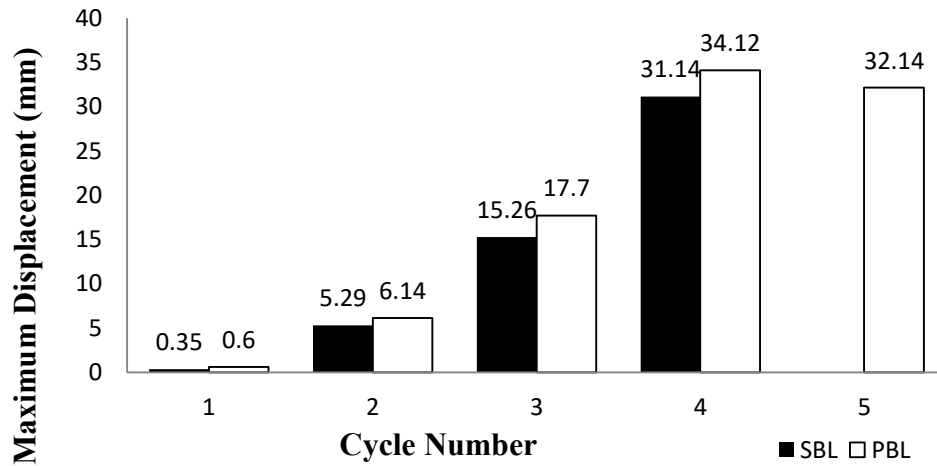


Figure 4.40: Maximum displacement at each cycle.

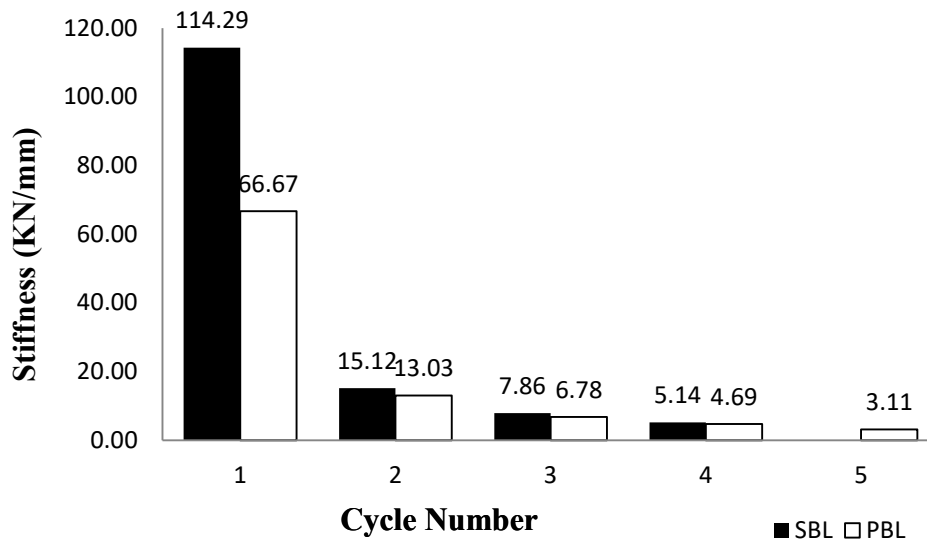


Figure 4.41: Stiffness at maximum displacement at each cycle.

Sample calculation of story drift, stiffness, and cumulative energy dissipation for a specimen (specimen SB is taken as an example) is shown in Appendix-I.

4.5 Overall Comparison of All Specimens

In the previous section, comparison was exhibited between two specimens. However, in this section the overall comparison is illustrated in Figure 4.42, 4.43, 4.44, 4.45, and 4.46. In summary, it is observed that PBL is the most effective specimen in terms of ductility,

whereas SB is the most effective specimen in terms of stiffness. PBL exhibited the most number of cracks. It indicates that it dissipated most energy among all specimens.

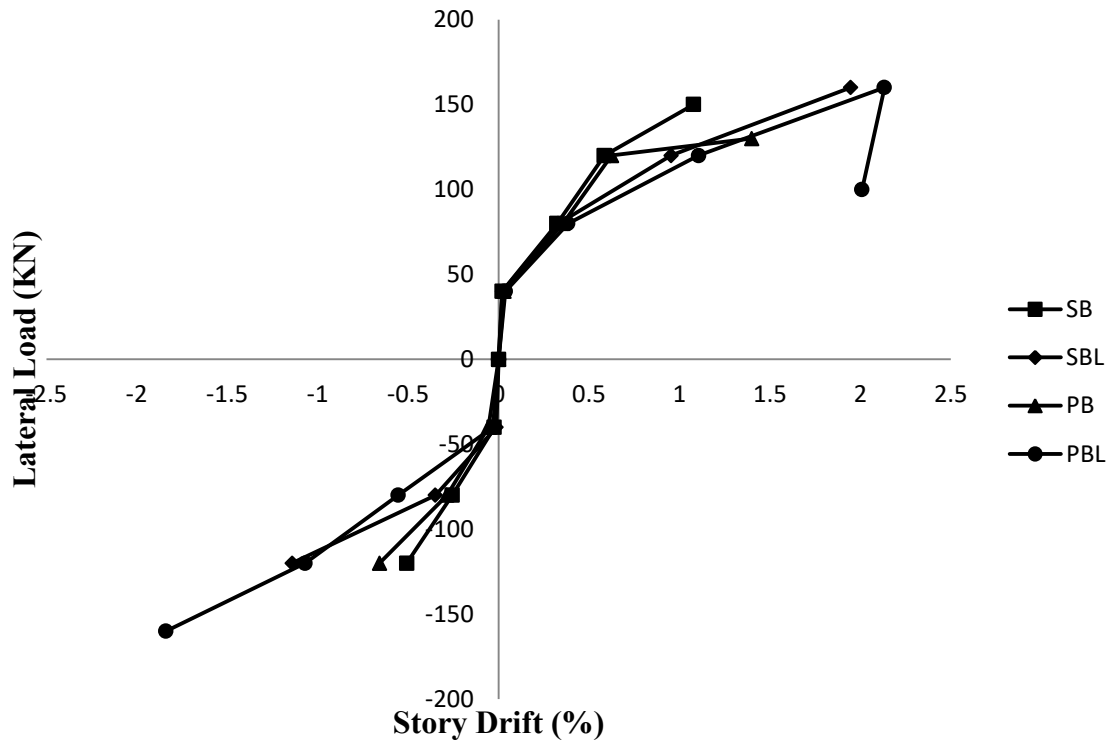


Figure 4.42: Relation between lateral load and story drift.

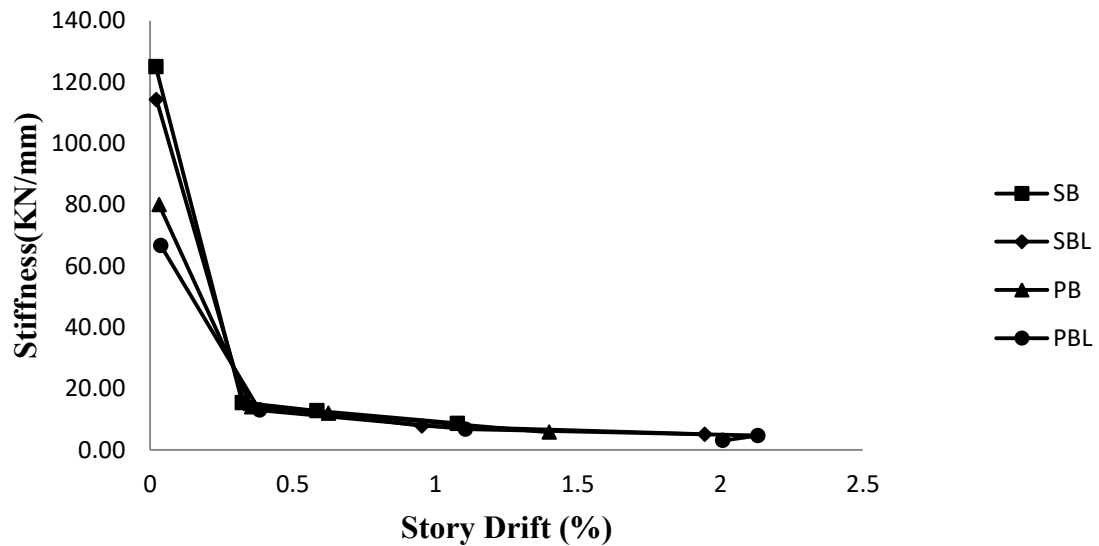


Figure 4.43: Relation between stiffness and story drift.

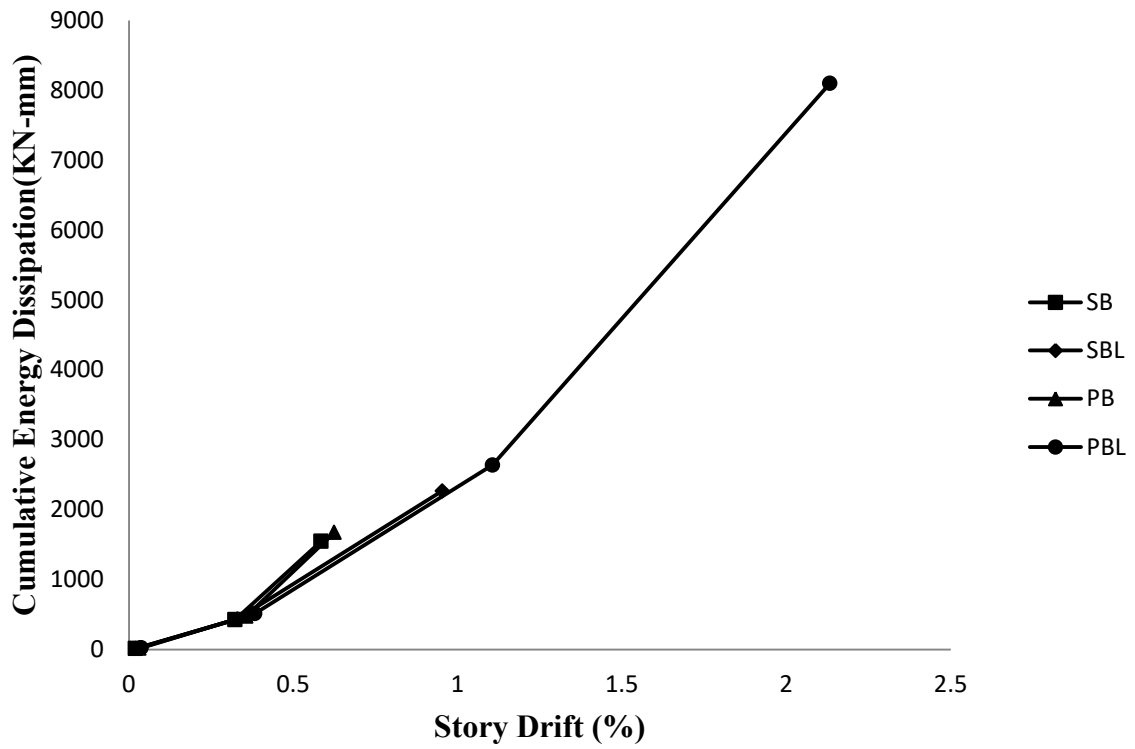


Figure 4.44: Relation between cumulative energy dissipation vs. story drift.

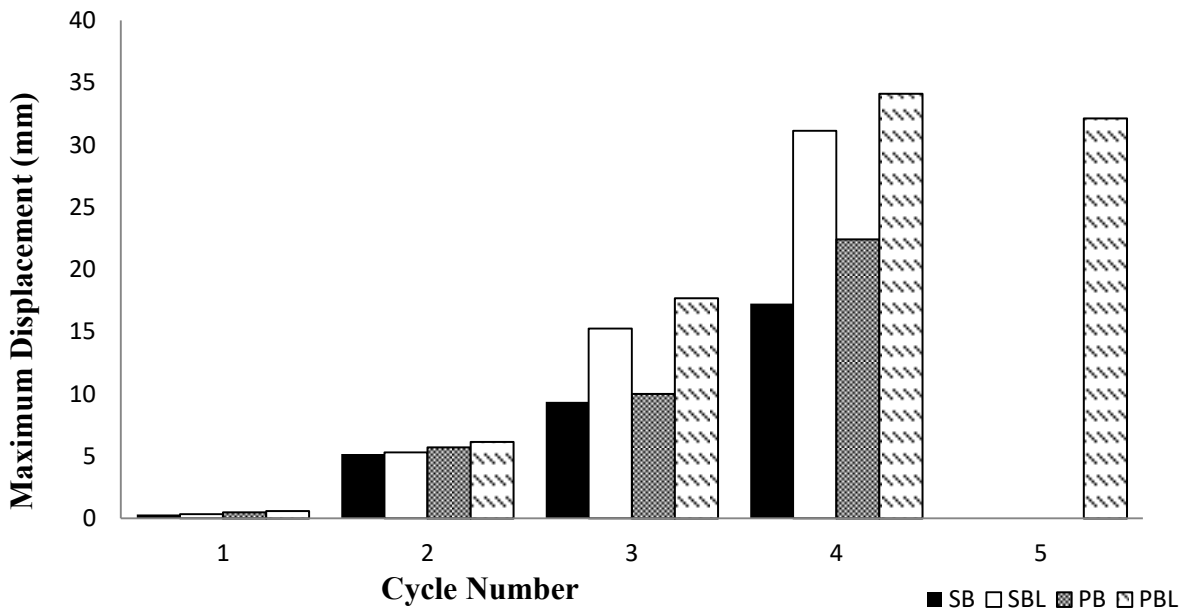


Figure 4.45: Maximum displacement at each cycle.

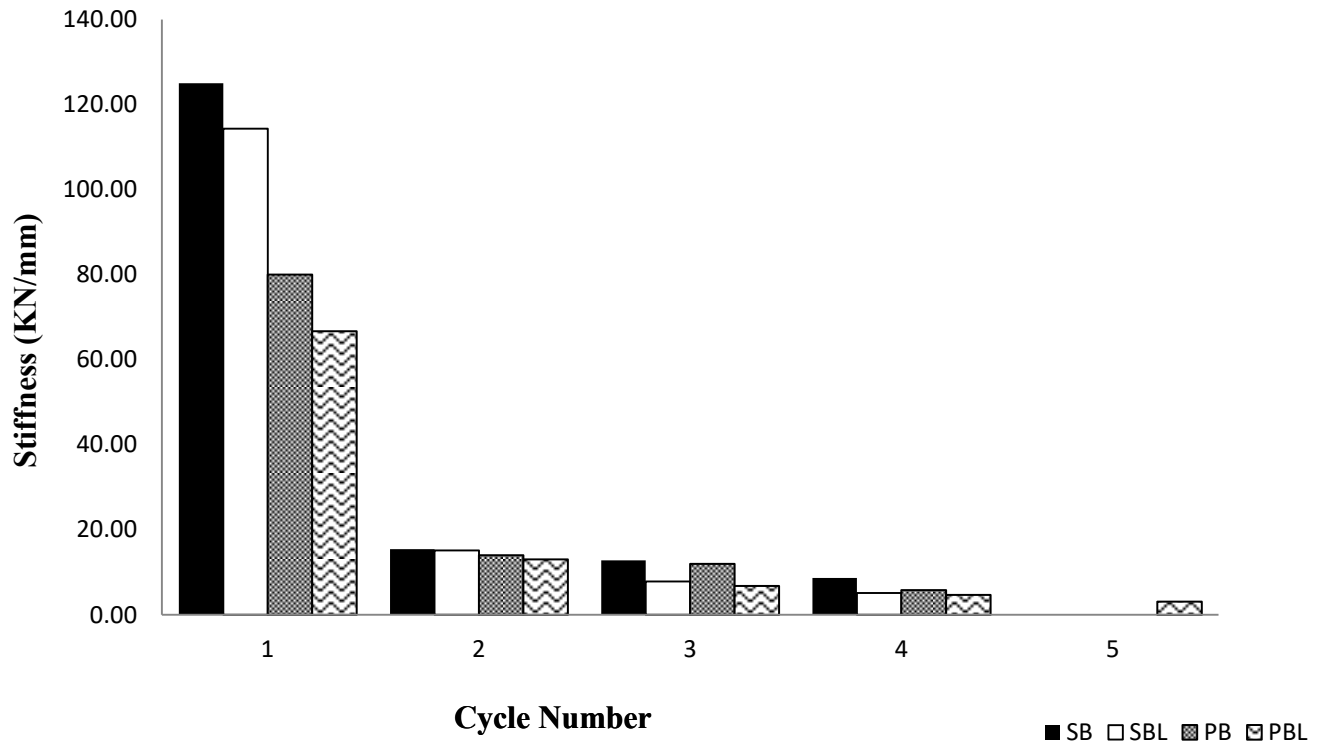


Figure 4.46: Stiffness at maximum displacement at each cycle.

Chapter 5

CONCLUSIONS AND RECOMMENDATIONS

5.1 Introduction

The principal purpose of this study is to assess the effect of lintel and perforated clay brick in infilled frames by experimental investigation. Four specimens were constructed. Two specimens contained lintel. Between these two, one was built with solid clay brick and another was constructed with perforated clay brick. The other two did not contain any lintel. Between these two, one was built with solid clay brick and another was constructed with perforated clay brick. After preparation, all of the specimens were subjected to cyclic loading and their structural behavior was carefully observed.

5.2 Conclusions from the Experiments

The important conclusions derived from the experiments are mentioned below.

- I. Lintel is effective to enhance the ultimate load-carrying capacity of MIRCFC structures. For example, SBL displayed 7% more ultimate load-carrying capacity than SB. Similarly, PBL demonstrated 23% more ultimate load-carrying capacity than PB.
- II. Infill masonry wall containing perforated clay brick did not show any clear contribution to the ultimate load-carrying capacity of the specimens. SBL and PBL failed at the same load, PB carried 13% less load than SB.
- III. Both perforated clay brick and lintel do not have any particular contribution to resist or delay the first cracking in the infill. As for illustrations, SB, SBL, PB, and PBL first cracked at the same load.
- IV. Both perforated clay brick and lintel are effective to increase the ductility of the specimens. For example, PB exhibited 30% more displacement before failure than SB and PBL showed 10% more displacement before failure than SBL. Similarly,

SBL exhibited 81% more displacement before failure than SB and PBL showed 52% more displacement before failure than PB.

- V. Both perforated clay brick and lintel have adverse effects on stiffness. For instance, PB exhibited 33% less stiffness before failure than SB and PBL showed 9% less stiffness before failure than SBL. Similarly, SBL exhibited 41% less stiffness before failure than SB and PBL showed 19% less stiffness before failure than PB.
- VI. Both perforated clay brick and lintel are effective to enhance the energy dissipating capacity of the specimens. For instance, PB dissipated 8% more cumulative energy than SB and PBL dissipated about 4 times more cumulative energy than SBL. Similarly, SBL dissipated 46% more cumulative energy than SB and PBL dissipated about 5 times more cumulative energy than PB.
- VII. The specimen having both perforated clay brick and lintel is the most effective structure in terms of ductility and energy dissipation.
- VIII. The specimen containing solid clay brick and devoid of the lintel is the most effective structure in terms of stiffness.

5.3 Recommendations for Future Study

In the future, there are a plethora of prospects to extend this study:

- I. Only two types of masonry units (solid clay brick and perforated clay brick) were used in this study. In the future, different types of masonry units can be investigated as infill masonry materials.
- II. In this experiment, reinforced concrete lintel was utilized. Lintel made with different materials can be used in the future.
- III. None of the specimens of this investigation contained openings. In the future, specimens can be constructed by using openings (doors, windows, etc.).

- IV. Perforated clay bricks were used in this experiment but their hole was not used to increase structural integrity. In the future, there is a huge scope to utilize these holes by inserting reinforcement throughout them along with partial or full grouting.
- V. In this study, all the specimens were taken in the same aspect ratio. However, there is always a scope to take any aspect ratio and observe the behavior change.
- VI. Mortar was the weakest point of the infill here and the initial cracking lines were found along the weak mortar joint. Considering this incident, high-strength mortar or rich mix mortar can be used in the future study.
- VII. In this study, it was observed that the infill masonry wall intended to get segregated from the frame in cyclic loading due to the weak mortar joint. In the future study, this joint can be strengthened by many means such as using dowel bars.
- VIII. The frame of this study was constructed with conventional concrete. However, in the future, special concrete such as ultra-high-performance concrete can be used.
- IX. This study was conducted fully experimentally. Nevertheless, the identical investigation can be committed numerically.
- X. All fresh or newly constructed specimens were tested in this study. However, there is always scope to repair or retrofit these specimens and test them again. And different retrofitting or repairing techniques can be adopted.

REFERENCES

AFPS-90, (1990) –Recommendations for the Redaction of Rules Relative to the Structures and Installations Built in Regions Prone to Earthquakes”, *French Association of Earthquake Engineering*, Paris, France.

Alam, M. T., (2014) *Behaviour of Randomly Infilled RC Frames with Soft Ground Floor Subjected to Seismic Loading*, M.Sc. Thesis, Department of Civil Engineering, Bangladesh University of Engineering and Technology.

Al-Chaar, G. K., Berman, J. B., and Sweeney, S.C., (2003) –Investigation of FRP for Seismic Rehabilitation of RC Structural Frames with URM Infill.” *Report No. ERDC/CERL TR-03- 10*, US Army Corps of Engineers.

Algerian Seismic Code, (1988) –Algerian Earthquake Resistant Regulations”, Ministry of Town planning and Construction, Algiers, Algeria.

Ali, M. M., Alam, M., Z., Asif, M. M., Purkayastha, S., and Ahsan, R., (2017) –Damage Assessment of Rural Infrastructure due to Cyclone in Bangladesh”, *Proceedings of International Conference on Disaster Risk Management*, Bangladesh.

Almusallam, T. H.; Al-Salloum, Y. A., (2007) –Behavior of FRP Strengthened Infill Walls under In-Plane Seismic Loading”, *The American Society of Civil Engineers (ASCE), Journal of Composites for Construction*, Vol. 11, No. 3, pp. 308-318, DOI: 10.1061/(ASCE)1090-0268(2007)11:3(308).

Alwashali, H., Sen, D., Jin, K., and Maeda, M., (2019) –Experimental Investigation Of Influences of Several Parameters on Seismic Capacity Of Masonry Infilled Reinforced Concrete Frame”, Elsevier, *Engineering Structures*, Vol. 189, pp. 11-24, DOI: 10.1016/j.engstruct.2019.03.020.

Akhter, S. H., (2010) –Earthquakes of Dhaka. Environment of Capital Dhaka—Plants Wildlife Gardens Parks Air Water and Earthquake”. *Asiatic Society of Bangladesh*, pp. 401-426.

Al-Zaman ,M. D., and Monira, N. J., (2017) –A Study of Earthquakes in Bangladesh and The Data Analysis of The Earthquakes That Were Generated in Bangladesh and Its' Very Close Regions for The Last Forty Years (1976-2016)", *Journal of Geology & Geophysics*, Vol. 6, No. 4, pp. 300, DOI: 10.4172/2381-8719.1000300.

American Society for Testing and Materials (ASTM) C33, (2020) Standard Specification for Concrete Aggregates, *ASTM International*, West Conshohocken, PA, United States of America.

American Society for Testing and Materials (ASTM) C67, (2020) Standard Test Methods for Sampling and Testing Brick and Structural Clay Tile, *ASTM International*, West Conshohocken, PA, United States of America.

American Society for Testing and Materials (ASTM) C109, (2020) Standard Test Method for Compressive Strength of Hydraulic Cement Mortars (Using 2-in. or [50-mm] Cube Specimens), *ASTM International*, West Conshohocken, PA, United States of America.

American Society for Testing and Materials (ASTM) C39, (2020) Standard Test Method for Compressive Strength of Cylindrical Concrete Specimens, *ASTM International*, West Conshohocken, PA, United States of America.

American Society for Testing and Materials (ASTM) C1314, (2020) Standard Test Method for Compressive Strength of Masonry Prisms, *ASTM International*, West Conshohocken, PA, United States of America.

Ansary, M. A., and Arefin, M. R., (2020) –Assessment of Predominant Frequencies in Dhaka City, Bangladesh Using Ambient Vibration", Springer, *Asian Journal of Civil Engineering*, Vol. 21, pp. 91-104.

Antoniadis, K. D., Assael, M. J., Tsiglifisi, C. A., and Mylona, S. K., (2012) –Improving the Design of Greek Hollow Clay Bricks", Springer, *International Journal of Thermophysics*, Vol. 33, pp. 2274–2290, DOI: 10.1007/s10765-012-1294-x.

Asif, M. M., Alam, M. Z., and Ahsan, R., (2021) –Experimental Study on Behavior of Ferrocement Retrofitted Unconfined URM Wall under Cyclic Loading", Springer, *Asian Journal of Civil Engineering*, Vol. 22, No. 6, pp. 1059–1074, DOI: 10.1007/s42107-021-

00365-0.

Asif, M. M., Alam, M. Z., and Ahsan, R., (2020) –An Experimental Investigation of Ferrocement Retrofitted Masonry Wall Units Subjected to Cyclic Loading, *Proceedings of 5th International Conference on Advances in Civil Engineering*, Bangladesh.

Asif, M. M., Alam, M., Z., and Ahsan, R., (2019) –Capacity of Roof Cladding of Rural Housing against Blowing due to Storm Wind”, *Proceedings of International Conference on Disaster Risk Management*, Bangladesh.

Asteris, P. G., Antoniou, S. T., Sophianopoulos, D. S., and Chrysostomou, C. Z., (2011) –Mathematical Macromodeling of Infilled Frames: State of the Art”, The American Society of Civil Engineers (ASCE), *Journal of Structural Engineering*, VOL. 137, No. 12, pp. 1508-1517 , DOI: 10.1061/(ASCE)ST.1943-541X.0000384.

Asteris, P. G., Demetrios, K., Chrysostomou, C. Z., and Smyrou, E., (2011) –Failure Modes of Infilled Frames,” *Electric Journal of Structural Engineering*, Vol. 11, No. 1, pp. 11-20.

BDS EN 197-1, (2003), Cement, Part-1, Composition, Specification and Conformity Criteria for Common Cements, *Bangladesh Standard*.

Bekele, L., (2016) *Effects of Masonry Infills on Reinforced Concrete Frame Buildings*, M.Sc. Thesis, School of Civil and Environmental Engineering, Addis Ababa University.

Biswas, R. N., Islam, M. N., and Islam, M. N., (2018) –Modeling on Management Strategies for Spatial Assessment of Earthquake Disaster Vulnerability In Bangladesh”, Springer, *Modeling Earth Systems and Environment*, Vol. 4, pp. 1377–1401,

BNBC, (1993) Housing and Building Research Institute and Bangladesh Standards and Testing Institution, *Bangladesh National Building Code*.

BNBC, Volume 2, Part 6-Structural Design, chapter 2, (2020) Loads on Buildings and Structures, Housing and Building Research Institute, Bangladesh, *Bangladesh National Building Code*.

BNBC, Volume 2, Part 6-Structural Design, chapter 7, (2020) Masonry Structures, Housing and Building Research Institute, Bangladesh, *Bangladesh National Building Code*.

BNBC, Volume 2, Part 6-Structural Design, chapter 8, (2020) Detailing of Reinforcement in Concrete Structures, Housing and Building Research Institute, Bangladesh, *Bangladesh National Building Code*.

Bolis, V., Starvridis, A., and Preti, M., (2017) –Numerical Investigation of the In-Plane Performance of Masonry-Infilled RC Frames with Sliding Subpanels”, The American Society of Civil Engineers (ASCE), *Journal of Structural Engineering*, Vol. 143, No 2, pp. 04016168-1-18. DOI: 10.1061/(ASCE)ST.1943-541X.0001651.

Buonopane, S. G., and White, R.N., (1999) –Pseudodynamic Testing of Masonry Infilled Reinforced Concrete Frame” The American Society of Civil Engineers (ASCE), *Journal of Structural Engineering*, Vol. 125, No 6, pp. 578-589. DOI: 10.1061/(ASCE)0733-9445(1999)125:6(578).

Calvi, G. M., Bolognini, D., and Penna, A., (2004) –Seismic Performance of Masonry Infilled RC Frames: Benefits of Slight Reinforcement.” *Proceedings of 6th Nat. Conf. on Seismology and Earthquake Engineering*, pp. 253-276, Portugal.

Cavaco, E., Grilo, I., Gouveia, J. P., Julio, E., and Neves, L., (2018) –Mechanical Performance of Eco-Efficient Hollow Clay Bricks Incorporating Industrial Nano-Crystalline Aluminium Sludge”, Taylor & Francis, *European Journal of Environmental and Civil Engineering*, Vol. 24, No. 12, pp. 1-18, DOI: 10.1080/19648189.2018.1492974.

Centeno J., Ventura, C. E., and Foo, S., (2008) –Shake Table Testing of Gravity Load Designed Reinforced Concrete Frames with Masonry Infill Walls.” *Proceedings of the 14th World Conference on Earthquake Engineering*, China.

Chiou, T. C., and Hwang. S. J., (2015) –Tests on Cyclic Behavior of Reinforced Concrete Frames with Brick Infill”, *Earthquake Engineering & Structural Dynamics*, Vol. 44, No. 12, pp. 1939-1958, DOI: 10.1002/eqe.2564.

Climent A. B., Marquez, A. R., and Pujol, S., (2018) –Seismic Strengthening of Low-Rise

Reinforced Concrete Frame Structures with Masonry Infill Walls: Shaking-Table Test”, Elsevier, *Engineering Structures*, Vol. 165, pp. 142-151, DOI: 10.1016/j.engstruct.2018.03.026.

Colangelo, F., (2013) –Pseudo-Dynamic Seismic Response of Reinforced Concrete Frames Infilled with Non-Structural Brick Masonry”, *Earthquake Engineering & Structural Dynamics*, Vol. 34, pp. 1219–1241, DOI: 10.1002/eqe.477.

Costa Rican Seismic Code, (1986) –Seismic Code of Costa Rica”, *Federal College of Engineers and Architects of Costa Rica*, San Jose, Costa Rica.

Crisafulli, F. J., (1997) *Seismic Behavior of Reinforced Concrete Structures With Masonry Infills*, Ph.D. Thesis, Department of Civil Engineering, University of Canterbury.

Dautaj, A. D., Kadiri, Q., and Kabashi, N., (2018) –Experimental Study on The Contribution of Masonry Infill In The Behavior of RC Frame Under Seismic Loading”, Elsevier, *Engineering Structures*, Vol. 165, pp. 27-35, DOI: 10.1016/j.engstruct.2018.03.013.

De Angelis, A., and Pecce, M. A., (2020) –The Role of Infill Walls in the Dynamic Behavior and Seismic Upgrade of a Reinforced Concrete Framed Building”, *Frontiers in Built Environment*, Vol. 6, pp. 1-14.

DM (Ministerial Decree), (2008) Nuove norme tecniche per le costruzioni [New technical codes for constructions]. Rome: *Ministry of Infrastructures and Transportations*.

Egyptian Seismic Code, (1988) –Regulations for Earthquake Resistant Design of Buildings in Egypt”, *Egyptian Society for Earthquake Engineering*, Cairo, Egypt.

Essa, A. S. A. T., Badr, M. R. K., and El-Zanaty, A. H., (2013) –Effect of Infill Wall on The Ductility And Behavior of High Strength Reinforced Concrete Frames”, Taylor and Francis, *HBRC Journal*, Vol. 10, pp. 258–264, DOI: 10.1016/j.hbrcj.2013.12.005.

Eurocode 8. Design of structures for earthquake resistance, (2004) Part 1: *General rules, seismic actions and rules for buildings*. Brussels: CEN.

Fardis, M. N., Calvi, G. M., and Panagiotakos, T. B., (1996) –Studies for the Development of Code Provisions for Infilled RC Frames,” *Proceedings of the 11th World Conference on Earthquake Engineering*, Mexico.

Fardis, M. N., Bousias, S. N., Franchioni, G., and Panagiotakos, T.B., (1999) –Seismic Response and Design of RC Structures with Plan-Eccentric Masonry Infills.” *Journal of Earthquake Engineering and Structural Dynamics*, Vol. 28, pp. 173-191.

FEMA 306, (1998) Evaluation of Earthquake Damaged Concrete and Masonry Wall Buildings. *Basic procedures manual*, Washington D.C.: Federal Emergency Management Agency.

FEMA 356, (2000) Pre-Standard and Commentary for The Seismic Rehabilitation of Buildings. *Basic procedures manual*, Washington, DC: Federal Emergency Management Agency.

Fiorato, A. E., Sozen, M. A., and Gamble, W. L., (1970) –An Investigation of The Interaction of Reinforced Concrete Frames with Masonry Filler Walls.” *Report No. UILU-ENG 70-100*, Dept. of Civ. Eng., University of Illinois at Urbana-Champaign.

Ghosh, A. K., and Amde, A. M., (2002) –Finite Element Analysis of Infilled Frames”, The American Society of Civil Engineers (ASCE), *Journal of Structural Engineering*, Vol. 128, No 7, pp. 881-889.

Gomez, J. M., (2012) *Innovative Retrofitting Materials for Brick Masonry Infill walls*, M.Sc. Thesis, Structural Analysis of Monuments and Historical Constructions, University of Minho.

Hashemi, A. and Mosalam, K. M., (2006) –Shake-Table Experiment on Reinforced Concrete Structure Containing Masonry Infill Wall.” *Journal of Earthquake Engineering and Structural Dynamics*, Vol. 9, No. 1, pp. 73-83.

Henderson, R.C., Fricke, K.E., Jones, W. D., Beavers, J. E. and Bennett, R. M., (2003) –Summary of a Large- and Small-Scale Unreinforced Masonry Infill Test Program”, The American Society of Civil Engineers (ASCE), *Journal of Structural Engineering*, Vol.129, No.12, pp. 1667-1675.

Holmes, M., (1961) –Steel Frames with Brickwork and Concrete Infilling”, *Proceedings of the Institution of Civil Engineers: Structures and Buildings*, Vol. 19, pp. 473–478.

Hossain, B., and Hossain, S. S., (2020) –Probabilistic Estimation of Seismic Parameters for Bangladesh”, *Arabian Journal of Geosciences*, Vol. 13, No. 6, pp. 262.

Huang, Q., Guo, Z., and Kuang, J. S., (2016) –Designing Infilled Reinforced Concrete Frames with The ‘Strong Frame-Weak Infill’ Principle”, Elsevier, *Engineering Structures*, Vol. 123, pp. 341–353, DOI: 10.1016/j.engstruct.2016.05.024.

IS-1893, (2002) Bureau of Indian Standards, Indian Standard Criteria for Earthquake Resistant Design of Structures—Part 1: *General Provisions and Buildings (Fifth Revision)*, New Delhi, India.

Islam, A. S., Bala, S. K., Hussain, M. A., Hossain, M. A., and Rahman, M. M., (2010) –Performance of coastal structures during cyclone Sidr”, The American Society of Civil Engineers (ASCE), *Natural Hazards Review*, Vol. 12, No.3, pp. 111-116.

Kakaletsis, D., (2010) –Comparison of CFRP and Alternative Seismic Retrofitting Techniques for Bare and Infilled RC Frames”, The American Society of Civil Engineers (ASCE), *Journal of Composites for Construction*, Vol. 15, No.4, pp. 565-577, DOI: 10.1061/(ASCE)CC.1943-5614.0000196.

Kareem, K., M., and Guneyisi, E. M., (2019) –Effect of Masonry Infill Wall Configuration and Modelling Approach on the Behaviour of RC Frame Structures”, Springer, *Arabian Journal for Science and Engineering*, Vol. 44, pp. 4309–4324, DOI: 10.1007/s13369-018-3389-6.

Khan, A. A., (2018) –The Geo-Genetic Status of Earthquake-Related Hazards And The Role of Human And Policy Dimensions in Impact Mitigation”, *Environmental Hazards*, Vol.17, No.4, pp. 276–291.

Li, S., Kose, M. M., Shan, S., and Sezen, H., (2019) –Modeling Methods for Collapse Analysis of Reinforced Concrete Frames with Infill Walls”, The American Society of Civil Engineers (ASCE), *Journal of Structural Engineering*, Vol. 145, No. 4, pp. 04019011-1-12, DOI: 10.1061/(ASCE)ST.1943-541X.0002285.

Liauw, T. C. and Kwan, K. H., (1985) –Unified Plastic Analysis for Infilled Frames”, The American Society of Civil Engineers (ASCE), *Journal of the Structural Engineering*, , Vol. 120, No.9, pp. 1861-1876.

Lourenco, P. B., Brost, R. D. and Rots, J. G., (1997) –A Plane Stress Softening Plasticity Model For Orthotropic Materials”, *International Journal For Numerical Methods In Engineering*, Vol. 40, pp. 4033-4057.

Madan, A., Reinhorn, A. M., Mander, J. B., and Valles, R. E., (1997) –Modeling of Masonry Infill Panels For Structural Analysis”, The American Society of Civil Engineers (ASCE), *Journal of Structural Engineering*, Vol. 123, No. 10, pp. 1295-1297.

Maidiawati, and Sanada, Y., (2017) –R/C frame–infill interaction model and its application to Indonesian Buildings” *Earthquake Engineering & Structural Dynamics*, Vol. 46, No.2, pp. 221-241, DOI: 10.1002/eqe.2787.

Mainstone, R. J., (1971) –On the stiffnesses and Strengths of Infilled Frame”, *Proceedings of the Institution of Civil Engineers*, Supplement IV, pp. 57-90.

Mallick, D. V., and Severn, R. T., (1971) –The Behavior of Infilled Frame under Static Loading”, *Proceedings of the Institution of the Civil Engineering*, Vol. 49, pp. 193-209.

Mander, J.B., Nair, B., Wojtkowski, K., and Ma, J., (1993) –An Experimental Study on the Seismic Performance of Brick-infilled Steel Frames with and without Retrofit”, *Rep. NCEER-93-0001*, State University of New York at Buffalo, United States of America.

Mehrabi, A. B., Shing, P. B., Schuller, M.P., and Noland, J. L., (1994) –Performance of Masonry-Infilled R/C Frames under In-Plane Lateral Loads.” *Report No. CU/SR-94/6*, University of Colorado at Boulder.

Mehrabi, A. B., Shing, P. B., Schuller, M. P., and Noland, J. N., (1996) –Experimental Evaluation of Masonry-Infilled RC Frames”, The American Society of Civil Engineers (ASCE), *Journal of Structural Engineering*, Vol. 122, No. 3, March, pp 228-237, DOI: 10.1061/(ASCE)0733-9445(1996)122:3(228).

Mehrabi, A. B., and Shing, P. B., (1997) –“Finite Element Modeling of Masonry-Infilled RC Frames”, The American Society of Civil Engineers (ASCE), *Journal of Structural Engineering*, Vol. 123, No. 5, pp. 604-613.

Misir, I. S., (2014) –“Potential Use of Locked Brick Infill Walls to Decrease Soft-Story Formation in Frame Buildings”, The American Society of Civil Engineers (ASCE), *Journal of Performance of Constructed Facilities*, Vol. 29, No. 5, pp. 04014133-1-10, DOI : 10.1061/(ASCE)CF.1943-5509.0000633.

Mohammadi, M., and Nikfar, F., (2013) –“Strength and Stiffness of Masonry-Infilled Frames with Central Openings Based on Experimental Results”, The American Society of Civil Engineers (ASCE), *Journal of Structural Engineering*, Vol. 139, No 6, pp. 974-984. DOI: 10.1061/(ASCE)ST.1943-541X.0000717.

Mondal, G., and Tesfamariam, S., (2013) –“Effects of Vertical Irregularity and Thickness of Unreinforced Masonry Infill on The Robustness Of RC Framed Buildings”, *Earthquake Engineering Structural Dynamics*, Vol. 43, No. 2, pp. 205-223, DOI: 10.1002/eqe.2338.

Moretti, M. L., Papatheocharis, T., and Perdikaris, P. C., (2014) –“Design of Reinforced Concrete Infilled Frames”, The American Society of Civil Engineers (ASCE), *Journal of Structural Engineering*, Vol. 140, No.9, pp. 04014062-1-10, DOI: 10.1061/(ASCE)ST.1943-541X.0001042.

Murthy, C. V. R., and Jain, S. K., (2000) –“Beneficial Influence of Masonry Infill Walls on Seismic Performance of RC Frame Buildings”, *12WCEE 2000 : 12th World Conference on Earthquake Engineering*, New Zealand.

Murty, T. S., and Neralla, V. R., (1992) –“On The Recurvature of Tropical Cyclones and The Storm Surge Problem in Bangladesh”, *Natural Hazards*, Vol. 6, pp. 275-279.

Negro, P., and Verzeletti, G., (1996) –“Effect of Infills on the Global Behavior of R/C Frames: Energy Considerations from Pseudo dynamic Response”, *Earthquake Engineering and Structural Dynamics*, Vol. 25, No. 8, pp. 753-773, DOI: 10.1002/(SICI)1096-9845(199608)25:8<753::AID-EQE578>3.0.CO;2-Q.

NBC-105, (1995) –“Nepal National Building Code for Seismic Design of Buildings in

Nepal”, *Ministry of Housing and Physical Planning, Department of Buildings, Kathmandu, Nepal.*

NSR-98, (1998) –Colombian Standards for Seismic Resistant Design and Construction”, Bogota, Colombia.

NZS-3101, (1995) –Code of Practice for the Design of Concrete Structures”, Part 1, *Standards Association of New Zealand, Wellington, New Zealand.*

Papia, M., (1998) –Analysis of Infilled Frames Using a Coupled Finite Element and Boundary Element Solution Scheme”, *International Journal For Numerical Methods In Engineering*, Vol. 26, 731-742.

Park, C. Y., Kim, H., Eom, C. D., Kim, G. C., and Lee, J. J., (2014) –Effect of lintel on horizontal load-carrying capacity in post-beam structure”, *Journal of Wood Science*, Vol. 60, pp. 30-38, DOI: 10.1007/s10086-013-1371-1.

Paul, A., and Rahman, (2006) –Cyclone Mitigation Perspectives in the Islands of Bangladesh: A Case of Sandwip and Hatia Islands”, *Coastal Management*, Vol. 34, No. 2, pp. 199-215.

Pavlik, Z., Fiala, L., Vejmelkova, E., and Cerny, R., (2012) –Application of Effective Media Theory for Determination of Thermal Properties of Hollow Bricks as a Function of Moisture Content”, Springer, *International Journal of Thermophysics*, Vol. 34, pp. 894–908, DOI: 10.1007/s10765-012-1183-3.

Polyakov, S. V., (1960) "On the Interaction between Masonry Filler Walls and Enclosing Frame when Loaded in the Plane of the Wall", *Translation in earthquake engineering*, pp. 36-42.

Preti M., and Bolis, V., (2017) –Masonry Infill Construction And Retrofit Technique For The Infill-Frame Interaction Mitigation: Test Results”, Elsevier, *Engineering Structures*, Vol. 132, pp. 597–608, DOI: 10.1016/j.engstruct.2016.11.053.

Rahman, S., and Rahman, M. A., (2015) –Climate extremes and challenges to

infrastructure development in coastal cities in Bangladesh”, Elsevier, *Weather and Climate Extremes*, Vol. 7, pp. 96-108.

Ricci, P., Domenico, M. D., and Verderame, G. M., (2018) –Empirical-Based Out-Of-Plane URM Infill Wall Model Accounting for The Interaction with In-Plane Demand”, *Earthquake Engineering Structural Dynamics*, Vol. 47, No. 3, pp. 802-827, DOI: 10.1002/eqe.2992.

Rodrigues, H., Furtado, A., Vila-Pouca, N., Varum, H., and Barbosa, A. R., (2018) –Seismic Assessment of a School Building in Nepal and Analysis of Retrofitting Solutions”, Springer, *International Journal of Civil Engineering*, Vol. 16, pp. 1573–1589.

Samai, M. L., (1984) *Behavior of Reinforced Concrete Frames With Lightweight Blockwork Infill Panels*, Ph.D. Thesis, Department of Civil and Structural Engineering, University of Sheffield.

Saneinejad, A. and Hobbs, B., (1995) –Elastic Design of Infilled Frames”, The American Society of Civil Engineers (ASCE), *Journal of Structural Engineering*, Vol. 121, No. 4, pp. 634-643.

Shailendra, S., and Babula, B. H., (2015) –Seismic Response of Soft Storey on High Rise Building Frame”, *International Journal of Engineering Technology and Computer Research*, Vol. 3, No.4, pp. 41-48.

Shing, P. B., and Mehrabi, A. B., (2002) –Behaviour and analysis of masonry-infilled frames”, *Progress in Structural Engineering and Materials*, Vol. 4, pp. 320-331.

Shing, P. B., Stavridis, A., Koutromanos, I., Willam, K., Blackard, B., Kyriakides, M. A., Billington, S. L., and Arnold, S., (2009) –Seismic Performance of Non-Ductile RC Frames with Brick Infill”, The American Society of Civil Engineers (ASCE), *ATC and SEI Conference on Improving the Seismic Performance of Existing Buildings and Other Structures*, pp. 1117–1128, DOI: 10.1061/41084(364)102.

Smith, B.S., (1966) –Behavior of the Square Infilled Frames”, The American Society of Civil Engineers (ASCE), *Journal of the Structural Division*, Vol. 2, No. 1, pp. 381-403.

Smith, B. S., and Coull, A. (1991) –Fall Building Structures Analysis and Design”, John Wiley & Sons, inc , *A Infilled-Frame Structures*, chapter. 8, pp.168-174, United States of America.

Smolira, M., (1974) –Analysis of Infilled Shear Walls”, *Proceedings of the Institution of Civil Engineers*, Vol. 55, pp. 895-912.

SNIP-II-7–81, (1996) –Building Code on Construction in Seismic Areas”, *The Ministry for Construction of Russia*, Moscow, Russia.

Soulis, V. J., (2019) –The Stress State Of Masonry Infilled Panel Under Different Surrounding Conditions of Contact with The RC Frame”, Springer, *Asian Journal of Civil Engineering*, Vol. 20, pp. 807–820, DOI: 10.1007/s42107-019-00146-w.

Stavroulaki, M. E., and Liarakos, V. B., (2012) –Dynamic analysis of a masonry wall with reinforced concrete lintels or tie-beams”, Elsevier, *Engineering Structures*, Vol. 44, pp. 23-33, DOI: 10.1016/j.engstruct.2012.05.041.

Su, Q., Cai, G., and Cai, H., (2016) –Seismic Behaviour of Full-Scale Hollow Bricks-Infilled RC Frames Under Cyclic Loads”, Springer, *Bulletin of Earthquake Engineering*. Vol. 15, No. 7, pp. 2981-3012, DOI: 10.1007/s10518-016-0074-6.

Tang, B., Chen, S., Li, X., Xiong, L., Chen, H., and Feng, Q., (2019) –Seismic Performance of RC Frames with EPSC Latticed Concrete Infill Walls”, Elsevier, *Engineering Structures*, Vol. 197, pp. 1-14, DOI: 10.1016/j.engstruct.2019.109437.

Tomazevic, M., (1999) –Earthquake - resistant design of masonry buildings”, London: Imperial College Press.

Trapani, F. D., Macaluso, G., Cavaleri, L., and Papia, M., (2015) –Masonry Infills and RC Frames Interaction: Literature Overview And State of The Art of Macromodeling Approach”, Taylor and Francis, *European Journal of Environmental and Civil Engineering*, Vil. 19, No. 9, pp. 1059-1095, DOI: 10.1080/19648189.2014.996671.

UBC, (1997) *Structural Engineering Design Provisions*, International Conference of

Building Officials, *Uniform Building Code*.

Vicente, R.S., Rodrigues, H., Varum, H., Costa, A., and Silva, J. A. R. M. D., (2012) –Performance of Masonry Enclosure Walls: Lessons Learned from Recent Earthquakes.” *Earthquake Engineering and Engineering Vibration*. Vol. 11, No. 1, pp. 23–34, DOI: 10.1007/s11803-012-0095-3.

Wararuksajja, W., Srechai, J., and Leelataviwat, S., (2020) –Seismic Design of RC Moment-Resisting Frames with Concrete Block Infill Walls Considering Local Infill-Frame Interactions”, Springer, *Bulletin of Earthquake Engineering*, Vol. 18, pp. 6445–6474, DOI: 10.1007/s10518-020-00942-9.

Yadav, R. K., Kumar, R., RajanKumar, and Nagarathinam, L., (2019) –Experimental Examination of Hollow Brick Masonry Wall with Reinforcement”, *International Journal of Recent Technology and Engineering*, Vol. 8, No.4, pp. 4690-4684.

Yadollahi, M. M., Benli, A., and Varolgunes, S., (2016) –Masonry Infill Walls Effect in Short Column Formation in Rc Buildings: A Case Study”, *Journal of Engineering Sciences*, Vol. 19, No. 2, pp. 78-83.

Venezuelan Seismic Code, (1988) Regulations for Earthquake Resistant Buildings, *Comision De Normas Industriales, Covenin*, Caracas, Venezuela.

Zarnic, R., Gostic S., Crewe A. J., and Taylor C.A., (2001) –Shaking table tests of 1:4 reduced-scale models of masonry infilled RC frame buildings.” *J. Earthquake Eng. Struct. Dyn.*, Vol. 30, pp. 819-834.

Zerin, A. I., (2018) *Experimental Investigation of the In-plane Cyclic Response of Infilled Reinforced Concrete Frame and Their Possible Retrofit Measures*, M.Sc. Thesis, Department of Civil Engineering, Bangladesh University of Engineering and Technology.

Zhang, H., Kuang, J. S., and Yuen, T. Y. P., (2017) –Low-Seismic Damage Strategies for Infilled RC Frames: Shake-Table Tests”, *Earthquake Engineering & Structural Dynamics*, Vol. 46, No. 4, pp. 2419-2438, DOI: 10.1002/eqe.2911.

Zovkic, J., Sigmund, V., and Guljas, I., (2013) –Cyclic Testing of A Single Bay Reinforced Concrete Frames with Various Types of Masonry Infill”, *Earthquake Engineering & Structural Dynamics*, Vol. 42, No. 8, pp. 1131–1149, DOI: 10.1002/eqe.2263.

Websites

Banglapedia (2021), <https://en.banglapedia.org/index.php/Cyclone>. (Date of access: 25/06/2022).

burro.case.edu (2002), <http://burro.case.edu/Academics/Astr221/SolarSys/tectonics.html>. (Date of access: 24/06/2022).

Civilclick (2020), <https://www.civilclick.com/lintel-beam/>. (Date of access: 27/06/2022).

Daily Civil (2022), <https://dailycivil.com/what-is-lintel-types-of-lintels-and-uses-in-building/#:~:text=A%20lintel%20is%20a%20horizontal,as%20that%20of%20the%20wall>. (Date of access: 27/06/2022).

Go Smart Bricks (2022), <http://gosmartbricks.com/hollow-bricks/>. (Date of access: 26/06/2022).

Hindustan Times (2015), <https://www.hindustantimes.com/india/five-major-earthquakes-to-have-struck-india/story-0TixSQULO1tYXGTEcOlqQL.html>. (Date of access: 25/06/2022).

SciJinks (2022), <https://scijinks.gov/hurricane/>. (Date of access: 25/06/2022).

Weather Underground (1999), <https://www.wunderground.com/hurricane/articles/deadliest-tropical-cyclones>. (Date of access: 25/06/2022).

Wikipedia: List of Earthquakes in Bangladesh (2022), https://en.wikipedia.org/wiki/List_of_earthquakes_in_Bangladesh. (Date of access: 25/06/2022).

Appendix-A

YIELD STRENGTH AND ULTIMATE STRENGTH OF REINFORCEMENT

Table A.1: Yield strength and ultimate strength of reinforcement

Dia (mm)	Weight /Length (kg/m)	Area of Bar (mm ²)	Yield Load (KN)	Yield Strength (MPa)	Average Yield Strength (MPa)	Ultimate Load (KN)	Ultimate Strength (MPa)	Average Ultimate Strength (MPa)	Elongation (%)
8	0.399	50	23.4	468	472	34.3	686	686	15
8	0.398	50	23.6	472		34.3	686		15
8	0.399	50	23.8	476		34.3	686		15
12	0.886	113	53.0	469	465	72.0	637	637	17
12	0.887	113	52.5	465		72.0	637		16
12	0.883	113	52.0	460		72.0	637		17



Figure A.1: Testing of rebar.

Appendix-B

COMPRESSIVE STRENGTH OF SOLID AND PERFORATED CLAY BRICK

Table B.1: Compressive strength of solid clay brick

Brick	Length (mm)	Width (mm)	Height (mm)	Area (mm ²)	Observed load (KN)	Actual load (KN)	Compressive Strength (MPa)	Average Compressive strength (MPa)
1	100.50	55.00	31.00	5527.50	276.00	266.40	48.20	40.39
2	100.50	53.50	33.00	5376.75	242.00	232.27	43.20	
3	99.50	55.50	31.00	5522.25	230.00	220.22	39.88	
4	99.50	51.50	32.00	5124.25	194.00	184.08	35.92	
5	100.00	53.00	31.00	5300.00	194.00	184.08	34.73	

Table B.2: Compressive strength of perforated clay brick

Brick	Length (mm)	Width (mm)	Height (mm)	Area (mm ²)	Observed load (KN)	Actual load (KN)	Compressive Strength (MPa)	Average Compressive strength (MPa)
1	102.50	58.00	30.00	5114.05	140.00	129.86	25.39	26.80
2	103.00	55.50	33.00	4885.55	196.00	186.08	38.09	
3	102.00	56.00	32.00	4881.05	112.00	101.75	20.85	
4	102.00	57.50	33.00	5034.05	124.00	113.80	22.61	
5	100.00	57.00	33.00	4869.05	142.00	131.87	27.08	



(a)



(b)

Figure B.1: (a) Capping of bricks before testing, (b) Compressive strength testing of brick.

Appendix-C

ABSORPTION CAPACITY OF SOLID AND PERFORATED CLAY BRICK

Table C.1: Absorption capacity of solid clay brick

Brick	SSD weight (gm)	Dry Weight (gm)	Absorption Capacity (%)	Average Absorption Capacity (%)
1	396.00	345.00	14.78	14.67
2	389.00	340.00	14.41	
3	404.00	352.00	14.77	
4	399.00	347.00	14.99	
5	366.00	320.00	14.38	

Table C.2: Absorption capacity of perforated clay brick

Brick	SSD weight (gm)	Dry Weight (gm)	Absorption Capacity (%)	Average Absorption Capacity (%)
1	353.00	313.00	12.78	12.84
2	351.00	310.00	13.23	
3	326.00	290.00	12.41	
4	346.00	306.00	13.07	
5	346.00	307.00	12.70	



(a)



(b)

Figure C.1: Weighting of (a) solid clay brick and (b) perforated clay brick during absorption capacity testing.

Appendix-D

COMPRESSIVE STRENGTH OF MORTAR CUBE

Each mortar cube size: 50 mm × 50 mm × 50 mm

Table D.1: Compressive strength of mortar cube

Days	Cube	Area (mm ²)	Observed load (KN)	Actual load (KN)	Stress (MPa)	Average stress (MPa)
7	1	2500	17.00	17.64	7.06	7.19
	2	2500	20.00	20.67	8.27	
	3	2500	15.00	15.63	6.25	
14	4	2500	28.60	29.33	11.73	12.61
	5	2500	30.50	31.25	12.50	
	6	2500	33.20	33.97	13.59	
28	7	2500	31.98	32.74	13.10	14.39
	8	2500	35.80	36.59	14.64	
	9	2500	37.78	38.59	15.43	



(a)



(b)

Figure D.1: (a) Prepared mortar cubes (b) mortar testing.

Appendix-E

COMPRESSIVE STRENGTH OF CONCRETE CYLINDER

Each cylinder size: 100 mm (Dia) × 200 mm (Height)

Table E.1: Compressive strength of concrete cylinder

Days	Cylinder	Average Dia (mm)	Area (mm ²)	Observed load (KN)	Actual load (KN)	Compressive Strength (MPa)	Average Compressive Strength (MPa)
14	1	101.225	8047.60	150.00	147.13	18.28	17.90
	2	101.05	8019.80	150.00	147.13	18.35	
	3	101.225	8047.60	140.00	137.28	17.06	
21	4	101	8011.87	185.00	183.14	22.86	20.72
	5	101.15	8035.68	170.00	168.12	20.92	
	6	101.3	8059.53	150.00	148.09	18.37	
28	7	101	8011.87	181.00	177.64	22.17	21.63
	8	101.325	8063.51	178.00	174.69	21.66	
	9	101.325	8063.51	173.00	169.77	21.05	



(a)



(b)

Figure E.1: (a) Prepared concrete cylinders (b) cylinder testing.

Appendix-F

COMPRESSIVE STRENGTH OF SOLID AND PERFORATED BRICK PRISM

Table F.1: Compressive strength of solid brick prism

Brick	Length h (mm)	Width (mm)	Height (mm)	Area (mm ²)	Applied load (KN)	Compressive Strength(MPa)	Average Compressive Strength (MPa)
1	110	100	180	11000	159	14.45	11.08
2	115	100	190	11500	119	10.35	
3	115	105	190	12075	102	8.45	

Table F.2: Compressive strength of perforated brick prism

Brick	Length h (mm)	Width (mm)	Height (mm)	Area (mm ²)	Applied load (KN)	Compressive Strength (MPa)	Average Compressive Strength (MPa)
1	120	100	190	10338.09	54	5.22	4.50
2	118	102	190	10374.09	40	3.86	
3	115	105	180	10413.09	46	4.42	



(a)



(b)

Figure F.1: (a) Prepared prisms (b) testing of prisms.

Appendix-G

HYDRAULIC JACKS

Hydraulic Jack 1 (Jack ID: 31431)

Piston diameter : 85 mm

Piston Perimeter : 267 mm

Ram area : 5675 mm²

Body Height : 370 mm

Operating Temperature : 24°C

Pump : Manual

Capacity : 50 Ton

Allowable Pressure Range of Pressure Gauge : 0-150 MPa

Calibration Device Used Digital (Display in Load (KN)) Load Cell: CCDHA-50t-004-000
s/n: 49625

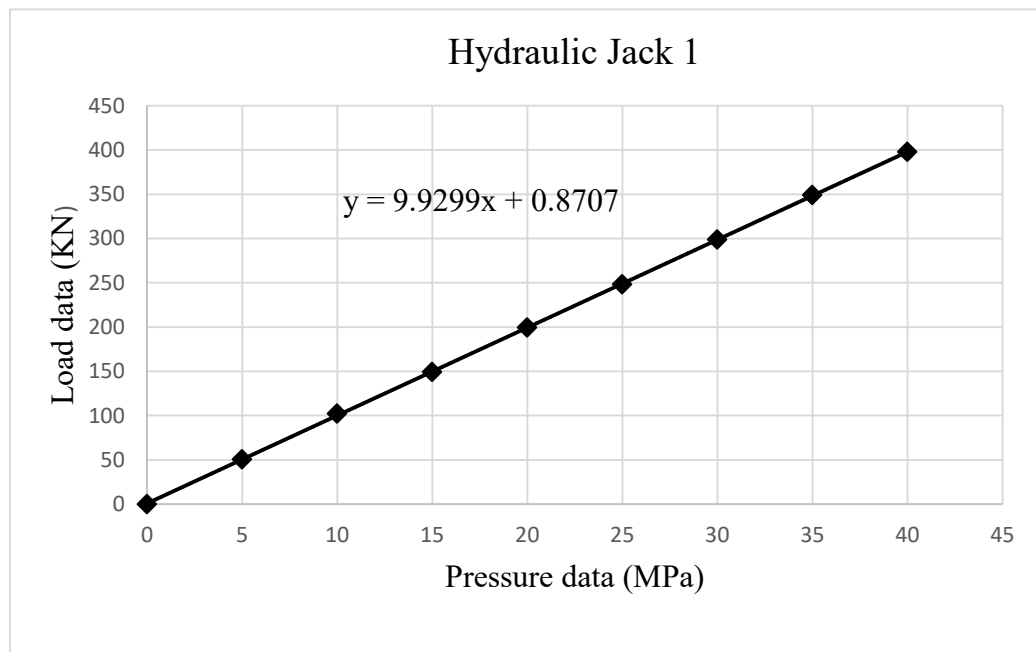


Figure G.1: Calibration curve of hydraulic jack 1.

Hydraulic Jack 2 (Jack ID: SM01)

Piston diameter : 50 mm

Piston Perimeter : 157 mm

Ram area : 1964 mm²

Body Height : 313 mm

Operating Temperature : 24°C

Pump : Manual

Capacity : 30 Ton

Allowable Pressure Range of Pressure Gauge : 0-60000 lbs

Calibration Device Used Digital (Display in Load (KN)) Load Cell: CCDHA-50t-004-000

s/n: 49625

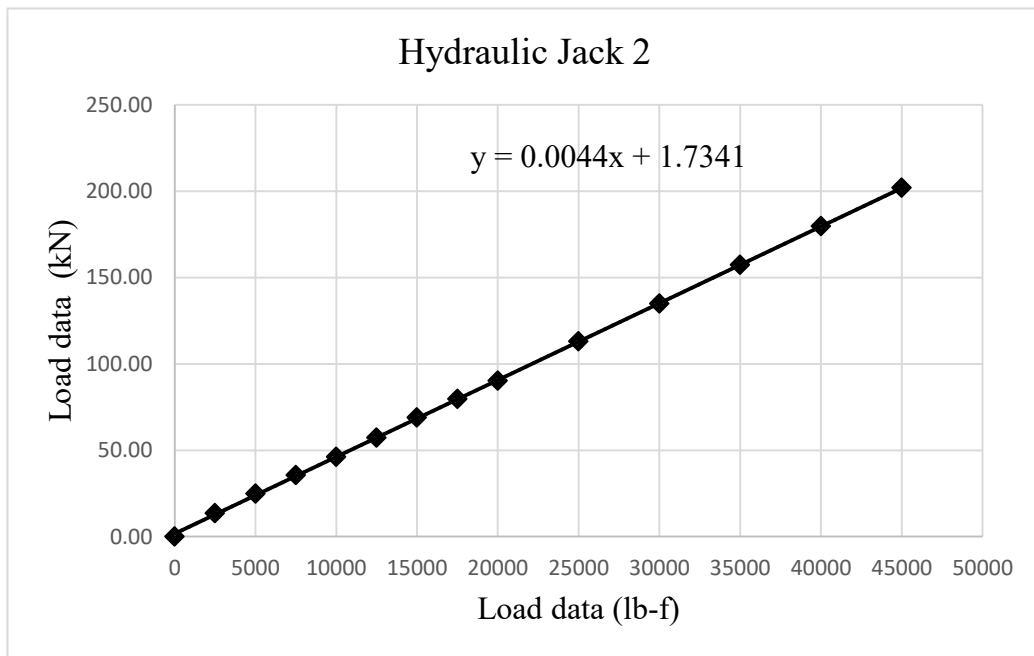


Figure G.2: Calibration curve of hydraulic jack 2.

Appendix-H

VALUES OF LOAD-DISPLACEMENT

Table H.1: Load-Displacement values for SB

Cycle	Maximum load	Load (KN)	Deflection (mm)
Cycle 1	40 KN	0	0
		10	0
		20	0.24
		30	0.27
		40	0.32
		30	0.31
		20	0.29
		10	0.28
		0	0.26
		-10	-0.21
		-20	-0.27
		-30	-0.33
		-40	-0.38
		-30	-0.37
		-20	-0.35
		-10	-0.34
		0	-0.12
Cycle 2	80 KN	0	-0.12
		20	0.16
		40	0.25
		60	2.3
		80	5.17
		60	5.1
		40	4.9
		20	4.5
		0	4.2
		-20	3.12
		-40	1.2
		-60	-2.2
		-80	-4.1
		-60	-3.6

		-40	-3.1
		-20	-2.7
		0	-1.4
Cycle 3	`120 KN	0	-1.4
		30	2.36
		60	4.93
		90	6.4
		120	9.36
		90	9.36
		60	9.36
		30	9.36
		0	6.34
		-30	0.5
		-60	-1
		-90	-3.2
		-120	-8.11
		-90	-8.07
		-60	-8.03
		-30	-7.8
		0	-1.3
Cycle 4	`160 KN	0	-1.3
		40	5.94
		80	8.12
		120	11.32
		150	17.25

Table H.2: Load-Displacement values for SBL

Cycle	Maximum load	Load (KN)	Deflection (mm)
Cycle 1	40 KN	0	0
		10	0.05
		20	0.1
		30	0.25
		40	0.35
		30	0.3
		20	0.28
		10	0.23
		0	0.04
		-10	-0.01
		-20	-0.01
		-30	-0.08
		-40	-0.2
		-30	-0.2
		-20	-0.08
		-10	-0.08
		0	-0.08
		Cycle 2	80 KN
20	1.08		
40	2.12		
60	3.58		
80	5.29		
60	5.01		
40	4.34		
20	3.45		
0	2.19		
-20	-0.2		
-40	-1.33		
-60	-3.56		
-80	-5.59		
-60	-5.59		
-40	-4.25		
-20	-3.2		
0	-1.5		

Cycle 3	120 KN	0	-1.5
		30	-2.13
		60	2.3
		90	6.12
		120	15.26
		90	14.45
		60	14.45
		30	14.45
		0	7.52
		-30	-2.5
		-60	-9
		-90	-15.23
		-120	-18.25
		-90	-18.25
		-60	-18.25
		-30	-12.45
		0	-4.59
Cycle 4	160 KN	0	-4.59
		40	6.14
		80	15.21
		120	24.45
		160	31.14

Table H.3: Load-Displacement values for PB

Cycle	Maximum load	Load (KN)	Deflection (mm)
Cycle 1	40 KN	0	0
		10	0
		20	0.1
		30	0.2
		40	0.5
		30	0.6
		20	0.5
		10	0.3
		0	0.1
		-10	-0.1
		-20	-0.3
		-30	-0.5
		-40	-0.9
		-30	-0.9
		-20	0.6
		-10	-0.2
		0	-0.1
		Cycle 2	80 KN
20	0.28		
40	2.45		
60	4.24		
80	5.7		
60	5.64		
40	4.26		
20	3.14		
0	1.25		
-20	-2.24		
-40	-3.15		
-60	-4.25		
-80	-4.57		
-60	-4.12		
-40	-3.45		
-20	-2.16		
0	-0.12		

Cycle 3	`120 KN	0	-0.12
		30	0.53
		60	1.45
		90	2.15
		120	10
		90	10
		60	7
		30	4.2
		0	1.5
		-30	0.8
		-60	0.1
		-90	-4.2
		-120	-10.52
		-90	-10.52
		-60	-7.43
		-30	-4
		0	-3.5
Cycle 4	`160 KN	0	-3.5
		40	3.75
		80	7.2
		120	13.2
		130	22.41

Table H.4: Load-Displacement values for PBL

Cycle	Maximum load	Load (KN)	Deflection (mm)
Cycle 1	40 KN	0	0
		10	0.09
		20	0.2
		30	0.41
		40	0.6
		30	0.53
		20	0.34
		10	0.22
		0	0.14
		-10	-0.08
		-20	-0.18
		-30	-0.37
		-40	-0.51
		-30	-0.47
		-20	-0.34
		-10	-0.27
		0	-0.16
		Cycle 2	80 KN
20	-0.02		
40	2.4		
60	4.54		
80	6.14		
60	6.01		
40	5.17		
20	4.43		
0	2.88		
-20	-0.01		
-40	-2.4		
-60	-4.07		
-80	-8.88		
-60	-9.42		
-40	-9.1		
-20	-8.23		
0	-2.02		

Cycle 3	120 KN	0	-2.02		
		30	3.5		
		60	7.08		
		90	10.05		
		120	17.7		
		90	16.5		
		60	16.5		
		30	16.32		
		0	11.02		
		-30	2.25		
		-60	-3.25		
		-90	-10.23		
		-120	-17.1		
		-90	-16		
		-60	-14.03		
		-30	-10.25		
		0	-1		
		Cycle 4	160 KN	0	-1
				40	3.21
80	8.12				
120	22.14				
160	34.12				
120	33.15				
80	32.15				
40	30.14				
0	17.52				
-40	5.25				
-80	-11.52				
-120	-19.52				
-160	-29.43				
-120	-27.65				
-80	-23.54				
-40	-18.52				
0	-14.52				
Cycle 5	200 KN			0	-14.52
				50	16.52
		100	32.14		

Appendix-I

SAMPLE CALCULATION FOR STIFFNESS, STORY DRIFT AND CUMULATIVE ENERGY DISSIPATION

Table I.1: Sample Calculation for stiffness, story drift and cumulative energy dissipation of SB

Cycle	Load (KN) x	Deflection (mm) y	Stiffness (KN/mm) x/y	Story Drift (%) (y/h)*100	Cumulative energy dissipation $\Sigma x*y$
1	40	0.32	125	0.02	12.8
2	80	5.17	15.47389	0.323125	426.4
3	120	9.36	12.82051	0.585	1549.6

Here, h= 1600 mm